Equation de transport, Level Set et mécanique eulérienne. Application au couplage fluide-structure

Emmanuel Maitre

Transport equations, Level Set and Eulerian mechanics. Application to fluid-structure coupling.

Report for "Habilitation à Diriger des Recherches"

Université de Grenoble

Emmanuel Maitre*

September 26, 2008

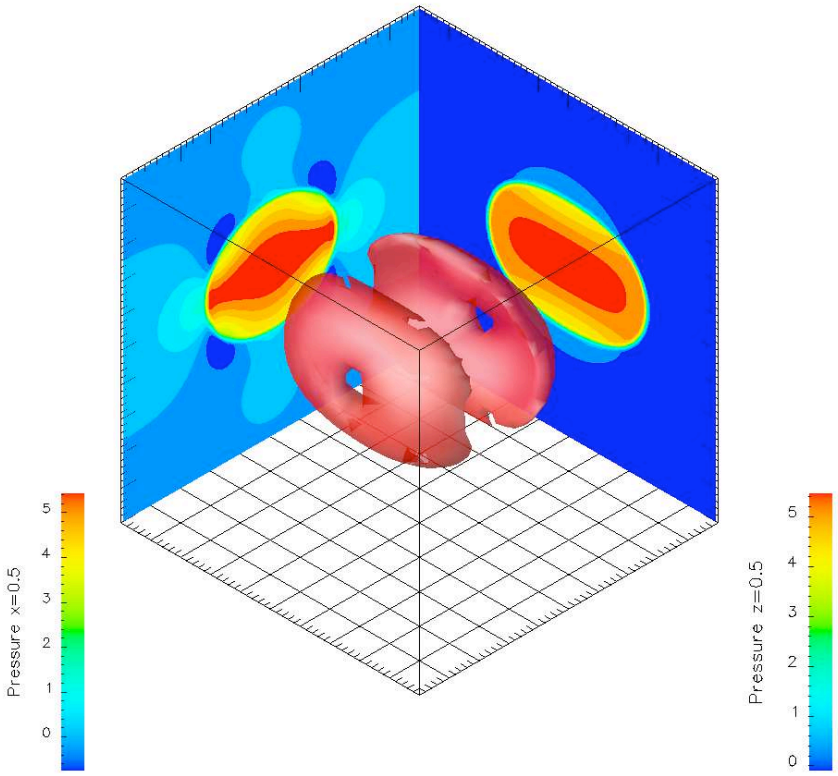

FIGURE 1: Iso-vorticity surface in the relaxation of an elastic immersed membrane

*Emmanuel.Maitre@imag.fr, http://ljk.imag.fr/membres/Emmanuel.Maitre/

Contents

1 Introduction

As an introduction I review some research directions I explored during last years, with a pointer to associated publications. The following pages develop into more details some of this fields, voluntarily ignoring those which I found less relevant.

After my PhD, my research in PDE was aimed toward doubly nonlinear elliptic-parabolic equations and a transport equation with boundary conditions involved in an elementary Level Set method [A13]. This Level Set method was developed to capture an interface in an injection molding process. The term elementary refers to the fact that there was no surface tension in this model by contrast with [45].

In September 1998, I obtained my first position in Mulhouse University and collaborated with S. Akesbi on his research themes which encompassed the study of numerical schemes for neutrons transport equations [A12, A11, A7]. I got also interested in the modeling and simulation of fabrics draping (Mulhouse is a town with a strong textile history, where there is a corresponding engineering school). I co-directed, with Alain Brillard, the PhD thesis of Nadjombé Faré on that subject (publication [A10]). This amounted to solve a nonlinear elasticity problem in large displacements. I also published articles on doubly nonlinear PDE, from the theoretical and numerical point of view (publications [A8, A9, A6]).

In September 2002 I moved back to Grenoble University on a position created to further develop interaction of applied mathematicians with Biologists and Physicists. In that direction I developed with Georges-Henri Cottet a new method for the modeling and computation of fluid-structure interaction problem (publications [A5, A4, A3]), applied to biological membranes (publications [B17, B16]) and cardiomyocyte contraction (publications [B15, A2]). This collaboration was supported by a local funding and a national grant for which I was coordinator. Moreover, two PhD thesis are about to be defended under our direction (Claire Bost and Thomas Milcent).

In connexion with the preceding, we developed a workgroup between our research team and a Physics laboratory in Grenoble (Chaouqi Misbah team) on the modeling of the behavior of phospholipidic vesicles in shear flow (article in preparation). A collaboration with John Stockie (U. Vancouver) about parametric instability of the immersed boundary model was initiated recently (work in progress).

At last during Spring and Summer 2007 I visited Fadil Santosa (U. Minnesota) and we developed a method for the minimization of functionals defined on curves moving on a surface [A1]. The motivation is the reconstruction of isocurves of activation potential on the myocardium.

2 Numerical analysis of elliptic-parabolic equations [A9]

2.1 Introduction and motivations

My interest for doubly nonlinear equations arose during my PhD, while I was modeling an injection moulding process [84]. Since the mold thickness was small, under a kinematic assumption of Hele-Shaw, it was possible by integration of Navier-Stokes equations to obtain a pressure equation which in turn could be written as a doubly nonlinear equation:

$$\frac{d}{dt}\mathcal{B}(u) + \mathcal{A}(u) = f \tag{1}$$

where $\mathcal{B}$ is a superposition et $\mathcal{A}$ an elliptic operator. A lot of publications have been devoted to this kind of equations from the pioneering work of [99] and [60] up to very recently [23, 100]. The problem we addressed in [A8] was to prove existence of a solution to (1) in the case where $\mathcal{B}$ can degenerate and therefore cannot bring all the compactness in time usually brought by the time derivative in parabolic equations, whereas operator $\mathcal{A}$ is not pseudo-monotone in the elliptic sense. This equation belongs to the class of elliptic-parabolic equations. We defined an *ad hoc* pseudo-monotony for these equations and prove existence of solutions in this class. The nonlinear semigroup approach [28] found in this kind of equation a new field of application initiated by F. Simondon [102] and more recently developed by Ph. Bénilan and P. Wittbold [29, 30] as well as F. Otto [94]. At last note that new results using renormalized solutions have been published very recently and weaken even more assumption on $\mathcal{B}$ to obtain existence.

The numerical analysis of related problems was first considered in [42][83] in the case where b^{-1} is Lipschitz continuous and the equation written as a porous-medium equation. This scheme was adapted to more general porous medium equations in [66][71]. More recently W. Jger and J. Kačur [67] and J. Kačur [72] studied the numerical approximation of (EP). However their numerical scheme was shown to converge for strictly increasing and Lipschitz continuous b, or in the particular case where a depends on u through $b(u)$.

In this article we introduce a numerical scheme for the case where b could become constant, but remains between two strictly increasing linear functions outside some compact set (see remark 1):

$(H2)$ b is a locally Lipschitz function on $\mathbb{R}$ and
$$\exists K \geq 0,\ \exists(\ell, L),\ 0 < \ell \leq L,\ \forall r \in \mathbb{R},\ |r| \geq K,\ \min(\ell r, Lr) \leq b(r) \leq \max(\ell r, Lr)$$

Note that under this assumption b can still become constant on some open set. However the constant steps have to be of bounded length.

Remark 1 *For example if we consider $b(r) = 0$ on $[-1, 1]$, $b(r) = r - 1$ on $[1, +\infty[$ and $b(r) = r + 1$ on $]-\infty, -1]$ (H2) is verified with $K = 2, L = 1, \ell = \frac{1}{2}$. However both $b(r) = \mathrm{sgn}(r)\sqrt{|r|}$ and $b(r) = \max(r, 0)$, fail to verify $(H2)$, the first one because it is non-Lipschitz in zero, the second one because it does not remain between to strictly increasing linear functions in the neighborhood of $-\infty$.*

2.2 Existence of mild solutions

Note that under assumptions $(H1)$ and $(H2)$, the existence of weak solutions is an open question, although some progress in that direction have been made recently [30] in dimension one. The good notion of solution there, is the notion of mild solutions since it is proved in [29] that there exists an exact mild solution u of (EP).

For an integer N we denote by $t_n = nh$, $n = 0, ..., N$ the subdivision of $[0, T]$ in N small intervals of length $h = \frac{T}{N}$ (see the remark below explaining why we work with a constant step subdivision). An exact mild solution of (EP) is a measurable function u verifying $v = b(u) \in C([0, T]; L^1(\Omega))$, $v(0) = v_0$ and, for any $\varepsilon > 0$, there exists $N \in \mathbb{N}$ such that for any

$$f_1, \dots, f_N \in L^\infty(\Omega) \text{ such that } \sum_n \int_{t_n}^{t_{n+1}} \|f(t) - f_{n+1}\|_1 dt \leq h,$$
$$u_0 \in L^\infty(\Omega) \text{ such that } \|v_0 - b(u_0)\|_1 \leq h,$$

there exists $(u_1, \dots, u_N)$ verifying for $n = 0, \dots, N-1$

$$\begin{cases} \dfrac{b(u_{n+1}) - b(u_n)}{h} - \operatorname{div} a(u_{n+1}, \nabla u_{n+1}) = f_{n+1} \text{ in } \mathcal{D}'(\Omega) \\ u_{n+1} \in W_0^{1,p}(\Omega) \cap L^\infty(\Omega). \end{cases} \tag{2}$$

and such that $\|v(t) - b(u_{n+1})\|_1 \leq \varepsilon$ for any $t \in (t_n, t_{n+1}]$, $n = 0, \dots, N-1$.

Remark 2 *The exact mild solution verifies more than the preceding, since the time subdivision needs not to be of constant step. It could be useful for an adaptative time step numerical scheme (see the final discussion and conclusion). However the technics developed thereafter can be adapted to a varying step subdivision without difficulty. So we chose for sake of readability to present the constant step algorithm.*

2.3 Existing schemes for related problems

The idea in [67] (under their assumptions a weak solution does exist) is basically to approach the solution of the equivalent equation

$$b'(u)u_t - \operatorname{div} a(u, \nabla u) = f \tag{3}$$

by the following scheme: for N integer and $h = \frac{T}{N}$ we denote by u_n the approximation of $u(t_n)$. Given u_n, to get u_{n+1} one first compute the solution θ_{n+1} of the elliptic problem

$$\lambda_n(\theta_{n+1} - u_n) - h \operatorname{div} a(u_n, \nabla \theta_{n+1}) = h f(t_{n+1}) \tag{4}$$

with the Dirichlet boundary condition, where $\lambda_n \in L^\infty(\Omega)$ should verify

$$\left\| \lambda_n - \frac{b_d((1-\alpha)u_n + \alpha\theta_{n+1}) - b_d(u_n)}{\theta_{n+1} - u_n} \right\|_\infty < h.$$

Then u_{n+1} is obtained by

$$u_{n+1} = (1-\alpha)u_n + \alpha\theta_{n+1}.$$

The function b_d is a regularization of b: $b_d(s) = b(s) + h^d s$; $d \in (0, \frac{1}{2})$ and α close to 1 are the parameters of the method. The coefficient λ_n is obtained eventually thanks to an iteration

$$\lambda_n^{k+1} = \frac{b_d((1-\alpha)u_n + \alpha\theta_{n+1}^k) - b_d(u_n)}{\theta_{n+1}^k - u_n}$$

where θ_{n+1}^k is obtained as the solution of (4) with $\lambda_n = \lambda_n^k$. This algorithm is proved to converge when b is strictly increasing and Lipschitz continuous. The numerical scheme we present now is stable even when b' is identically zero on some open set, or does not satisfy a global Lipschitz condition (see $(H2)$).

2.4 Numerical algorithm

Given $f_1, \ldots, f_N$, u_0, we are now addressing the problem of the numerical resolution of (2). We point out that the initial condition in (EP) is in fact given on $b(u)$ instead of u for a parabolic problem. This is because in (EP), in general, one has only the time continuity of $b(u)$. If b has some constant steps in its graph, then the initial condition on u can be undetermined.

For the same reason, the explicit scheme

$$\begin{cases} \dfrac{b(u_{n+1}) - b(u_n)}{h} - \operatorname{div} a(u_n, \nabla u_n) = f_{n+1}, \quad n = 0, \ldots, N-1 \\ b(u_0) = v_0, \end{cases}$$

could easily be solve in $v_{n+1} := b(u_{n+1})$ but nothing could prevent v_{n+1} from going out of the range of b. Then u_{n+1} could not be recovered. And even if v_{n+1} remains in the range of b, its degeneracy could bring a bad numerical behavior.

So we have to solve the implicit scheme directly in u. For this we introduce the following iterative process to get u_{n+1} from u_n:

$$(S) \qquad \begin{cases} \text{Let } u_{n+1}^0 \in L^\infty(\Omega) \text{ (e.g. } u_n), \text{ solve for } k = 0, 1, \ldots, \\ \\ u_{n+1}^{k+1} - \rho \operatorname{div} a(u_{n+1}^{k+1}, \nabla u_{n+1}^{k+1}) = \lambda_k u_{n+1}^k - \frac{\rho}{h}\left(b(\lambda_k u_{n+1}^k) - b(u_n)\right) + \rho f_{n+1} \end{cases}$$

where $\rho > 0$ is a given parameter, and (λ_k) is a sequence of $]0, 1[$ such that

$$\lim_{k\to\infty} \lambda_k = 1, \qquad \prod_{k\geq 0} \lambda_k = 0, \qquad \sum_{k\geq 0} |\lambda_{k+1} - \lambda_k| < \infty. \tag{5}$$

For example $\lambda_k = 1 - \frac{1}{k+1}$ is a convenient choice. Note that the introduction of λ_k in this scheme is an application of the ideas of B. Halpern [61] sharpened by P.-L. Lions [81] and more recently by H. Bauschke [25]. Indeed, in the interesting case, where b can degenerate, the iteration (S) with $\lambda_k = 1$ is non-expansive but not strictly contractant.

Remark 3 *Let us compare (S) (with $\lambda_k = 1$) with the scheme of Jger and Kačur that we recalled before, in the simpler case where $\alpha = 1$ and without regularization of b: in this case*

we have $\theta_{n+1} = u_{n+1}$ *and* $\lambda_n^{k+1} = \frac{b(u_{n+1}^k) - b(u_n)}{u_{n+1}^k - u_n}$ *and we make the following iteration to get* u_{n+1}^{k+1} *from* u_{n+1}^k*:*

$$\lambda_n^{k+1}(u_{n+1}^{k+1} - u_n) - h \operatorname{div} a(u_n, \nabla u_{n+1}^{k+1}) = hf(t_{n+1}).$$

Setting $\rho_n^{k+1} = \frac{h}{\lambda_n^{k+1}}$ *we get*

$$u_{n+1}^{k+1} - \rho_n^{k+1} \operatorname{div} a(u_n, \nabla u_{n+1}^{k+1}) = u_n + \rho_n^{k+1} f(t_{n+1}).$$

Thus our scheme appears as an analog of this scheme, with a correction term in the right hand side. The first advantage, from the computational point of view, is that there is no need to compute these λ_n^{k+1} *for which one has to test whether* $u_{n+1}^k = u^n$ *or not. Another point is that this scheme could exhibit a bad numerical behavior at times where* $u(t)$ *is discontinuous. Indeed, solutions* u *of* (EP) *need not to be continuous in time. Only* $b(u)$ *have to. If such a discontinuity happens, the estimation of the derivative of* b *in* λ_n^{k+1} *is nonsense. On contrary numerical tests we made (see at the end of article) show that our method works even in case of discontinuous* u*.*

2.5 Convergence of the algorithm

First we prove that under assumptions $(H1) - (H2)$ there exists a solution u_{n+1}^{k+1} to the equation involved in (S). This is performed by first truncating the u dependence of a, and by invoking a classical result of [82]. Then we are able to prove that u is bounded independently of the truncation level, so that existence is obtained for the equation without truncation. In order to rpove the convergence of the whole sequence (and not of some subsequence) we further assume:

$$(UC) \qquad \begin{cases} \forall f \in L^\infty(\Omega) \text{ il existe au plus une solution de} \\ u \in W_0^{1,p}(\Omega) \cap L^\infty(\Omega), \quad b(u) - \operatorname{div} a(u, \nabla u) = f \quad \text{dans } \mathcal{D}'(\Omega). \end{cases}$$

This assumption is for example fulfilled when a is strictly monotonic.

We prove the following convergence results that gives an explicit bound for the choice of ρ in (S) depending of the data.

Proposition 1 *Assume (H1)(H2) and (UC) hold. Let* M *defined by*

$$M = \max(\|u_{n+1}^0\|_\infty, \frac{1}{\ell}\|hf_{n+1} + b(u_n)\|_\infty, \frac{2K}{1 - \frac{\rho\ell}{h}}, \frac{2\frac{\rho}{h}}{1 - \frac{\rho\ell}{h}} \max_{[-K,K]} |b|)$$

where K *is defined in* $(H2)$*. Let* L_M *the Lipschitz constant of* b *on* $[-M, M]$*. Then for* $\rho < \min(\frac{h}{L}, \frac{2h}{L_M})$ *the iterative scheme* (S) *converges, i.e.*

$$\lim_{k \to \infty} u_{n+1}^k = u_{n+1} \quad \textit{strongly in } L^1(\Omega),$$

where u_{n+1} *verifies (2).*

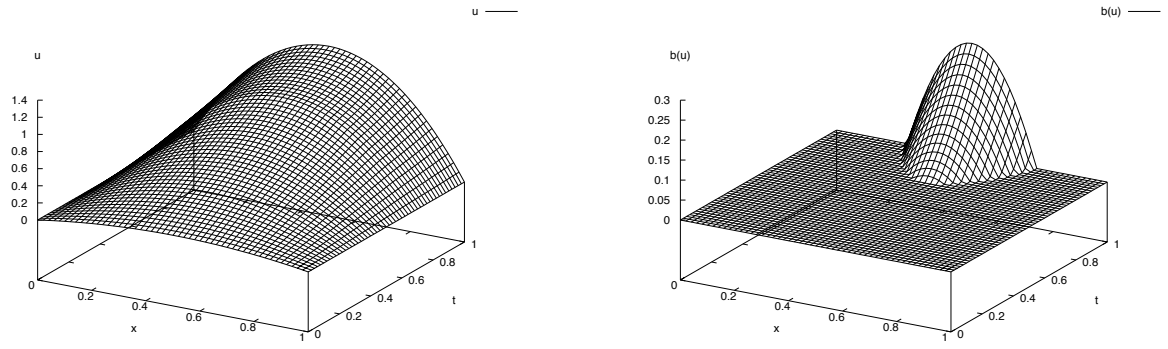

FIGURE 2: Test 2: Degenerate case $b(u) = 0$ for $|u| \leq 1$ and linear outside.

Let us point out that our bound on ρ, is easily computable so that we can implement this algortihm. Constant M appears when we estimate $\|u_{n+1}^k\|_\infty$ independently of k, see Lemma 6.2 of [A9].

Note that in [67], an iteration on k is performed until convergence to get the right coefficient λ_n in (4). Each iteration solves a linear scheme. When u_{n+1} is known, they prove the convergence of the step function $u_N(t) = u_{n+1}$ on $(t_n, t_{n+1}]$ toward the weak solution $u(t)$ as the time step goes to zero.

Under our assumptions on a and b, the existence of a weak solution is still an open question (see [30] for one dimension). For a mild solution we do not need to show the convergence in time since it is included in its definition: once convergence in k is achieved for u_{n+1}, then by definition of mild solution $b(u_{n+1})$ approaches $b(u)$ on $(t_n, t_{n+1}]$ up to ε. If b is non-degenerate, as in [67], this gives information on the behavior of u_{n+1}. On the contrary, note that if $b = 0$ we do not get a real convergence result; the point is that in this case, from the definition of [29], every measurable function u is a mild solution !

Note however that under some additional assumptions on a, it is proved in [29] that there exists a weak solution w of (EP) such that $b(w) = b(u)$ a.e. We thus have in this case the convergence of our scheme (in the same meaning) toward this weak solution.

2.6 Numerical tests

The stop criterium for iterations, in all the following tests is $\frac{\|u^{k+1}-u^k\|_2}{\|u^{k+1}\|_2} \leq 10^{-6}$ where $\|\cdot\|_2$ is the Euclidean norm and u^k the vector approaching, at iteration k, the space-discretization of u. The first numerical test is to emphasize the ability of our scheme to converge for really degenerated b. We chose $b(u) = 0$ for $|u| \leq 1$, $b(u) = u - 1$ for $u > 1$ and $b(u) = u + 1$ for $u < -1$, with $u_0(x) = \frac{1}{2}x(1-x)$ (thus $v_0(x) = b(u_0(x)) = 0$) and $f(x,t) = 10t + 1$.

Note that the value of u_0 plays no role, we just take this value so that it solves the equation at $t = 0$, ensuring a continuity of u. Here we are in a totally degenerate case since we start in a zone where b is identically zero. One see that u increases (in time) as f increases whereas b remains zero until u reach 1. The time for which $\|u(t)\|_\infty$ reaches 1 can be computed

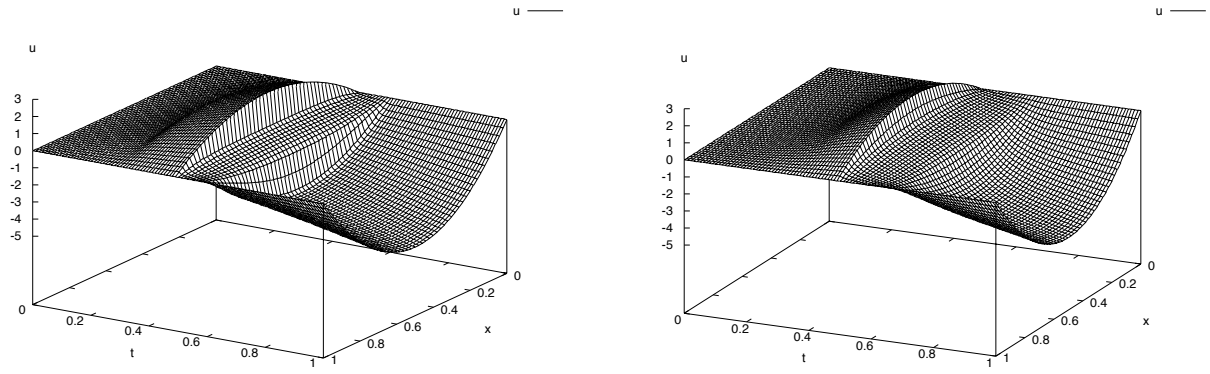

FIGURE 3: When u is discontinuous, our algorithm (left) and the method of Jäger and Kačur (right).

explicitly and is $t_c = 0.7$. Thus for $t < t_c$, we solve a pure elliptic problem and starting from $t = t_c$ we solve a parabolic problem. We can see on figure 2 that t_c is well computed.

In the two previous cases, u was continuous in time (and space). We compared our method with Kačur algorithm, and found that the two methods give exactly the same results. For the parameters of Kačur algorithm, we took $\alpha = 1$, and $d = 5$ (see [67]). Note that $d = 5$ is not permitted theoretically, but it works here and gave better results than $d = 1$ (since the regularisation term of b, h^d is smaller). In test 2 Kačur algorithm converges in even less iterations than our scheme.

We turn now to a case where u is discontinuous. On the same space-time domain, take the odd function b defined on $\mathbb{R}^+$ by $b(r) = 1$ for $r > 1$, and $b(r) = -r^2 + 2r$ for $0 \leq r < 1$. With $f(x,t) = 40t$ for $t < 0.5$, and $-40t$ for $t \geq 0.5$, and $u_0 = v_0 = 0$. The point is that the discontinuity of f occurs when (EP) is elliptic (because $u > 1$), so u has a jump too, at $t = 0.5$, and falls into $[-1, 1]$ where the equation is parabolic. There is a parabolic transition while u remains in $[-1, 1]$, and then the equation becomes elliptic so the rapidly varying f acts directly on u. Trying to make algorithm of [67] converging is hard, we had to rely on relaxation with $\alpha = 0.9$ and with a great regularisation term h^d with $d = 0.2$, or it does not converge for $t = 0.5$. Then there is a large smoothing of the profile induced by the method. Thus our method can handle discontinuities in u that seem hard to compute with the other algorithm. On figure 3 the superposed graphs of u (resp. $b(u)$) obtain by the two methods are plotted.

2.7 Conclusion and possible extensions

We develop a new algorithm to deal with the numerical computation of solution to degenerate elliptic-parabolic equations, which performs better in that case than known algorithms.

Note that as indicated before, the time step needs not to be constant in the definition of mild solution, leading to an adaptative time step method. This may be interesting, when the solution is expected to present a jump (in u) at a certain time. Indeed in this case one could operate thiner time discretization around this discontinuity time.

Some works extending our approach have been recently published [103].

3 Neutrons transport equation [A11, A7]

Efficient algorithms to solve the neutrons transport equation have been an active field of research (see [111, 59, 22, 75, 89, 74, 85, 86] and references therein). Among these schemes, some introduced by Samir Akesbi (Université de Mulhouse) and co-authors [19, 20, 21], make use of a splitting of the tranport operator taking into account its characteristics [18]. In the present work we introduced a new algorithm based on this splitting and an adaptation of minimal residual methods to the infinite dimensional case. Some very recent publications [111, 112] extend this results further.

We present both the case where the velocity space is of dimension 1 (slab geometry) and 2 (plane geometry), because the splitting is simpler in the former.

3.1 The equations and their resolution without splitting

3.1.1 Transport equations

Dimension 1 The evolution of neutrons in a one-dimensional domain $(0, L)$, in interaction with them, is described by a function $f(x, \mu)$ which represents the angular flux of neutrons at the position x traveling in the direction cosine $\mu \in (-1, 1)$. The cross section $\sigma(x)$ accounts for neutrons-domain interaction, whereas a kernel $k(x, \mu, \mu')$ describes collisions between neutrons. At last, a neutrons source is represented by a function $S(x, \mu)$.

Let $L > 0$ and $\Omega = (0, L) \times (-1, 1)$. We consider the following problem: given a source term $S \in L^2_+(\Omega)$, find $f : \Omega \to \mathbf{R}$ solution of the transport equation

$$(P) \quad \begin{cases} Tf(x,\mu) = Kf(x,\mu) + S(x,\mu) & \text{in } \Omega, \\ f(0,\mu) = 0 & \text{for } \mu \in I_1 := (0,1), \\ f(L,\mu) = 0 & \text{for } \mu \in I_2 := (-1,0), \end{cases}$$

where $Tf(x, \mu) = \mu \dfrac{\partial f}{\partial x}(x, \mu) + \sigma(x) f(x, \mu)$ with

$$\mathcal{D}(T) = \left\{ f \in L^2(\Omega) \ : \ \mu \frac{\partial f}{\partial x}(x,\mu) \in L^2(\Omega), \ f(0,\mu) = f(L,-\mu) = 0 \text{ for } \mu > 0 \right\},$$

and K an integral operator of *positive* kernel k:

$$Kf(x,\mu) = \int_{-1}^{1} k(x,\mu,\mu') f(x,\mu') d\mu'.$$

We make the following **assumptions** (where L^1_+ denotes the positive cone of L^1):

(A1) $\sigma \in L^1_+(0, L)$.

(A2) $(\mu, \mu') \to k(\mu, \mu') \in L^2_+((-1, 1)^2)$.

(A3) If k is symmetric and even and σ constant (see remark 1), we assume:

$$\exists c < 1, \ \left(\int_{-1}^{1} \int_{-1}^{1} k(\mu,\mu')^2 d\mu d\mu' \right)^{\frac{1}{2}} \leq \sigma c.$$

Assumptions in the general case are given in [A12], and are satisfied by usual neutrons kernels.

(A4) $k(\mu, \mu') = \sum_{l=1}^{N_k} a_l(\mu) a_l(\mu')$.

Dimension 2 The behaviour of neutrons in a two dimensional domain D, in interaction with them, is described by a function $f(x, \Omega)$ which represents, up to some factor, the flux of neutron density at the position x with velocity $\Omega \in B(0,1)$. A function $\sigma(x)$ accounts for neutron-domain interaction, whereas a kernel $k(x, \Omega, \Omega')$ describes collisions between neutrons. At last, a neutron source is represented by a non-negative function $S(x, \Omega)$.

Let D bet a bounded open set of $\mathbf{R}^2$ with lipschitz boundary ∂D, and $Q = D \times B$ where $B = B(0,1) = \left\{\Omega \in \mathbf{R}^2, \quad \|\Omega\|_2 < 1\right\}$. The outer normal $\mathbf{n}(\mathbf{x})$ to ∂D exists almost everywhere, and we define

$$\Gamma^- := \{(x, \Omega) \in \partial D \times B, \quad \Omega \cdot \mathbf{n}(x) < 0\}.$$

We consider the following problem: given a source term S, find $f : Q \to \mathbf{R}$ solution of the transport equation

$$(P) \quad \begin{cases} Tf(x,\Omega) = Kf(x,\Omega) + S(x,\Omega) & \text{in } Q, \\ f(x,\Omega) = 0 & \text{on } \Gamma^-, \end{cases}$$

where T is the transport operator, $Tf(x, \Omega) = \Omega \cdot \nabla_x f(x, \Omega) + \sigma(x) f(x, \Omega)$ whose domain is

$$\mathcal{D}(T) = \left\{f \in L^2(\Omega) \ : \ \Omega \cdot \nabla_x f \in L^2(\Omega), \ f = 0 \text{ on } \Gamma^-\right\},$$

and K an integral operator of *positive* kernel k:

$$Kf(x, \Omega) = \int_B k(x, \Omega, \Omega') f(x, \Omega') d\Omega'.$$

We make the following
Assumptions:

(A1) $\sigma \in L^\infty(D)$, $\exists \sigma_0 > 0, \quad \sigma(x) \geq \sigma_0$ a.e. on D.

(A2) $k(x, \Omega, \Omega') = k(x, \Omega', \Omega)$ and k is positive.

(A3) $\exists c \in [0, 1), \quad \forall i \in \{1, 2, 3, 4\}, \quad \int_{B_i} k(x, \Omega, \Omega') d\Omega' \leq \frac{\sigma_0 c}{4}$ a.e. on Q, where B_i is the i-th quarter of the disk B, see figure 4.

(A4) $k(x, \Omega, \Omega') = C(x) \sum_{l=1}^{N_k} a_l(\Omega) a_l(\Omega')$.

Assumption (A4) is not used for theoretical proof of convergence. However, it is necessary to assume this form for k for the numerical splitting method to work [21, 18].

3.1.2 Source Iteration method

The standard method to solve (P), called the source iteration method, is based on a decoupling between the differential and integral parts, through the following iterative scheme: given $f^0 \in \mathcal{D}(T)$, solve

$$(P_s) \quad \begin{cases} Tf^{n+1} = Kf^n + S & \text{in } Q, \\ f^{n+1} \in \mathcal{D}(T). \end{cases}$$

Close to the critical case ($c \approx 1$), this algorithm becomes extremly slow. Several acceleration methods of the convergence of (P_s) have been introduced and studied. In particular the Diffusion Synthetic Acceleration (DSA) method [75][24] and multigrid algorithms [86][89].

The main difficulties encountered while studying these methods lead the authors either to consider the discretized equation in the angular variable [74][85], or the continuous equation with a truncated expansion of k with respect to this angular variable [89][74].

To our knowledge, the only theoretical proof for the acceleration of the convergence in the continuous case (in space an angular variables) has been obtained for reflexive boundary conditions by [75].

The idea of [19] and [20] is to introduce and study better algorithms than (P_s), adapted from the methods of Jacobi, Gauss-Seidel and SOR, in the infinite dimensional case. These algorithms can be accelerated by an adapted DSA method. This approach has been studied in dimension one and two by [21], and successfully compared to standard DSA method.

Our aim is to propose a new algorithm, replacing Jacobi, Gauss-Seidel or SOR algorithms, based on an adaptation of the minimal residual method in infinite dimensional case. As others algorithms, it relies on a natural splitting of k.

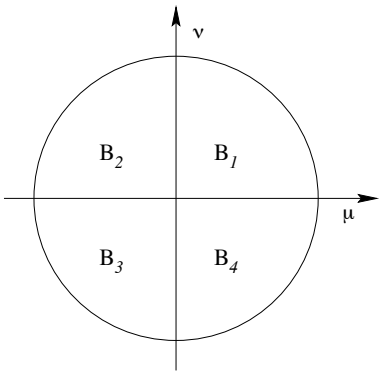

FIGURE 4: Decomposition of B in dimension 2.

3.2 Splitting of transport operator

Dimension 1. Let k_{ij}, $i, j \in \{1, 2\}$ be the positive kernel defined by

$$k_{ij}(x, \mu, \mu') = k(\mu, \mu') \times \mathbf{1}_{\Omega_i}(x, \mu) \times \mathbf{1}_{\Omega_j}(x, \mu'),$$

with $\Omega_1 = (0, L) \times (0, 1)$, $\Omega_2 = (0, L) \times (-1, 0)$, and $\mathbf{1}_{\Omega_i}$ the indicator function of Ω_i. We introduce the associated integral operator $K_{i,j}$:

$$K_{ij}(f)(x, \mu) = \int_{-1}^{1} k_{ij}(x, \mu, \mu') f(x, \mu') d\mu'.$$

Since we have $K_{ij}(f) = K_{ij}(f.\mathbf{1}_{\Omega_j})\mathbf{1}_{\Omega_i}$, operator K splits into $K = K_{11} + K_{12} + K_{21} + K_{22}$. Note that K_{ij} is an operator acting from $L^2(\Omega)$, using only the values of f on Ω_j, such that $K_{ij}f$ has its support in Ω_i.

The solution of (P) is given by $f = f_1 + f_2$ with $f_1, f_2 \in \mathcal{D}(T)$ solution of

$$\begin{pmatrix} T - K_{11} & -K_{12} \\ -K_{21} & T - K_{22} \end{pmatrix} \begin{pmatrix} f_1 \\ f_2 \end{pmatrix} = \begin{pmatrix} S_1 \\ S_2 \end{pmatrix}. \tag{6}$$

It is easy to prove that $f_i = f\mathbf{1}_{\Omega_i}$, $i = 1, 2$. (cf [21]).

Dimension 2. Let K_{ij}, $i, j \in \{1, \ldots, 4\}$ be the integral operator whose kernel is

$$k_{ij}(x, \Omega, \Omega') = k(x, \Omega, \Omega') \times \mathbf{1}_{Q_i}(x, \Omega) \times \mathbf{1}_{Q_j}(x, \Omega'),$$

with $Q_i = D \times B_i$, B_i being the i-th quarter of the unit disk (see figure 4) and $\mathbf{1}_{Q_i}(x, \Omega)$ the indicator function of Q_i. Since we have $K_{ij}(f) = K_{ij}(f.\mathbf{1}_{Q_j})\mathbf{1}_{Q_i}$, operator K splits into $K = \sum_{i,j=1}^{4} K_{ij}$. Note that K_{ij} is an operator acting from $L^2(Q)$, using only the values of f on Q_j, such that $K_{ij}f$ has its support in Q_i. The solution of (P) is given by $f = f_1 + f_2 + f_3 + f_4$ with $f_1, f_2, f_3, f_4 \in \mathcal{D}(T)$ solution of

$$\begin{pmatrix} T - K_{11} & -K_{12} & -K_{13} & -K_{14} \\ -K_{21} & T - K_{22} & -K_{23} & -K_{24} \\ -K_{31} & -K_{32} & T - K_{33} & -K_{34} \\ -K_{41} & -K_{42} & -K_{43} & T - K_{44} \end{pmatrix} \begin{pmatrix} f_1 \\ f_2 \\ f_3 \\ f_4 \end{pmatrix} = \begin{pmatrix} S_1 \\ S_2 \\ S_3 \\ S_4 \end{pmatrix} \tag{7}$$

where $S_i = S \times \mathbf{1}_{Q_i}$. Then we have $f_i = f \times \mathbf{1}_{Q_i}$ for $i \in \{1, \ldots, 4\}$. T (cf [18]). The SOR method introduced by [21] gives excellent results, but needs the computation of its optimal parameter, which in turn can be very slow in the critical case. For these reasons we seeked a method that gives good rate of convergence, but do not need any extra parameter calculation.

3.3 Minimal residual algorithm

3.3.1 Algorithm

This method was introduced by O. Axelsson [76], in the finite dimensional case, and proved to converge provided the matrix of the linear system has a definite positive symetric part. Using the operator splitting deviced by S. Akesbi and M. Nicolet, the transport equation is equivalent to the following system, that we present for the case of dimension 2 only.

$$\begin{pmatrix} I - \theta_{11} & -\theta_{12} & -\theta_{13} & -\theta_{14} \\ -\theta_{21} & I - \theta_{22} & -\theta_{23} & -\theta_{24} \\ -\theta_{31} & -\theta_{32} & I - \theta_{33} & -\theta_{34} \\ -\theta_{41} & -\theta_{42} & -\theta_{43} & I - \theta_{44} \end{pmatrix} \begin{pmatrix} f_1 \\ f_2 \\ f_3 \\ f_4 \end{pmatrix} = \begin{pmatrix} \widetilde{S_1} \\ \widetilde{S_2} \\ \widetilde{S_3} \\ \widetilde{S_4} \end{pmatrix},$$

where we applied on components the operator T^{-1}, and set $\theta_{ij} = T^{-1}K_{ij}$, $\widetilde{S}_i = T^{-1}S_i$. The matrix of operators of our system will be preconditionned by the inverse of diagonal i.e.

$$\begin{pmatrix} (I-\theta_{11})^{-1} & 0 & 0 & 0 \\ 0 & (I-\theta_{22})^{-1} & 0 & 0 \\ 0 & 0 & (I-\theta_{33})^{-1} & 0 \\ 0 & 0 & 0 & (I-\theta_{44})^{-1} \end{pmatrix},$$

leading to the following matrix of operators

$$\mathcal{A} = \begin{pmatrix} I & -(I-\theta_{11})^{-1}\theta_{12} & -(I-\theta_{11})^{-1}\theta_{13} & -(I-\theta_{11})^{-1}\theta_{14} \\ -(I-\theta_{22})^{-1}\theta_{21} & I & -(I-\theta_{22})^{-1}\theta_{23} & -(I-\theta_{22})^{-1}\theta_{24} \\ -(I-\theta_{33})^{-1}\theta_{31} & -(I-\theta_{33})^{-1}\theta_{32} & I & -(I-\theta_{33})^{-1}\theta_{34} \\ -(I-\theta_{44})^{-1}\theta_{41} & -(I-\theta_{44})^{-1}\theta_{42} & -(I-\theta_{44})^{-1}\theta_{43} & I \end{pmatrix}$$

In order to perform a minimal residual method, we have to make clear which operations between matrix and vectors, appearing in the method, can be calculated from a numerical point of view.
We are willing to solve $\mathcal{A}F = B$, where $F = {}^t(f_1, f_2, f_3, f_4) \in \mathcal{D}(T)^4$. We denote by $\langle , \rangle$ the scalar product in $(L^2(\Omega))^4$, i.e. $\langle F, G\rangle = (f_1, g_1) + (f_2, g_2) + (f_3, g_3) + (f_4, g_4)$ where $(,)$ is the standard $L^2(\Omega)$ scalar product. Similarly, $\|\|_2$ will represent the norm in $(L^2(\Omega))^4$ associated to this scalar product.
The minimal residual method, minimizing $\mathcal{E}(F) = \|B - \mathcal{A}F\|_2^2$, takes the following form:
Let $f^0 \in \mathcal{D}(T)$, $F^0 = (f^0 \mathbf{1}_{Q_i})_{i=1,\dots,4}$, $R^0 = B - \mathcal{A}F^0$, $P^0 = R^0$, $Q^0 = \mathcal{A}P^0$.
While $\left\|R^k\right\|_2 > \varepsilon$ do
begin

$$\begin{aligned} \alpha^k &= \frac{\langle R^k, Q^k\rangle}{\langle Q^k, Q^k\rangle} \\ F^{k+1} &= F^k + \alpha^k P^k \\ R^{k+1} &= R^k - \alpha^k Q^k \\ \beta^{k+1} &= -\frac{\langle \mathcal{A}R^{k+1}, Q^k\rangle}{\langle Q^k, Q^k\rangle} \\ P^{k+1} &= R^{k+1} + \beta^{k+1} P^k \\ Q^{k+1} &= \mathcal{A}R^{k+1} + \beta^{k+1} Q^k \end{aligned}$$

end
In the previous algorithm, we have to make clear how we compute the product $\mathcal{A}$ times a vector, since $\mathcal{A}$ contains some inverse operator.
So let $g \in \mathcal{D}(T)$, $\mathcal{G} = (g\mathbf{1}_{Q_i})_{i=1,\dots,4}$ and see how to compute $\mathcal{Z} = (z_1, z_2, z_3, z_4)$ verifying

$$\mathcal{Z} = \mathcal{A}\mathcal{G}$$

Componentwise, this equality means for $i = 1, \dots, 4$,

$$z_i = g_i - \sum_{j\neq i} (I - \theta_{ii})^{-1}\theta_{ij} g_j.$$

Applying $T(I-\theta_{ii}) = T - K_{ii}$ to the first equation we get

$$(T - K_{ii})(g_i - z_i) = \sum_{j \neq i} K_{ij} g_j \tag{8}$$

These integro-differential equations can be calculated numerically [18] thanks to the splitting and the special form of the kernel assumed in (A4).

3.3.2 Convergence

In order to prove the convergence of our algorithm, we have to estimate from below the quadratic form associated to the operator matrix $\mathcal{A}$. It is indeed well known (direct adpatation of [76]) that the minimal residual method produces a sequence of residual such that

$$\mathcal{E}(F^{k+1}) \leq \mathcal{E}(F^k) \left(1 - \frac{\langle R^k, \mathcal{A}R^k \rangle}{\langle R^k, R^k \rangle} \frac{\langle R^k, \mathcal{A}R^k \rangle}{\langle \mathcal{A}R^k, \mathcal{A}R^k \rangle}\right). \tag{9}$$

In [A12, A7] we prove the following by estimation the transport operator T and the integral kernels K_{ii}:

Proposition 2 *Under assumptions (A1)-(A3) operator $\mathcal{A}$ has a positive definite symmetric part and verifies*

$$\textit{1D case:} \qquad \forall F \in \mathcal{D}(T)^2,\ \langle \mathcal{A}F, F \rangle \geq \frac{1-c}{1-\frac{c}{2}} \|F\|_2^2, \qquad \langle \mathcal{A}F, F \rangle \geq \frac{1-\frac{c}{2}}{1+\left(\frac{c}{2}\right)^2} \langle \mathcal{A}F, \mathcal{A}F \rangle$$

$$\textit{2D case:} \qquad \forall F \in \mathcal{D}(T)^4,\ \langle \mathcal{A}F, F \rangle \geq \frac{1-c}{1-\frac{c}{4}} \|F\|_2^2, \qquad \langle \mathcal{A}F, F \rangle \geq \frac{1-\frac{c}{4}}{1+\frac{c}{2}} \langle \mathcal{A}F, \mathcal{A}F \rangle .$$

Therefore we get the following convergence result:

Proposition 3 *Under assumptions (A1)-(A3), the minimal residual method converges, that is F^k converges toward the unique solution of (6) or (7), and the residual decreases when $k \geq 0$ following:*

$$\textit{1D case:} \qquad \mathcal{E}(F^{k+1}) \leq \mathcal{E}(F^k) \left(1 - \frac{1-c}{1+\left(\frac{c}{2}\right)^2}\right)$$

$$\textit{2D case:} \qquad \mathcal{E}(F^{k+1}) \leq \mathcal{E}(F^k) \left(1 - \frac{1-c}{1+\frac{c}{2}}\right).$$

Our estimate of the convergence rate (15) is not optimal. Indeed, the forthcoming numerical tests will show that our algorithm works for values of c greater than one. In dimension 2 we observed the convergence for $\sigma = 50$ up to $c < 4$. Figure 5 displays a comparison our algorithm for $\sigma = 50$ with SOR. Recall that the latter requires the computation of an optimal parameter which is not taken into account. In dimension 1 it appears clearly that SOR explodes for c close to 1, and Figure 6 shows the same for the dimension 2. However our method allows to exceed the critical value $c = 1$. Moreover our algorithm displays a good behavior for large σ (see Figure 7) converging more and more rapidly.

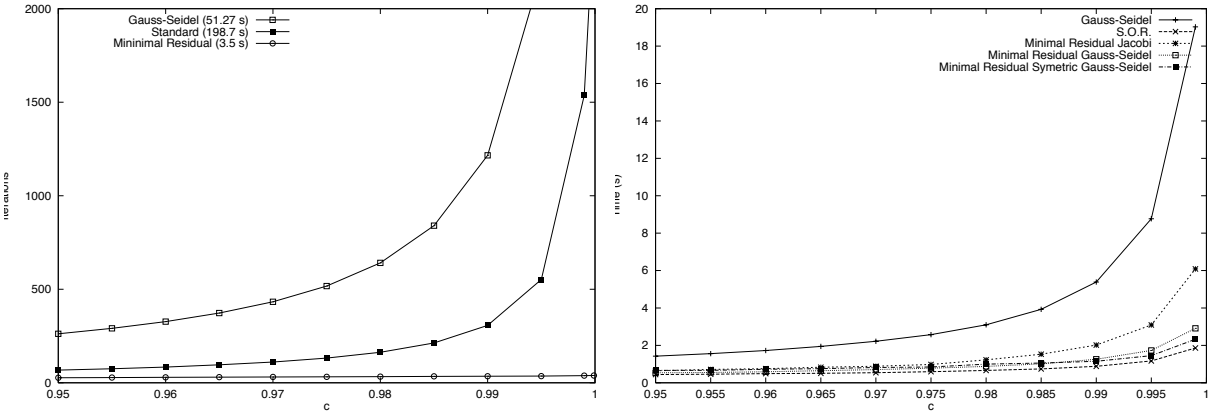

FIGURE 5: Computational costs for $\sigma = 50$ up to $c = 0.999$. Left: 1D. Right: 2D for several implementation of the resolution of (8)

3.4 Conclusion

We showed through the previous numerical tests that our methods are as performant as SOR for non-critical cases (c close to 1 or large σ), and converge even faster for critical cases. Moreover, their implementation is as easy as standard algorithm (P_s). They are naturally deviced for parallelization. A work is in progress for the acceleration of this algorithm by an adapted DSA method [21], and its comparison with standard DSA. One important point would be to be able to prove that the method indeed converges for $c > 1$, which would be definitive argument for ou r method. Very recently Samir Akesbi and Abdelkader Tizaoui implemented a GMRes algorithm which seems to beat out algorithm [112].

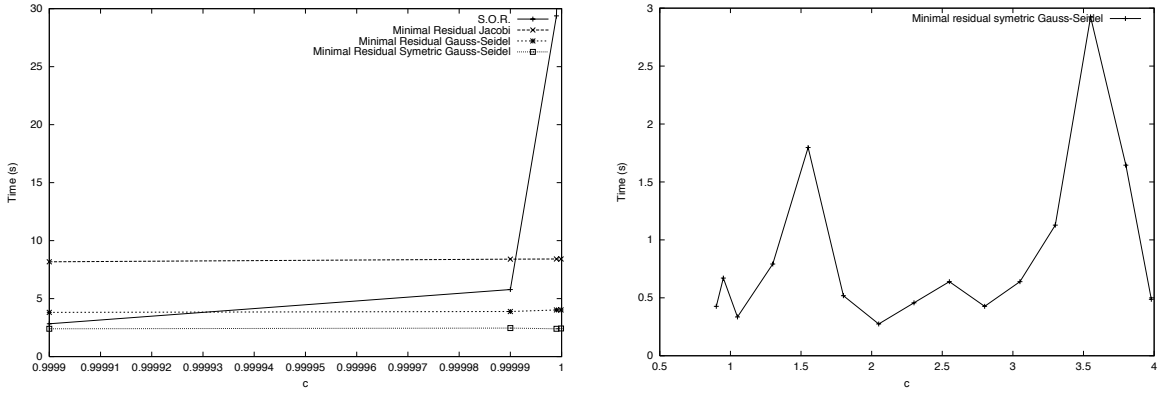

FIGURE 6: Comparison in the 2D case of computational cost, for $\sigma = 50$ in the neighborhood of $c = 1$ and for values $1 < c < 4$

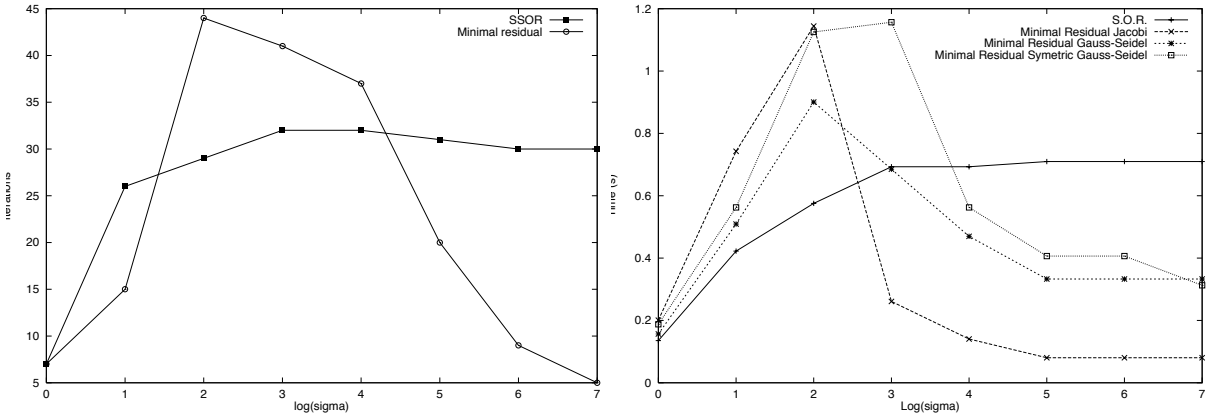

FIGURE 7: Comparison of cpu time at fixed $c = 0.98$, for large σ.

4 Fabrics modeling [A10]

4.1 Introduction

This work was developed during the PhD of Nadjombé Faré in Mulhouse University. This town in north-east of France has a strong history of textile industry, so that a one century old engineering school devoted to that topic is present. We interacted with fabrics specialists to model textiles as continuum media, of a special kind.

One toy problem is the drape problem, in which one studies the folds formed by a textile which subject to its own weight and attached on a part of it boundary. There even exist drape meter which measure the shadow area formed by those folds to characterize the textile. We got interested in the modeling and simulation of this problem.

In that case, as the fabric only undergoes gravity, we neglected the stretching of its fibers. Thus the model we study only take into account shear in the tangent plane to the fabric and flexion.

In the following, greek subscripts α, β ... take values 1 or 2 and we adopt the Einstein convention on repeated indices. We denote by $f_{,\alpha}$ lthe partial derivative of f with respect to x_α and by $f_{,\alpha\beta}$ the second order derivatives. If X is a vector of $\mathbb{R}^3$, $\|X\|$ denotes its Euclidian norm; the vector product between u and v is written $u \wedge v$, and the scalar product $u \cdot v$. The norm $\| \|_2$ depending of its argument, stands for $L^2(\Omega, \mathbb{R}^3)$ or $L^2(\Omega, \mathbb{R})$ norm.

Assume that the fabric initially occupies a domain $\Omega \times \{0\}$ of $\mathbb{R}^3$ where $\Omega \subset \mathbb{R}^2$ is an open bounded subset with piecewise C^1 boundary. Let Γ_0 be a subset of $\partial\Omega$ of positive measure, where the fabrics is fixed. The reference configuration coincides with the initial one and a point X has coordinates $X = \varphi_0(x_1, x_2) = (x_1, x_2, 0)$ in some fixed frame (e_1, e_2, e_3). An admissible deformation of the initial configuration is an application φ sufficiently smooth, injective in Ω and $\mathbb{R}^3$ valued i.e.:

$$\varphi : \begin{cases} \Omega \to \mathbb{R}^3 \\ x = (x_1, x_2) \to \varphi(x) = (\varphi_1(x), \varphi_2(x), \varphi_3(x)) \end{cases}$$

which moreover verifies:

(i) $\|\varphi_{,1}\| = 1$, $\|\varphi_{,2}\| = 1$ (non extensible fibers),

(ii) $\|\varphi_{,1} \wedge \varphi_{,2}\| \geq C_0$, where $0 < C_0 \leq 1$ depends on the fabric.

Remark 4 *1. Condition (ii) means that weft and warp fibers cannot become parallel.*

2. D. Coutand [51] considered the case of a shell with $C_0 = 1$, that is without membrane shear. We ourselves assumed a plane configuration since this is often the case for fabrics, but this is not a technical limitation of our method. We make use of technics introduced in [51] and [49].

4.2 Mechanical derivation of our model

In [A10] we start from a 3D model where the fabrics occupied the domain $\Theta = \Omega \times]-h, +h[\subset \mathbb{R}^3$. The fabric thickness $h > 0$ being very small, we make a kinematic assumption of Cosserat, considering that deformation of the initial configuration are of the following form:

$$\Phi(x_1, x_2, x_3) = \varphi(x_1, x_2) + x_3 t(x_1, x_2)$$

where $t(x_1, x_2)$ is unitary.
By computing the three dimensional Green Saint-Venant deformations tensor, we get

$$E_{\alpha\beta} = \frac{1}{2}(\varphi_{,\alpha}.\varphi_{,\beta} - \delta_{\alpha\beta}) + \frac{1}{2}x_3(\varphi_{,\alpha}.t_{,\beta} + \varphi_{,\beta}.t_{,\alpha}) + \frac{1}{2}x_3^2 t_{,\alpha}.t_{,\beta} \quad E_{3\alpha} = \frac{1}{2}\varphi_{,\alpha}.t \quad E_{33} = 0.$$

Using the small thickness assumption, we neglect terms of order higher than 1 in x_3, so that the three following tensors are involved: the membrane deformation tensor, the flexural tensor and the transverse shear tensor:

$$\left\{ \begin{array}{lcl} e_{\alpha\beta} & = & \frac{1}{2}(\varphi_{,\alpha} \cdot \varphi_{,\beta} - \delta_{\alpha\beta}) \\ \chi_{\alpha\beta} & = & \frac{1}{2}(\varphi_{,\alpha} \cdot t_{,\beta} + \varphi_{,\beta} \cdot t_{,\alpha}) \\ \gamma_{\alpha} & = & \frac{1}{2}\varphi_{,\alpha} \cdot t \end{array} \right.$$

where $\delta_{\alpha\beta}$ is the Kronecker symbol.
From the fabric structure, we assume no transverse shear, which corresponds to cancel the last tensor, which means $\gamma_\alpha = \frac{1}{2}\varphi_{,\alpha} \cdot t = 0$. In that case t is normal to the textile mean surface. From now we denote it $N(\varphi)$. Differentiating γ, one may eliminate derivatives of t from $\chi_{\alpha\beta}$ which turns to: $\chi_{\alpha\beta} = -\varphi_{,\alpha\beta} \cdot N(\varphi)$.
Assuming for the sake of simplicity a linear relationship between the strain and stress tensor (note that the material is still geometrically nonlinear) we have $\Sigma_{ij} = R_{ijkl}E_{kl}$, where Σ is the second Piola-Kirchhoff tensor and R the stiffness matrix which contains elasticity coefficients depending of the fabrics.

Static equilibrium is characterized by application of the principle of virtual works (see [47][48], [73]), which by integration in the thickness of the second Piola-Kirchhoff tensor leads to the following energy:

$$I(\varphi) = \frac{1}{2}\int_\Omega \left[G\left(\varphi_{,1} \cdot \varphi_{,2}\right)^2 + d_{\alpha\beta}\left(\varphi_{,\alpha\beta} \cdot N(\varphi)\right)^2 \right] dx - \int_\Omega \sigma g \varphi_3 dx$$

where the coefficients G and $d_{\alpha\beta}$ depends on the material properties. Under this general form, we are not able to prove existence of minimizers due to the lack of coerciveness of $I(\varphi)$. More specifically, terms of the form $\varphi^n_{,\alpha\alpha}.\varphi^n_{,\beta}$ for a minimizing sequence seem hard to control.

After discussion with fabric specialists[1] we considered a regularized energy with an extra term accounting for the variation of shear angle.

[1] among who Ron Postle, invited by the local engineering school

4.3 Regularized energy and existence of a minimizer

Adding this regularizing term, we obtain a two-dimensionnal mechanical model that we now study from the mathematical point of view. The energy is given by:

$$W(\varphi) = \frac{1}{2}\int_\Omega \left[G\left(\varphi_{,1}\cdot\varphi_{,2}\right)^2 + g_\alpha\left(\left(\varphi_{,1}\cdot\varphi_{,2}\right)_{,\alpha}\right)^2 + d_{\alpha\beta}\left(\varphi_{,\alpha\beta}\cdot N(\varphi)\right)^2\right]dx - \int_\Omega \sigma g\varphi_3 dx$$

where $N(\varphi):\Omega\to\mathbb{R}^3$, $N(\varphi)=\frac{\varphi_{,1}\wedge\varphi_{,2}}{\|\varphi_{,1}\wedge\varphi_{,1}\|}$ is normal to the fabrics mean surface, $g_\alpha>0$, $d_{\alpha\beta}>0$ and $G>0$ are fabric elasticity coefficients, $\sigma>0$ is its surface density and $g>0$ gravity. In the following we write N for $N(\varphi)$.
The first term represents the membrane shear deformation energy, the second one accounts for shear angle variation and the last one records flexural effects. Note that W is not convex with respect to φ.

We study W on the following (non-convex) set of admissible deformations $V\subset H^2(\Omega,\mathbb{R}^3)$ defined by:

$$V=\left\{\varphi\in H^2(\Omega,\mathbb{R}^3)\ :\ \|\varphi_{,1}\|=\|\varphi_{,2}\|=1,\ \|\varphi_{,1}\wedge\varphi_{,2}\|\geq C_0 \text{ in } \Omega \text{ and } \varphi=\varphi_0 \text{ on } \Gamma_0\right\}$$

with the topology of $H^2(\Omega,\mathbb{R}^3)$. We look for a $\varphi\in V$ such that $W(\varphi)=\inf_V W$.
In [A10] we prove existence of such a minimizer. We first prove that W is a proper and coercive functional. Then we obtain *a priori* estimates leading to a weak convergence in H^2 of a minimizing sub-sequence. At last we prove some weak lower semicontinuity of W.

Proposition 4 *There exists $\varphi\in V$ such that $W(\varphi)=\inf\limits_V W$.*

The key point in the proof is to use and differentiate the constraints to get estimates on higher derivatives of the minimizing sequence [49, 51]. The shear angle penalization term gives some control on cross derivatives of second order of φ.

4.4 Numerical simulations

We implemented a descent algorithm to minimize the energy and produce a dynamic-like animation. In the case of a very soft textile hanging on the corner of a square table, we obtained animations that are available here:

http://www-ljk.imag.fr/membres/Emmanuel.Maitre/Drape/.

Note that this animations corresponds to a false dynamic, since we don not account for inertia or air effects. With the tools that we now developed with level-set, we could think of a more sound simulation, but note that orthotropy is not so trivial to implement in a simple manner in the Level Set framework. This is an undergoing research which has applications in simulations involving red blood cells, see new section.
For the textile problem, we did not go further since after my leaving from Mulhouse Nadjombé Faré did not get a position. Figure 8 shows resultats obtained in 2002 and contains several cases: a rectangular table with more or less flexible fabrics hanging from it, the case of a circular table and the case of a spherical obstacle. There is no collision test, which explains some strange behavior in the sphere case.

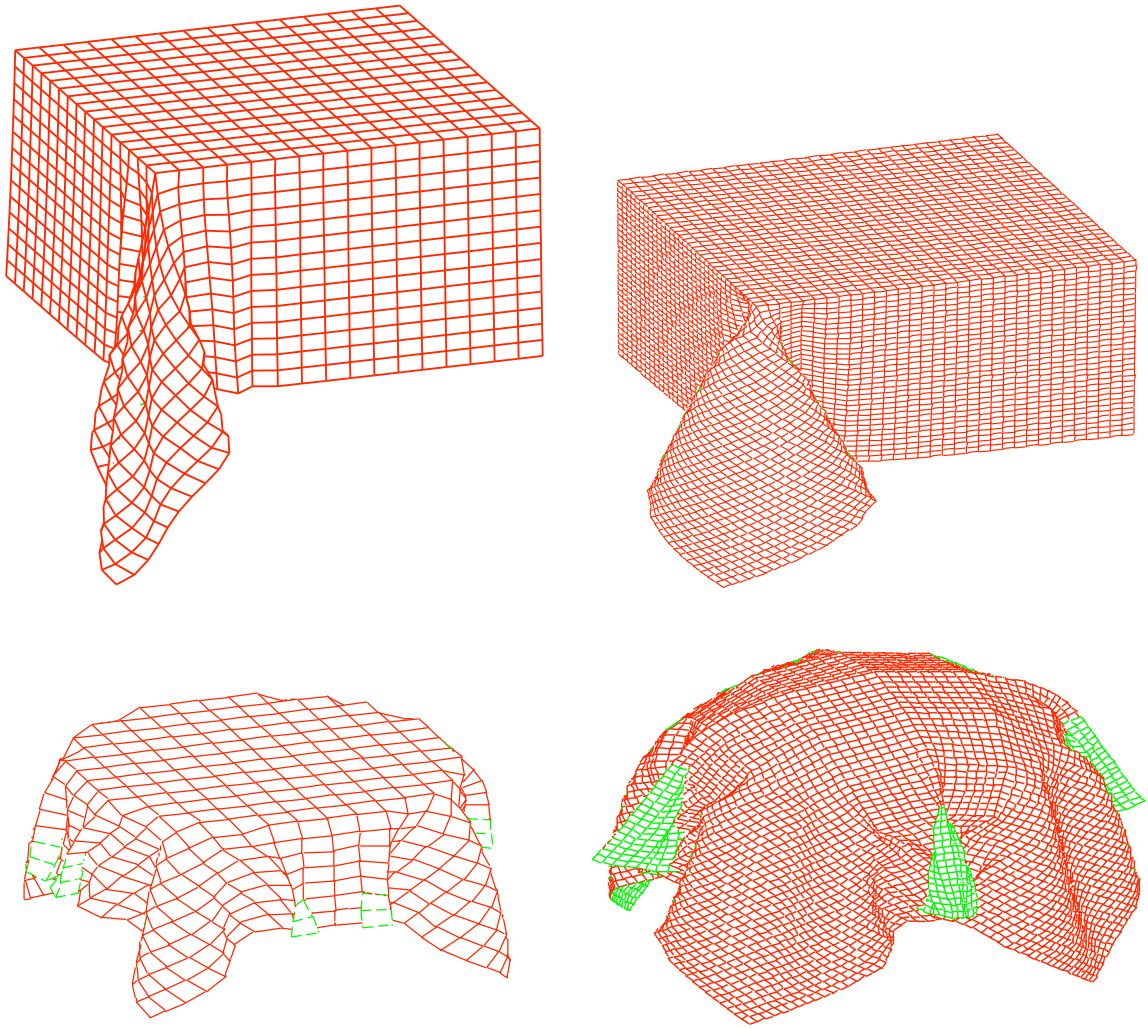

FIGURE 8: Four drape situations: a more or less flexible fabric hanging on the corner of a square table; a fabric hanging on a round table; a fabric falling on a sphere.

5 Level-set method in continuum mechanics [A5, A4, A3, A2, A14]

5.1 Motivations

We were interested in mechanical modeling, and more specifically in fluid-structure problems in a biomedical context.

Our first interest was concerned with the oscillation of a cell membrane, as observed and studied in a partner laboratory of biology. In that case the membrane had a simple elasticity and a changing area. The aimed application was the study of cell motion through a mechanical model consisting of an immersed elastic membrane in a fluid.

Some biological membrane have a degenerate energy. They do not undergo area changes since they are constituted of a bi-layer of molecules the number of which is fixed. This phospholipidic membranes are studied by physicists as model of the red blood cell membrane. The energy driving their equilibrium shape is a curvature energy with a constraint of constant surface area and enclosed volume.

Other biological objects are not membranes. For example biologists in Grenoble study isolated cardiomyocytes (in a Petri box). The auto oscillation they exhibit results from the coupling between a reaction-diffusion equation which drives the calcium dynamics inside the myocyte, its elasticity and the surrounding fluid motion.

Those three examples share the common point of coupling the motion of a fluid and an immersed elastic body. This is an interesting setting in order to develop a multi-physics model of this coupling. The first difficulty that we encounter in this modeling is the difference between natural coordinates for fluid (Eulerian) or structure (Lagrangian). In our work we decided to develop an Eulerian elasticity for the structure. The first case is an Eulerian formulation of the immersed boundary method with Level Set method, where we succeeded in expressing the elasticity of an immersed elastic membrane thanks to a single function. The generic case of an immersed body make use of 3D elasticity written in Eulerian coordinates.

Thanks to this formulation, we are able to turn the fluid-structure coupling problem into a flow problem of some complex visco-elastic fluid of Korteweg type. This permits us to tackle existence problems as well as numerical challenges. In the case of biomechanics, in which coupled entities have comparable densities but are more flexible than in e.g. aerodynamics, this approach seems to be promising.

5.2 Lagrangian elasticity of an immersed interface

We start from a Lagrangian representation of the membrane since it is more usual, and then show that our Eulerian formulation is equivalent. Let a smooth elastic surface $\widetilde{\Gamma}$ in $\mathbb{R}^3$ in a rest configuration, parametrized by a regular $\theta : [0, M]^2 \to \mathbb{R}^3$, $M > 0$ (we thus assume that the surface is not closed so that such a regular map exists). We assume that this surface reacts only to membrane deformation (no flexural effects), and more specifically to area change, and not to membrane shear. This last assumption is verified in the case of phospholipidic membranes, which are made of a fixed amount of molecules which may slip one with respect to the others on the membrane. Flexural effects are present and important in the study of vesicles shape but we will add this effect later. As well, we considered a surface with a boundary which is not coherent with a vesicle, but this is to introduce the Lagrangian

representation. This will be worked around automatically by the Level Set representation. For the sake of simplicity we assume the membrane to react only to tangential stress and more specifically to area change. We will add curvature effects afterwards, since it plays a central role in e.g. vesicle dynamics. The assumption of neglecting membrane shear is physically sound in the case of phospholipidic vesicles since their membrane is constituted of molecules which can slip along each other.

The membrane surface density in that configuration is denoted by $\lambda_\theta(r,s)$. The surface is moving between time $t=0$ et $t=T$, and we call Γ_t, its position at time t. In particular Γ_0 is its initial position, and generally $\Gamma_0 \neq \widetilde{\Gamma}$ unless the elastic surface is initially at rest. We denote by $(r,s) \to \gamma_0(r,s)$ and $(r,s) \to \lambda_0(r,s)$ a regular parametrization and surface density for Γ_0 such that $\lambda_0|\gamma_{0,r} \times \gamma_{0,s}| = \lambda_\theta|\theta_r \times \theta_s|$. Let $\gamma : [0,M]^2 \times [0,T] \to \gamma(r,s,t)$ the regular parametrization of Γ_t transported by the velocity field u of the continuous medium, that is $\gamma(r,s,t) = X(t;\gamma_0(r,s))$ or equivalently:

$$\begin{cases} \gamma_t(r,s,t) = u(\gamma(r,s,t),t), & (r,s) \in [0,M]^2, t \in]0,T] \\ \gamma(r,s,0) = \gamma_0(r,s), & (r,s) \in [0,M]^2. \end{cases} \tag{10}$$

Γ_t is immersed into a Newtonian incompressible and homogeneous fluid with give density ρ_f and visocity μ. This example corresponds to consider a singular density for the whole continuous medium defined by:

$$\rho = \rho_f + \lambda \delta_{\Gamma_t}$$

where δ_{Γ_t} is the measure supported by Γ_t, which is defined by

$$\forall h \in \mathcal{C}_0^0(\Omega), \qquad \langle \delta_{\Gamma_t}, h \rangle = \int_{\Gamma_t} h(x) d\sigma.$$

5.2.1 Some notations

In the following we will make extensive use of the characteristic curves of u. We will denote by $(x,t) \to X(x,t)$ the forward characteristic(resp. $(x,t) \to Y(x,t)$ the backward characteristic) which are solutions of $X_t = u(X,t)$ with $X(0,x) = x$ (resp. $Y_t + u \cdot \nabla Y = 0$ with $Y(0,x) = x$). Under regularity assumptions on the velocity field (for instance $W^{1,\infty}$ in space) $x \to X(x,t)$ and $x \to Y(x,t)$ are two differentiable maps which are inverse one of the other: $X(Y(x,t),t) = x$ and $Y(X(x,t),t) = x$. Therefore their jacobians do not vanish and if we set $J(x,t) = \det \nabla Y(x,t)$, we have $J_t + u \cdot \nabla J = -J \operatorname{div} u$.

5.2.2 Volume conservation: incompressibility

A continuous medium is said incompressible if every open set ω is deformed into $\omega(t) = X(\omega,t)$ of same measure for all time t. Therefore

$$\frac{d}{dt} \int_{\omega(t)} dx = 0$$

thus applying Reynolds formula there holds $\int_{\omega(t)} \operatorname{div} u dx = 0$ for all $\omega(t)$, which give the incompressibility condition

$$\operatorname{div} u = 0$$

From PDE verified by J we see that this condition also reads $J = 1$.

5.2.3 Mass conservation

Consider an open subset $\omega \subset \Omega$. Let Γ_ω^0 the maybe empty part of Γ_0 meeting ω. Let $K \subset [0,M]^2$ such that $\gamma_0(K) = \Gamma_\omega^0$. We set $\omega(t) = X(\omega,t)$ (which is open since X is differentiable with differentiable inverse) and $\Gamma_\omega(t) = X(\Gamma_\omega^0, t)$. By conservation of the mass inside $\omega(t)$ we have

$$\frac{d}{dt}\int_{\omega(t)} \rho = 0$$

which in our case gives

$$\frac{d}{dt}\left\{\rho_f \,\mathrm{mes}(\omega(t)) + \int_K \lambda(r,s,t)|\gamma_r \times \gamma_s| dr ds\right\} = 0.$$

From the incompressibility and as the fluid is homogeneous $\rho_f \,\mathrm{mes}(\omega(t))$ is constant, thus

$$\int_K \frac{\partial}{\partial t}\left(\lambda(r,s,t)|\gamma_r \times \gamma_s|\right) dr ds = 0$$

As the domain is arbitrary, K is also arbitrary, thus

$$\frac{\partial}{\partial t}\left(\lambda(r,s,t)|\gamma_r \times \gamma_s|\right) = 0 \tag{11}$$

This relation once integrated gives $\lambda(r,s,t)|\gamma_r \times \gamma_s| = \lambda(r,s,0)|\gamma_r^0 \times \gamma_s^0| = \lambda_\theta(r,s)|\theta_r \times \theta_s|$. The known quantity that we can measure is this last density.

5.2.4 Conservation of linear momentum for the elastic surface

We assumed the membrane to react only to local area change, and not to membrane shear or flexion. Therefore a natural energy associated should depend on its local area in the deformed configuration compared to the rest configuration. Thefore we introduce the following energy:

$$\mathcal{E}[\gamma] = \int_{[0,M]^2} E\left(\frac{|\gamma_r \times \gamma_s|}{|\theta_r \times \theta_s|}\right) dr ds \tag{12}$$

where $r \to E(r)$ is an elastic constitutive law. The simplest choice is a truncated quadratical law as $E(r) = \lambda \max(r-1,0)^2$. This law has been justified by an asymptotic analysis on a thin elastic body with $3D$ elasticity following a Saint Venant - Kirchhoff law [79]. Now let us compute the time derivative of this energy during motion of the membrane:

$$\frac{d}{dt}E[\gamma] = \int_{[0,M]^2} E'\left(\frac{|\gamma_r \times \gamma_s|}{|\theta_r \times \theta_s|}\right)\frac{|\gamma_r \times \gamma_s|_t}{|\theta_r \times \theta_s|} dr ds.$$

As $\gamma_t = u(\gamma,t)$ and $\operatorname{div} u = 0$ we show in [A5] that

$$(\gamma_r \times \gamma_s)_t = -\nabla u^T(\gamma_r \times \gamma_s)$$

which immediately gives, if we set $N(r,s) = \frac{\gamma_r \times \gamma_s}{|\gamma_r \times \gamma_s|}$,

$$\begin{aligned}|\gamma_r \times \gamma_s|_t = -\frac{(\gamma_r \times \gamma_s)^T \nabla u (\gamma_r \times \gamma_s)}{|\gamma_r \times \gamma_s|} &= -|\gamma_r \times \gamma_s|(N(r,s)\otimes N(r,s)) : \nabla u \\ &= |\gamma_r \times \gamma_s|(\mathbb{I} - N(r,s)\otimes N(r,s)) : \nabla u = |\gamma_r \times \gamma_s| \operatorname{div}_{\Gamma_t} u,\end{aligned}$$

using $\mathbb{I} : \nabla u = \operatorname{div} u = 0$ and the definition of surface density. Thus the sought derivative is given by

$$\frac{d}{dt}E[\gamma] = \int_{[0,M]^2} E'\left(\frac{|\gamma_r \times \gamma_s|}{|\theta_r \times \theta_s|}\right)\frac{|\gamma_r \times \gamma_s|}{|\theta_r \times \theta_s|}(\operatorname{div}_{\Gamma_t} u)(\gamma, t)drds.$$

In this expression the surface measure $d\sigma = |\gamma_r \times \gamma_s|drds$ appears and we can use Murat-Simon integration by part formula on manifolds without boundary:

$$\int_{\Gamma_t} \nabla_{\Gamma_t} f \cdot u d\sigma + f \operatorname{div}_{\Gamma_t} u d\sigma = \int_{\Gamma_t} \kappa f u \cdot n d\sigma,$$

where κ is the manifold mean curvature. We wrote for simplicity the formula for a manifold without boundary while we chose a surface with a boundary to be able to consider a regular parametrization of it. We implicitly assume that boundary terms cancels, which correspond to some boundary condition on the membrane. Recall that our aim is to model closed object, thus we did not take care of these boundary terms, which will be irrelevant once we will skip to the Level Set representation. This formula gives in our case

$$\frac{d}{dt}E[\gamma] = -\int_{\Gamma_t} [\nabla_{\Gamma_t} T(r,s) - T(r,s)\kappa N(r,s)] \cdot u d\sigma$$

where $T(r,s) = E'\left(\frac{|\gamma_r \times \gamma_s|}{|\theta_r \times \theta_s|}\right)\frac{1}{|\theta_r \times \theta_s|}$. From the principle of virtual powers, the power of internal constraints corresponds to the time variation of energy, so that the elastic force per unit of surface is given by:

$$F(r,s,t) = \nabla_{\Gamma_t} T(r,s) - T(r,s)\kappa N(r,s) \tag{13}$$

which includes a tangential and a normal component. The conservation of momentum for the elastic surface is therefore expressed by

$$(|\gamma_r \times \gamma_s|\lambda(r,s,t)\gamma_t(r,s,t))_t = (F(r,s,t) + f_e(r,s,t))|\gamma_r \times \gamma_s|$$

where $\lambda(r,s,t)$ is the surface mass density, and f_e the exterior force density per unit of surface that we will consider to be reduced to gravity, i.e. $\lambda(r,s,t)g$. This also reads, by conservation of the surface mass,

$$\lambda(r,s,t)|\gamma_r \times \gamma_s|\gamma_{tt}(s,t) = (F(r,s,t) + \lambda(r,s,t)g)|\gamma_r \times \gamma_s|. \tag{14}$$

5.2.5 Conservation of linear momentum for the continuous medium

We use the same notations as in 5.2.3. The total linear momentum for volume $\omega(t)$ is given by

$$\int_{\omega(t)} \rho u dx = \int_{\omega(t)} \rho_f u dx + \int_{\Gamma_\omega(t)} \lambda u d\sigma = \int_{\omega(t)} \rho_f u dx + \int_K \lambda|\gamma_r \times \gamma_s|\gamma_t drds$$

For the first integral, which corresponds to the fluid alone, the time derivative of the momentum of some part $\omega(t)$ of continuous medium is equal by principle to the sum of forces applied to $\omega(t)$. Those forces are either volume or surface forces. Volume forces are restricted to gravity $\rho_f g$. Surface forces take by the Cauchy theorem (see Duvaut [52] or Ciarlet [47])

the particular form $\boldsymbol{\sigma} n$ where $\boldsymbol{\sigma}$ is the Cauchy stress tensor and n the exterior normal to $\partial\omega(t)$. Furthermore we just computed the time derivative of the second integral. Therefore

$$\frac{d}{dt}\int_{\omega(t)} \rho u dx = \int_{\omega(t)} \rho_f g dx + \int_{\partial\omega(t)} \boldsymbol{\sigma} n d\sigma + \int_K (F(r,s,t) + \lambda(r,s,t)g)|\gamma_r \times \gamma_s| dr ds$$

which using Reynolds formula and divergence theorem gives

$$\int_{\omega(t)} \rho(u_t + u\cdot\nabla u)dx = \int_{\omega(t)} \rho_f g dx + \int_{\Gamma_\omega(t)} \lambda(r,s,t) g d\sigma + \int_{\omega(t)} \operatorname{div}\boldsymbol{\sigma} dx + \int_{\Gamma_\omega(t)} F(r,s,t) d\sigma.$$

For the fluid domain $\boldsymbol{\sigma}$ is a function of the deformation tensor given by

$$D(u) = \frac{1}{2}(\nabla u + \nabla u^t).$$

In particular if we consider a Newtonian fluid this function is affine. For an incompressible flow we get

$$\boldsymbol{\sigma} = -p\mathbb{I}_d + 2\mu D(u)$$

where p is the pressure and μ the fluid viscosity.

Immersed boundary model Formally, we obtain a non-homogeneous Navier-Stokes equation with a singular forcing term and a density with a singular part. We write it under the following short way:

$$\begin{cases} (\rho_f + \lambda\delta_{\Gamma_t})(u_t + u\cdot\nabla u) - 2\operatorname{div}\mu D(u) + \nabla p & \\ \qquad = \{\nabla_{\Gamma_t} T(r,s) - T(r,s)\kappa N(r,s)\}\,\delta_{\Gamma_t} + (\rho_f + \lambda\delta_{\Gamma_t})g & \text{sur } \Omega\times]0,T[\\ \operatorname{div} u = 0 & \text{on } \Omega\times]0,T[\\ \gamma_t = u(\gamma,t) & \text{on } [0,M]\times]0,T[\end{cases}$$

where we recalled (10) which dictates the curve motion.

This formulation is exactly the immersed boundary method from Peskin [95, 96] although it is written in a different form, and for an elastic surface rather than a volume collection of fibers. Indeed using Peskin's notations the immersed boundary condition amounts to mix Eulerian and Lagrangian quantities. Fluid unknowns are Eulerian while Lagrangian markers are used for the surface. The interaction of these two representations is done thanks to a discrete Dirac measure. With the not so mathematical notations of [96], adapted to the surface case (terms in $|\theta_r \times \theta_s|$), this reads:

Immersed boundary method: *Eulerian description* of velocity field and *Lagrangian description* of immersed structure (made of a family of elastic fibers), interpolated in the Eulerian domain.

- A velocity field $(x,t) \in \Omega \times [0,T] \to u(x,t)$.
- $(r,s,t) \in U \times [0,T] \to \gamma(r,s,t)$ position of points on the elastic surface Γ_t.
- Force density with respect to the surface measure (r,s) in the reference configuration is a known function $F_\theta(r,s,t)$.
- The surface density in the reference configuration is a known function $\lambda_\theta(r,s,t)$.
- Equations of motion (stress coupling):

$$(\rho_f + \Lambda)(u_t + u \cdot \nabla u) - \nu \Delta u + \nabla p = f \tag{15}$$
$$\operatorname{div} u = 0 \tag{16}$$
$$f(x,t) = \int_U |\theta_r \times \theta_s| F_\theta(r,s,t) \delta(x - \gamma(r,s,t)) dr ds \tag{17}$$
$$\Lambda(x,t) = \int_U |\theta_r \times \theta_s| \lambda_\theta(r,s,t) \delta(x - \gamma(r,s,t)) dr ds \tag{18}$$
$$\gamma_t = u(\gamma(r,s,t),t) = \int_\Omega u(x,t) \delta(x - \gamma(r,s,t)) dx \tag{19}$$
$$F_\theta(r,s,t) = \mathcal{F}_\theta[\gamma(r,s,t)] \tag{20}$$

Equation (17) converts the Lagragian force into the Eulerian domain; equation (19) converts the velocity field into a velocity on the Lagrangian markers. If we write the precise definition of (17) thanks to a test function $\psi : \Omega \to \mathbb{R}$, we get integrating on Ω

$$\begin{aligned}\int_\Omega f(x,t)\psi(x,t)dx &= \int_U |\theta_r \times \theta_s| F_\theta(r,s,t) \int_\Omega \delta(x - \gamma(r,s,t))\psi(x,t) dx dr ds \\ &= \int_U |\theta_r \times \theta_s| F_\theta(r,s,t)\psi(\gamma(r,s,t),t) dr ds = \int_{\Gamma_t} F_\theta(r,s,t) \frac{|\theta_r \times \theta_s|}{|\gamma_{,r} \times \gamma_{,s}|} \psi(x,t) d\sigma\end{aligned}$$

therefore formally

$$f(x,t) = \frac{|\theta_r \times \theta_s|}{|\gamma_r \times \gamma_s|} F_\theta(r,s,t) \delta_{\Gamma_t} = F(r,s,t)\delta_{\Gamma_t}$$

if F represents a surface density in the deformed configuration. Similarly, from (18), Λ is a measure given by

$$\Lambda(x,t) = \frac{|\theta_r \times \theta_s|}{|\gamma_r \times \gamma_s|} \lambda_\theta(r,s,t)\delta_{\Gamma_t} = \lambda(r,s,t)\delta_{\Gamma_t}, \qquad \text{with } x = \gamma(r,s,t).$$

We exactly recover the former expression for F, up to the choice of constitutive law.

The immersed boundary method we just described is simple and attrative. However, at each time iteration one has to convert back and forth the coordinates, which introduces serious volume conservation issues. Indeed the interpolated velocity field is not divergence free thus the curve described does not enclose a volume of constant measure. This volume

loss is acknowledged and in a good extent cured in [97, 78, 77], but the method looses its inherent simplicity. The foremost aim of our Eulerian formulation, introduced in [A5, A4] was to maintain the method simplicity while introducing an Eulerian localization of the interface which suppress these interpolation problems. The original immersed boundary method can be implemented so that it is order 2 in the case of thick interfaces, but order 1 for thin structures [58]. Stability studies have been developed in [33, 34, 107].

Let us point out that our Eulerian formulation will by structure make natural the handling of closed membrane, which was more delicate in Lagrangian coordinates. Moreover, the variable viscosity or density case, which is not considered in the IBM is very simply handled in our formulation. This is important as our cell models often exhibits a viscosity contrast between the inner and outer fluids to take into account the biological material inside it.

5.3 Eulerian Elasticity of an immersed membrane

5.3.1 Level Set formulation

We now skip to a new representation of the interface to avoid caveats encountered with the Lagrangian formulation. We consider Γ_t, that we now assume closed[2] as the zero level set of a function $\phi : \Omega \times [0,T] \to \mathbb{R}$ so that

$$\Gamma_t = \{x \in \Omega, \quad \phi(x,t) = 0\}.$$

As $\phi(\gamma(r,s,t),t) = 0$ on $[0,M]^2 \times [0,T]$, and $\gamma_t = u(\gamma,t)$, we get by time differentiation

$$\phi_t(\gamma(r,s,t),t) + u(\gamma(r,s,t),t) \cdot \nabla\phi(\gamma(r,s,t),t) = 0.$$

The Level Set method [93] takes as initial condition a function ϕ_0 whose zero level set is Γ_0 and amounts to find a function ϕ which is solution to the above transport equation on the whole computational domain:

$$\begin{cases} \phi_t + u \cdot \nabla\phi = 0 & \text{on } \Omega \times]0,T[\\ \phi = \phi_0 & \text{on } \Omega \times \{0\}. \end{cases} \tag{21}$$

A common choice for ϕ_0 is the signed distance to the interface:

$$\phi_0(x) = \begin{cases} -\operatorname{dist}(x,\Gamma_0) & \text{if } x \text{ is inside } \Gamma_0, \\ \operatorname{dist}(x,\Gamma_0) & \text{if } x \text{ is outside } \Gamma_0. \end{cases}$$

With this choice of ϕ_0 the exterior normal to the domain enclosed by Γ_t, and the surface mean curvature are expressed in terms of ϕ as follows:

$$n(x) = \frac{\nabla\phi}{|\nabla\phi|} \qquad \kappa(x) = \operatorname{div} \frac{\nabla\phi}{|\nabla\phi|}$$

[2] We could get rid of this assumption by introducing a supplementary function, but once again the physical objects we intend to model are closed.

5.3.2 Deformations and Level Set

What is more original and proved in [A5] is that in the case of an incompressible flow, the surface stretching is recorded in the function ϕ, which allows us to rephrase our fluid-structure problem with this function. There is several ways to prove this intuitive fact, which generalizes well to compressible case with the adjunction of J (this aspect has been recently developed in [40, 41] in the framework of tumor growth simulation and also in [26]). We could also start from the stretching written in Lagrangian and prove that $|\nabla\phi|$ verifies the same equation, as in [A5] that is to say

$$|\nabla\phi|_t + u\nabla|\nabla\phi| = -|\nabla\phi|\frac{\nabla\phi^T\nabla u\nabla\phi}{|\nabla\phi|^2} = -|\nabla\phi|\frac{\nabla\phi}{|\nabla\phi|}\otimes\frac{\nabla\phi}{|\nabla\phi|} : \nabla u \tag{22}$$

However I will present the following more intrinsic demonstration which relies on the two following propositions.

Lemma 1 *Let $\phi : \mathbb{R}^d \to \mathbb{R}$ Lipschitz on $\mathbb{R}^d$ and $g : \mathbb{R}^d \to \mathbb{R}$ integrable. We assume the exists $\eta_0 > 0$ such that $\operatorname{ess\,inf}_{|\phi|<\eta_0} |\nabla\phi| > 0$. Then for $\eta \in]0, \eta_0[$, there holds*

$$\int_{|\phi(x)|<\eta} g(x)dx = \int_{-\eta}^{\eta}\int_{\phi(x)=\nu} g(x)|\nabla\phi|^{-1}d\sigma d\nu.$$

Proof. In [54], proposition 3 page 118, it is shown under the same assumptions that

$$\frac{d}{ds}\left(\int_{\phi>s} g(x)dx\right) = -\int_{\phi=s} g|\nabla\phi|^{-1}d\sigma \qquad \text{a.e. } s$$

The above result is a straightforward consequence of that identity by setting $s = -t$, choosing ϕ and $-\phi$ and adding the obtained relations. Then we integrate from $-\eta$ to η.

A more intuitive proof is to write, in a neighborhood of x the volume dx as $dx = d\sigma \times dh$, where dh is along the normal $\frac{\nabla\phi}{|\nabla\phi|}$ and to remark that

$$\nu \pm d\nu := \phi(x \pm dh\frac{\nabla\phi}{|\nabla\phi|}) = \phi(x) \pm dh|\nabla\phi| + O(dh^2)$$

from which we get $dx = |\nabla\phi|^{-1}d\sigma d\nu$. □

Under the following assumption on the level sets of ϕ,

(H_ϕ) $\quad \forall t \in [0,T], \forall f \in \mathcal{C}_c(\mathbb{R}^n), \quad s \to \displaystyle\int_{\{|\phi(x,t)|<s\}} f(x)dx$ is of class $\mathcal{C}^1$ in a neighborhood of $s = 0$

we have the following:

Proposition 5 *Let $u : \mathbb{R}^d \times [0,T] \to \mathbb{R}^d$ of class $\mathcal{C}^1$ with $\operatorname{div} u = 0$ and ϕ solution of class $\mathcal{C}^1$ of $\phi_t + u\cdot\nabla\phi = 0$, $\phi = \phi_0$ with $|\nabla\phi| \geq \alpha > 0$ in a neighborhood of $\{\phi = 0\}$ and verifying (H_ϕ). Then for every function f continuous and with compact support,*

$$\int_{\{\phi_0(\xi)=0\}} f(\xi)|\nabla\phi_0|^{-1}(\xi)d\sigma(\xi) = \int_{\{\phi(x,t)=0\}} f(Y(x,t))|\nabla\phi|^{-1}(x,t)d\sigma(x) \tag{23}$$

which means that $|\nabla\phi|/|\nabla\phi_0|$ represents the variation of surface measure between Γ_t and Γ_0.

Proof. From assumption (H_ϕ) follows using the above Lemma that

$$s \to \int_{\{\phi_0=s\}} f(\xi)|\nabla\phi_0|^{-1}(\xi)d\sigma(\xi)$$

is continuous. Therefore using Lemma 1,

$$\int_{\{\phi_0(\xi)=0\}} f(\xi)|\nabla\phi_0|^{-1}(\xi)d\sigma(\xi) = \lim_{\eta\to 0}\frac{1}{\eta}\int_{-\frac{\eta}{2}}^{\frac{\eta}{2}}\int_{\phi_0=\nu} f(\xi)|\nabla\phi_0|^{-1}(\xi)d\sigma(\xi)d\nu = \lim_{\eta\to 0}\frac{1}{\eta}\int_{|\phi^0|<\frac{\eta}{2}} f(\xi)d\xi.$$

With the change of variables $\xi = Y(x,t)$ whose jacobian $J(x,t)$ is 1 since $\operatorname{div} u = 0$. As ϕ is solution to a transport equation we have $\phi^0(Y(x,t)) = \phi(x,t)$ and thus

$$\int_{\{\phi_0(\xi)=0\}} f(\xi)d\sigma(\xi) = \lim_{\eta\to 0}\frac{1}{\eta}\int_{|\phi(x,t)|<\frac{\eta}{2}} f(Y(x,t))dx$$

which gives the announced result thanks to 1. □

Remark 5 *Another proof is possible using the Reynold formula for surfaces. We give it here in the more general compressible case to show what differs. For a $\mathcal{C}^1$ function g, we have*

$$\frac{d}{dt}\int_{\{\phi(x,t)=0\}} g(x,t)d\sigma = \int_{\{\phi(x,t)=0\}} g_t + \operatorname{div}(gu) - g[\nabla u]n\cdot n d\sigma$$

and on $\{\phi = 0\}$ we have using (22)

$$[\nabla u]n\cdot n = [\nabla u]\frac{\nabla\phi}{|\nabla\phi|}\cdot\frac{\nabla\phi}{|\nabla\phi|} = -\frac{1}{|\nabla\phi|}\left(|\nabla\phi|_t + u\cdot\nabla|\nabla\phi|\right)$$

Gathering terms leads to

$$\frac{d}{dt}\int_{\{\phi(x,t)=0\}} g(x,t)d\sigma = \int_{\{\phi(x,t)=0\}} \left((g|\nabla\phi|)_t + u\cdot\nabla(g|\nabla\phi|)\right)\frac{1}{|\nabla\phi|} + g\operatorname{div} u d\sigma$$

Moreover as $J_t^{-1} + u\cdot\nabla J^{-1} = J^{-1}\operatorname{div} u$, we can eliminate $\operatorname{div} u$ which gives

$$\frac{d}{dt}\int_{\{\phi(x,t)=0\}} g(x,t)d\sigma = \int_{\{\phi(x,t)=0\}} \left((gJ^{-1}|\nabla\phi|)_t + u\cdot\nabla(gJ^{-1}|\nabla\phi|)\right)\frac{J}{|\nabla\phi|}d\sigma$$

We now apply this formula with $g(x,t) = f(Y(x,t))J(x,t)|\nabla\phi|^{-1}(x,t)$, by computing

$$(gJ^{-1}|\nabla\phi|)_t + u\cdot\nabla(gJ^{-1}|\nabla\phi|) = f(Y)_t + u\cdot\nabla[f(Y)] = 0$$

since $f(Y)$ is just the transported function f. Finally we obtain

$$\frac{d}{dt}\int_{\{\phi(x,t)=0\}} f(Y(x,t))J(x,t)|\nabla\phi|^{-1}(x,t)d\sigma = 0$$

which after integration from 0 to t gives (23), if $J = 1$. In the compressible case we recover results from [41, 26] where the stretching is expressed as $J^{-1}|\nabla\phi|$.

Remark 6 *From a theoretical point of view the formula (23) just says that the measure* $|\nabla\phi_0|^{-1}(x)\delta_{\{\phi_0=0\}}$ *is the image of* $|\nabla\phi|^{-1}(x,t)\delta_{\{\phi=0\}}$ *by the map* $x \to Y(x,t)$.

Corollary 1 *In dimension* 2, *we consider a parametrization* $s \in [0,M] \to \gamma(s,0) \in \mathbb{R}^2$ *of* $\Gamma(0)$ *which is transported into a parametrization* $s \to \gamma(s,t)$ *of* $\Gamma(t)$. *Expressing the surface measure in terms of the parametrization we get since* $Y(\gamma(s,t),t) = \gamma(s,0)$:

$$\int_0^M f(\gamma(s,0))|\nabla\phi_0|^{-1}(\gamma(s,0))|\gamma_s|(s,0)ds = \int_0^M f(\gamma(s,0))|\nabla\phi|^{-1}(\gamma(s,t),t)|\gamma_s|(s,t)ds$$

for all continuous f *with compact support. Thus*

$$\frac{|\nabla\phi|(\gamma(s,t),t)}{|\nabla\phi_0|(\gamma(s,0))} = \frac{|\gamma_s(s,t)|}{|\gamma_s(s,0)|}.$$

In dimension 3, *if* $(r,s) \in \omega \to \gamma(r,s,t) \in \mathbb{R}^3$ *is a (patch of) parametrization of* $\Gamma(t)$, *we still have* $Y(\gamma(r,s,t),t) = \gamma(r,s,0)$ *which gives*

$$\int_\omega f(\gamma(r,s,0))|\nabla\phi_0|^{-1}(\gamma(r,s,0))|\gamma_r \times \gamma_s|(r,s,0)drds$$
$$= \int_\omega f(\gamma(r,s,0))|\nabla\phi|^{-1}(\gamma(r,s,t),t)|\gamma_r \times \gamma_s|(r,s,t)drds$$

therefore

$$\frac{|\nabla\phi|(\gamma(r,s,t),t)}{|\nabla\phi_0|(\gamma(r,s,0))} = \frac{|\gamma_r \times \gamma_s|(r,s,t)}{|\gamma_r \times \gamma_s|(r,s,0)}.$$

More precisely we construct ϕ_0 such that its zero level set is Γ_0, and such that

$$|\nabla\phi_0|(\gamma(r,s,0)) = \frac{|\gamma_r \times \gamma_s|(r,s,0)}{|\theta_r \times \theta_s|(r,s)}$$

which corresponds to the area change between the initial and rest configuration. Then we have

$$|\nabla\phi|(\gamma(r,s,t),t) = \frac{|\gamma_r \times \gamma_s|(r,s,t)}{|\theta_r \times \theta_s|(r,s)}.$$

If the initial stretching does not depend on (r,s) (uniform stretching) this amounts to initialize ϕ_0 to this stretching times the signed distance to the surface.

5.3.3 Energy and elastic force expressed in Level Set

We are now in a position to express the elastic energy of an elastic membrane in terms of the Level Set function. But we must first cope with the surface integral, which leads us to consider as analog of (12) the following energy (here for a surface with stretching 1 at rest)

$$\mathcal{E}[\phi] = \int_{\{\phi=0\}} E(|\nabla\phi|)\frac{1}{|\nabla\phi|}d\sigma.$$

Then we could differentiate this energy with respect to t in order to identify the singular elastic force (Thomas Milcent in his thesis [87] inspected this direction). We could then

develop a finite element method to give a weak meaning to measure, which is made in [33, 34] in the framework of immersed boundary method. However we chose, as in the usual Level Set method, to approximate the surface measure by a non singular function. Then we can use a finite difference method on a cartesian grid with fast FFT solver for Poisson equation. In this aim we have the following Lemma (proved in [A4] and originally in [45]) which gives a volume approximation of a Dirac Measure supported by an hypersurface localized by a level set:

Proposition 6 *Let $r \to \zeta(r)$ be a continuous function with support in $[-1, 1]$, such that $r \to \frac{1}{\varepsilon}\zeta(\frac{r}{\varepsilon})$ converges toward δ_0 in the sense of distributions. Then under assumption (H_ϕ), when $\varepsilon \to 0$,*

$$\frac{1}{\varepsilon}\zeta\left(\frac{\phi}{\varepsilon}\right)|\nabla\phi| \rightharpoonup \delta_{\{\phi=0\}} \quad \text{in } \mathcal{M}(\mathbb{R}^d).$$

Therefore we see that a sound numerical approximation of $\delta_{\{\phi=0\}}$ is given by $|\nabla\phi|\frac{1}{\varepsilon}\zeta\left(\frac{\phi}{\varepsilon}\right)$, which allows to define a regularized energy by

$$\mathcal{E}_\varepsilon(\phi) = \int_\Omega E(|\nabla\phi|)\frac{1}{\varepsilon}\zeta(\frac{\phi}{\varepsilon})dx. \tag{24}$$

Remark 7 *This approximation is not so innocent it could first appear. Indeed we replaced a purely geometrical object, namely $\delta_{\{\phi=0\}}$, independent of ϕ representing the same geometrical surface (and therefore scale independent), by an object which does depend of ϕ. This is the origin of numerical issues in the Level Set method that we discuss later, and probably of stability problems in some situations (Claire Bost adressed this issue in her Thesis [36]).*

Differentiating this energy we get (up to a gradient term, see [A3] the details)

$$F_\varepsilon(x,t) = \operatorname{div}\left(E'(|\nabla\phi|)|\nabla\phi|(\mathbb{I} - \frac{\nabla\phi\otimes\nabla\phi}{|\nabla\phi|^2})\frac{1}{\varepsilon}\zeta(\frac{\phi}{\varepsilon})\right). \tag{25}$$

Expanding the divergence operator leads after some algebra

$$F_\varepsilon(x,t) = \left\{\mathbb{P}_{\nabla\phi^\perp}\left(\nabla[E'(|\nabla\phi|)]\right) - E'(|\nabla\phi|)\kappa(\phi)\frac{\nabla\phi}{|\nabla\phi|}\right\}|\nabla\phi|\frac{1}{\varepsilon}\zeta(\frac{\phi}{\varepsilon})$$

which is in agreement with (13) obtained in Lagrangian coordinates. Gradients terms are irrelevant in the incompressible case, since pressure forces do not work under an isochoric displacement vanishing on the boundary.

Remark 8 *Thomas Milcent proved in his thesis [87] the consistency of this approximation (in the case of a far more general energy) in comparison with computation of this force directly by differentiation of a sharp energy. In other words, the force obtained by differentiation of the regularized energy converges when ε to 0 toward the force that we obtain by differentiation of the singular energy.*

5.3.4 Multiphysics model

Let $H(r) = \int_{-\infty}^{r} \zeta(s)ds$. We have $H(r) = 0$ for $r < -1$, and $H(r) = 1$ for $r > 1$. We finally set

$$\rho(\phi) = \rho_1 + H(\frac{\phi}{\varepsilon})(\rho_2 - \rho_1) + \lambda_\theta \frac{1}{\varepsilon}\zeta\left(\frac{\phi}{\varepsilon}\right)$$

assuming for now on that λ_θ is constant, and

$$\mu(\phi) = \mu_1 + H(\frac{\phi}{\varepsilon})(\mu_2 - \mu_1)$$

Then we obtain the following model (wrote here in the case where $f = 0$): Find (u, ϕ) solution on $\Omega \times]0, T[$ of

$$\begin{cases} \rho(\phi)(u_t + u \cdot \nabla u) - \operatorname{div}\left(\mu(\phi)D(u) - E'(|\nabla\phi|)|\nabla\phi|\frac{\nabla\phi\otimes\nabla\phi}{|\nabla\phi|^2}\frac{1}{\varepsilon}\zeta(\frac{\phi}{\varepsilon})\right) + \nabla\pi = 0 \\ \operatorname{div} u = 0 \\ \phi_t + u \cdot \nabla\phi = 0 \end{cases}$$

Note that $\rho(\phi)$ also verifies the transport equation and thus the conservation law associated since $\operatorname{div} u = 0$. In that respect we proposed a complex fluid model for our fluid-structure problem in which the stress tensor is modified on a neighborhood of the membrane. This model is a generalization of the Korteweg fluid model [110] and this is precisely from this remark that we will attack the existence of solution to our model. The starting point is the following energy equality which states that the spreading of elastic force does not introduce an artificial dissipation. This is a simple consequence of how we defined our elastic energy.

Proposition 7 *If ϕ is such that $|\phi| > \varepsilon$ on $\partial\Omega$, we have*

$$\frac{1}{2}\int_\Omega \rho_\varepsilon(\phi(x,T))u^2(x,T)dx + \int_0^T \int_\Omega \mu(\phi)D(u)^2 dxdt + \int_\Omega E(|\nabla\phi|)\frac{1}{\varepsilon}\zeta(\frac{\phi}{\varepsilon})dx = \frac{1}{2}\int_\Omega \rho_\varepsilon(\phi_0(x))u_0^2(x)dx + \int_\Omega E(|\nabla\phi_0|)\frac{1}{\varepsilon}\zeta(\frac{\phi_0}{\varepsilon})dx \quad (26)$$

5.3.5 Existence of a solution to the multiphysics problem

For a sake of simplicity we fix $\epsilon = 1$, $\rho_1 = \rho_2$, $\mu_1 = \mu_2$ and we consider the following model

$$\rho(\phi)\left(u_t + (u \cdot \nabla)u\right) - \mu\Delta u + \nabla\pi = -\operatorname{div}\left(\Sigma(\phi, \nabla\phi)\right) \quad (27)$$

$$\phi_t + u \cdot \nabla\phi = 0 \quad (28)$$

$$\operatorname{div}(u) = 0, \quad (29)$$

where

$$\rho(\phi) = \overline{\rho} + \lambda\zeta(\phi) \quad (30)$$

and $\overline{\rho}, \lambda$ are two strictly positive coefficients (the fluid background and membrane surface densities). Σ derives from the energy E of the membrane through the following formula

$$\Sigma(\phi, \nabla\phi) = \frac{E'(|\nabla\phi|)}{|\nabla\phi|}\zeta(\phi)\nabla\phi \otimes \nabla\phi \quad (31)$$

which corresponds to (25) where the gradient term has been absorbed by the pressure π. This system is supplemented by initial conditions for u and ϕ

$$u(x,0) = u_0(x)\ ,\ \phi(x,0) = \phi_0(x) \tag{32}$$

and boundary conditions for u. We will focus on no-slip boundary conditions (our result easily extends to periodic boundary conditions): $u = 0$ on $\partial\Omega$. ζ denotes a C^∞ positive cut-off function. Throughout this section we will assume that

$$r \to E'(r) \in \mathcal{C}^1([0,+\infty)). \tag{33}$$

Note that the case of a linear response is given by $E'(r) = \lambda(r-1)$ (however the material is still geometrically nonlinear).

Note also our formulation allows to recover Korteweg fluids [110] as a particular case, when $E'(r) = r$, the Level Set function ϕ playing the role of density. Indeed if we choose $E'(r) = r$ and if we introduce a function $Z(.)$ such that its derivative is $\sqrt{\zeta(.)}$, setting $\psi = Z(\phi)$ gives

$$\zeta(\phi)\nabla\phi \otimes \nabla\phi = \nabla\psi \otimes \nabla\psi.$$

Clearly, ψ is, like ϕ solution of the transport equation. Moreover, since $\mathrm{div}(\nabla\psi \otimes \nabla\psi) = \Delta\psi\nabla\psi + D^2\psi\nabla\psi = \Delta\psi\nabla\psi + \frac{1}{2}\nabla|\nabla\psi|^2$, we obtain for the right hand side of the Navier-Stokes equations, up to a gradient term that can be absorbed in the pressure term, the usual Korteweg source term.

In [A3] we prove the following result.

Theorem 1 *Let $p > 3$. Assume Ω is a smooth connected bounded domain in $\mathbb{R}^3$, $\phi_0 \in W^{2,p}(\Omega)$, such that $|\nabla\phi_0| \geq \alpha > 0$ in a neighborhood of $\{\phi_0 = 0\}$, and $u_0 \in W_0^{1,p}(\Omega) \bigcap W^{2,p}(\Omega)$, with $\mathrm{div}\, u_0 = 0$. Then there exists $T^* > 0$ only depending on the initial data such that a solution of (27), (28), (29) exists in $[0,T^*]$ with*

$$\phi \in L^\infty(0,T^*;W^{2,p}(\Omega)),\ u \in L^\infty(0,T^*;W_0^{1,p}(\Omega)) \cap L^p(0,T^*;W^{2,p}(\Omega)),\ \nabla\pi \in L^p(0,T^*;L^p(\Omega)).$$

Our proof is based on a compactness argument. We classically start by considering a sequence of mollified problems for which smooth solutions are available. We consider a time-retarded mollification of the velocity (see [43], p. 823) and a spatial regularization of the Level Set function. We then obtain estimates using results of Solonnikov [106] on Stokes problem in L^p. The use of Sobolev spaces for $p > 3$, instead of Hilbert spaces, provides more regularity thanks to Sobolev injection theorems (in particular $W^{1,p} \subset L^\infty$ for the velocity) without climbing in the order of derivatives. This avoids clumbersome differentiation of the pde.

5.3.6 Numerical components

Reinitialization or renormalization of ϕ ? It is commonly acknowledged that the function ϕ, through the calculation process should remain close to a (signed) distance function, that is with a gradient norm equal to one. The invoked reason is that the spreading formula induces a support width which depends on $|\nabla\phi|$ in contrast with the sharp interface measure $\delta_{\{\phi=0\}}$. Thus maintaining a constant $|\nabla\phi| = 1$ ensures a constant width smeared interface.

However, starting from a distance function ϕ_0, the solution of the advection equation for ϕ does not in general give a distance function $\phi(t,\cdot)$ for $t>0$. Three solutions may circumvent this behavior:

- *Reinitialization by an Hamilton-Jacobi equation.* This is the classical method [108, 109] which is achieved by solving the following partial differential equation

$$d_\tau = \text{sign}(\phi)(1-|\nabla d|)$$

with initial condition $d(x,0)=\phi(x,t)$ a time t, and where sign takes values in $\{-1,0,1\}$ depending on the sign of ϕ. We will see that this equation is an hyperbolic one, a fact which appears even more clearly if we write it as

$$d_\tau + w\cdot\nabla d = \text{sign}(\phi)$$

and its characteristic are starting from $\{\phi=0\}$. Thus solving this equation results in a reconstruction of ϕ starting from the interface. As we are interested by a unity gradient only on a neighborhood of the interface, this reinitialization PDE is solved for small τ only (about 1.5ε for instance).

Solving exactly this HJ equation certainly provides a distance function whose zero level set coincide with those of ϕ, but numerically this is not true, a fact which leads to a correcting constraint to add to the HJ equation to ensure volume conservation [108]. This is partly due to the fact that w is not a divergence-free velocity field, except in the case of a flat interface, thus advection with this field does not provide automatic volume conservation.

A new and radical method proposed by Smolianski [105] to correct this volume leaking is to lower or raise the distance function to ensure volume conservation. The shift quantity needed may be computed from the exact volume (usually known when the fluids are incompressible) and the length of interface. Let V_0 be the volume of $\{\phi_0>0\}$, which should be conserved during the incompressible flow. At time $t>0$, due to numerical errors, $V:=\text{meas}\{\phi>0\}$ differs a little from V_0. We look for a level set $\{\phi>C\}$ such that $\text{meas}\{\phi>C\}=V_0$. Using [54], p. 118,

$$\frac{d}{ds}\left(\int_{\{\phi>s\}} g(x)dx\right) = -\int_{\{\phi=s\}} g|\nabla\phi|^{-1}d\sigma \qquad \text{p.p. } s$$

which for $g=1$ and a distance function (recall that HJ equation has been solved) reads

$$\frac{d}{ds}\,\text{meas}\{\phi>s\} = -L(\{\phi=s\})$$

where L denotes the length of a curve. Thus integrating between 0 and C give

$$V_0 - V = -\int_0^C L(\{\phi=s\})ds$$

Thus at first order in C one has $V_0-V\approx -CL(\{\phi=0\})$. We thus conclude that an approximative value for C is

$$C\approx\frac{V-V_0}{L(\{\phi=0\})}$$

and we correct ϕ by $\phi-C$ to get our volume conserved.

- *Modifying the advection equation outside of the interface.* Gomes and Faugeras (as observed by H.-K. Zhao *et al* (JCP, 1996) from a remark by Evans and Spruck) partially proved that if one replaces the advection equation by the non-local PDE

$$\phi_t(x,t) + (u \cdot \nabla\phi)(x - \phi\nabla\phi, t) = 0$$

then $\{\phi = 0\}$ is still advected with velocity u, and ϕ remains a distance function for all times. While this algorithm seems to be applicable in the context of image processing, the non-locality of the equation is a serious obstacle to its practical use in fluid flows.

- *Renormalize ϕ by its gradient.* As observed by G.-H. Cottet, though ϕ is not a distance function, one could get a reasonable approximation of the distance to the interface using $\frac{\phi}{|\nabla\phi|}$, at least close enough from this interface. Numerical tests in [A4] indicate that this is a realistic counterpart to reinitialization, for length calculation (a prototype of singular force calculation, see figure 9). Moreover, this avoids reinitialization and subsequent

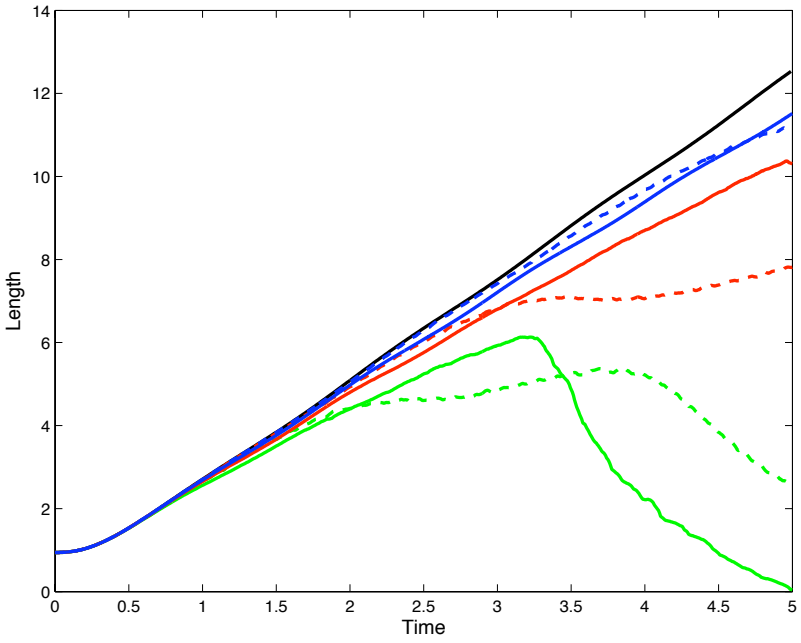

FIGURE 9: Comparison between reinitialization (dashed lines) and renormalization (continuous lines) for $N = 64, 128, 256$, in a test where an interface is stretched by a rotating velocity field. Top curve is a high resolution front tracking solution.

volume loss, which leads to excellent volume conservation properties. One striking example of this good behavior has been recently obtained on an accuracy test in [104]. In this paper the author introduces two discrete delta functions which are supposed to be used efficiently for interface length calculation. We used the renormalization trick to achieve results which show order two convergence, except for really rough grids. Although less accurate than the second order delta function proposed by the author,

this simple method seems thus a good counterpart (this kind of approximation was also studied in [53]).

Mesh Size	Smereka 1		Renormalization		Smereka 2	
	Rel. Error	Order	Rel. Error	Order	Rel. Error	Order
0.2	9.38×10^{-3}		1.5×10^{-1}		2.68×10^{-3}	
0.1	2.23×10^{-3}	2.07	5×10^{-3}		5.49×10^{-4}	2.29
0.05	8.12×10^{-4}	1.46	1.3×10^{-3}	1.9	1.32×10^{-4}	2.05
0.025	2.71×10^{-4}	1.58	3×10^{-4}	2.1	2.90×10^{-5}	2.18
0.0125	7.58×10^{-5}	1.83	8×10^{-5}	1.9	7.79×10^{-6}	1.90
0.00625	3.04×10^{-5}	1.32	2×10^{-5}	2	1.84×10^{-6}	2.08

Numerical method used Il all the simulations proposed we used mostly the same ingredients. The Navier-Stokes equations were discretized by a finite difference method on a MAC mesh where the velocity and pressure unknowns are located in such a way that the discrete divergence is exactly zero. This permits to enforce the volume constraint very accurately. The incompressibility constraint is enforced by a projection method of Chorin type. The transport equations are solved by a WENO5 scheme. Note that this high order is motivated by the fact that the advected quantities are regular in space and their derivatives are used to compute the elastic stress.

5.3.7 Numerical stability of the coupling

The model we discretize consists of Navier-Stokes equations with a source term which can be expressed, in the case where $E'(r) = \lambda(r-1)$ as:

$$F(x,t) = \lambda \left\{ \mathbb{P}_{\nabla\phi^\perp}\left(\nabla|\nabla\phi|\right)) - (|\nabla\phi| - 1)\kappa(\phi)\frac{\nabla\phi}{|\nabla\phi|} \right\} |\nabla\phi| \frac{1}{\varepsilon}\zeta(\frac{\phi}{\varepsilon}),$$

where $\mathbb{P}_{\nabla\phi^\perp}$ is the projector onto the tangent plane, $\kappa(\phi)$ the mean curvature, and λ the membrane stiffness (we do not consider curvature forces here). As the advection terms are explicited we have a classical CFL condition to respect. Moreover, we have to write some kind of CFL condition for this elastic force such that in one time step, it would not create a displacement greater than a mesh cell. This type of extra condition for the stability of curvature driven flow has been computed initially by Brackbill [37] in the case of a two-phase flow by estimating capillary waves speed. In [105], this condition is rediscovered by arguing on a CFL condition for the source term. Applied to our elastic force, we computed a stability condition which takes the following expression:

$$\Delta t < \Delta t_e = \sqrt{\frac{\rho\alpha}{\lambda|\nabla\phi|(2|\nabla\phi| - 1)}} h^{\frac{3}{2}}$$

where $\varepsilon = \alpha h$ is the interface width. This condition corresponds to the one of [37], up to a constant, if we consider $|\nabla\phi| = 1$ and $\alpha = 1$. In our case however, the width of interface as well as the stretching is involved. This condition could become very restrictive in the case of a stiff membrane (large λ), as in phospholipidic vesicles, since it behaves as $h^{\frac{3}{2}}$.

On another hand, Paul Vigneaux in his thesis and an article with Cédric Galusinski [57, 56] exhibits a stability condition for low Reynolds number and large surface tension (the case of micro-fluid dynamics). In that case their condition reads, neglecting gravity,

$$\Delta t < C\frac{\mu}{\sigma}h$$

where μ is the viscosity and σ the surface tension. In that case, where inertia is neglected, we obtain a less restrictive condition, of order 1 in h.

In her thesis [36] Claire Bost clarifies these stability conditions by introducing a simplified 1D problem, which exhibits both of the two stability conditions. Thanks to a Fourier analysis she found a stability condition compatible with the former two.

An important question for the stability of these fluid-structure coupling problems is the conservation of some discrete energy, after time and/or space discretization. This kind of questions has been addressed in the framework of the ALE method [55, 44] and the second gradient theory [68] by Jamet *et al* [69]. They introduced a method to conserve energy at a discrete level and in doing so suppressed some parasitic currents appearing is the numerical simulations when the surface tension is large.

In the framework of immersed boundary method, stability questions have been addressed by [113, 107, 33, 34], which defined explicit, semi-implicit or fully implicit schemes and studied their stability. In particular Boffi et al [33, 34] in the implementation of IBM with a sharp interface term computed through a finite element formulation, found an explicit scheme stable under a Brackbill type condition and an unconditionally stable implicit scheme (in dimension 2). Another approach still in dimension 2 was proposed by T. Y. Hou and Z. Shi [63, 64] where the interface is parametrized by curvilinear coordinate and the angle of tangent vector to the curve. They were able in this formulation to develop a spectral analysis and produce a semi-implicit scheme stable under a Brackbill condition.

With Claire Bost we tried to construct numerical schemes that conserve a discrete energy. We faced the problem of the spreading of the elastic force through the cut-off function, which brings an extra nonlinearity. We are indeed able to produce such a scheme, but for which we are not able to control the width of interface. This problem of interface width is also present in the phase-field method where we introduce an *ad hoc* extra term in the transport equation to control it. This seems to be the major difference between the two methods and maybe an explanation of the possible better behavior of phase field in that context.

5.3.8 Application: cellular motility and parametric instability

Several tests have been developed in order to validate our numerical code [A4, A3]. We present an application of our method to the study of vesicle protrusions. This is a joint work with John Stockie (U. Vancouver). Cells, for example for their motion, create protrusions on their membrane. The underlying mechanism is still controversial in the Biologists community. It is attributed to polymerization / depolymerization process of actin filaments in the neighborhood of the membrane, but this is modeled differently between authors (cf [90, 35] and references therein). As a two-phase continuous medium, or a visco-elastic medium, or as a microscale network. As I am not specialist to decide between these models, I got interested in an article of Cortez, Peskin, Stockie and Varela [50] into which the authors study the parametric instability of the system formed by an elastic membrane immersed in a $2D$ fluid. Parametric instability is well known to everybody who once use a swing. In the immersed

membrane case, we could imagine that the periodic variation of somme parameter of the system, as the stiffness for example, could lead to large unstable deformations. This is what is proved in [50] and that we study in dimension 3 with John Stockie.

From a numerical point of view the tests we developed with our membrane model clearly illustrated that a spherical membrane slightly perturbed, and with a stiffness varying with a precise periodicity, could exhibit an instability, which means very large displacements compared with the initial perturbation. We want to stress out that this does not correspond to a resonance phenomenon under a suitably chosen forcing term. For example without initial perturbation of the membrane the periodic fluctuations of its stiffness do not create any motion.

Some videos are available on my web page. The following example (figure 10) is academic: it corresponds to a membrane with stiffness 1 immersed in a fluid of Reynolds 100. The spherical membrane is perturbed in the following way: we consider a meridian on this sphere that we perturb by a small amplitude (2.5%) oscillation in $\cos(4\theta)$. Then we consider the surface generated by this perturbed meridian. The membrane stiffness is oscillating between 0.5 and 1.5. The pictures below show the deformed immersed membrane (the fluid is not represented). The colors on the surface give the stretching. The pressure slices in the middle of the vesicle are plotted on the edges of the graphical box.

5.4 Flexural membrane with constant local area

5.4.1 Curvature force

In the case of the study at equilibrium or in a shear flow of phospholipidic vesicles, the method developed above gives an interesting counterpart to phase-field methods [31]. Il this setting, the elastic surface is nearly inextensible and therefore the curvature forces drive the geometrical equilibrium shape. In our model, we in fact somehow penalize the area invariance constraint by considering a membrane with a very large stiffness, and we add a curvature energy. We can consider the following general form:

$$\mathcal{G}_\varepsilon(\phi) = \int_\Omega G(\kappa(\phi))|\nabla\phi|\frac{1}{\varepsilon}\zeta(\frac{\phi}{\varepsilon})dx$$

the standard case corresponding to $G(r) = \frac{1}{2}r^2$. As above the time derivative of the curvature energy will compare to the power of curvature forces $H_\varepsilon(x,t)$, and we have

$$\frac{d}{dt}\mathcal{G}_\varepsilon(\phi) = d\mathcal{G}_\varepsilon(\phi)(\phi_t) = d\mathcal{G}_\varepsilon(\phi)(-u\cdot\nabla\phi) = -\int_\Omega H_\varepsilon(x,t)\cdot u dx \tag{34}$$

which give by identification (see article in preparation [A14]):

$$H_\varepsilon(x,t) = \operatorname{div}\left[-G(\kappa(\phi))\frac{\nabla\phi}{|\nabla\phi|} + \frac{1}{|\nabla\phi|}\mathbb{P}_{\nabla\phi^\perp}\left(\nabla[|\nabla\phi|G'(\kappa(\phi))]\right)\right]\frac{1}{\varepsilon}\zeta(\frac{\phi}{\varepsilon})\nabla\phi.$$

It is possible to obtain a divergence form for the curvature forces which involves the second fundamental form. We obtained in [A14] l'expression $H_\varepsilon(x,t) = \operatorname{div}\sigma_c^\varepsilon$ with

$$\sigma_c^\varepsilon = \left\{|\nabla\phi|\left[G(\kappa(\phi))\mathbb{I} + \frac{\nabla\phi}{|\nabla\phi|}\otimes\nabla G'(\kappa(\phi))\right]\left(\mathbb{I} - \frac{\nabla\phi\otimes\nabla\phi}{|\nabla\phi|^2}\right)\right.$$
$$\left. -G'(\kappa(\phi))\left(\mathbb{I} - \frac{\nabla\phi\otimes\nabla\phi}{|\nabla\phi|^2}\right)D^2\phi\left(\mathbb{I} - \frac{\nabla\phi\otimes\nabla\phi}{|\nabla\phi|^2}\right)\right\}\frac{1}{\varepsilon}\zeta(\frac{\phi}{\varepsilon}) \tag{35}$$

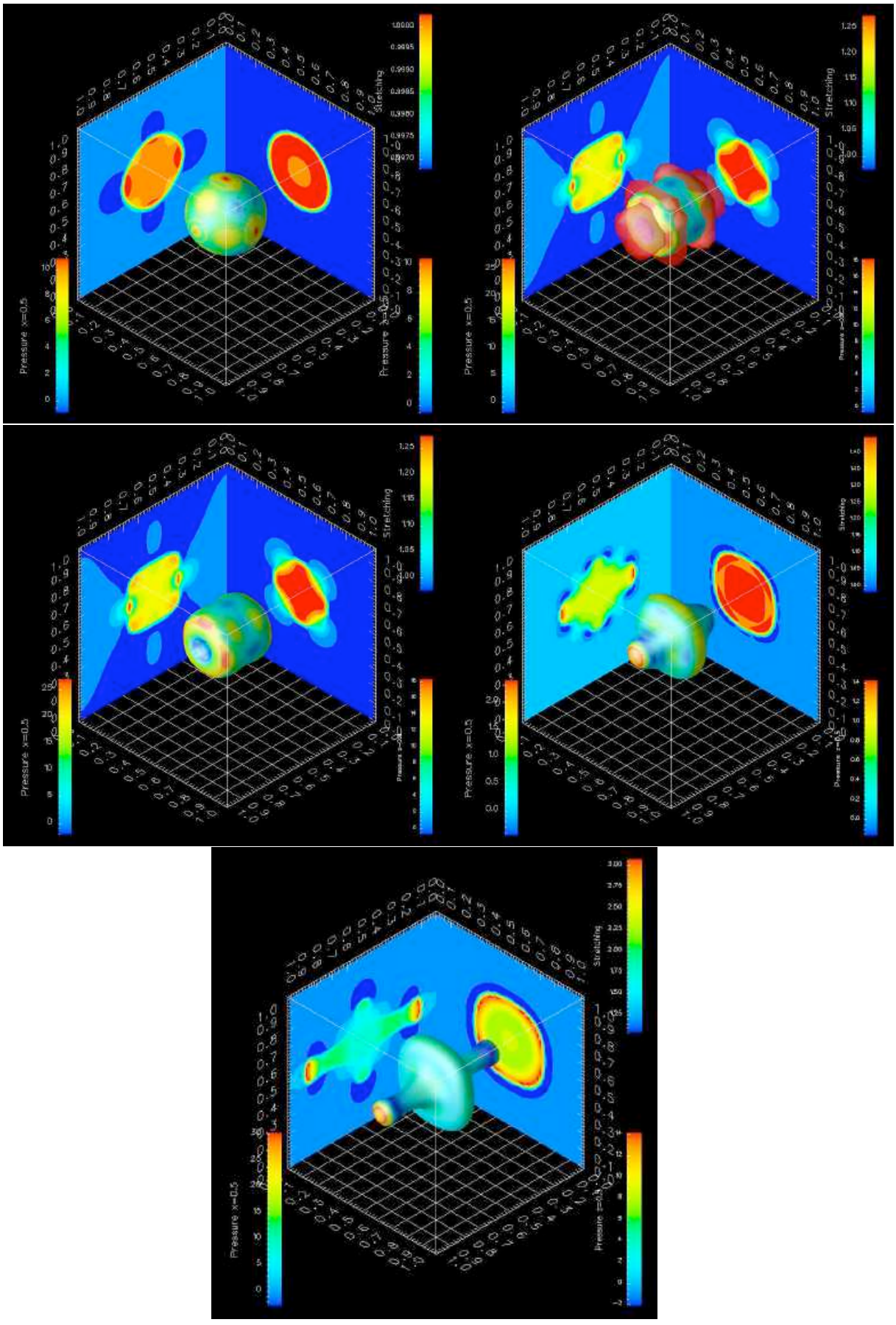

FIGURE 10: Parametric instability of an immersed elastic membrane

5.4.2 Links with phase field method and second gradient theory

The behavior of vesicles in shear flow, which is a physics model of red blood cells in arteries, has been studied extensively in the Laboratory of Spectrometry (LSP) in Grenoble by J. Beaucourt, Th. Biben, C. Misbah and their co-authors [31, 27, 32] and experimentally by M. Mader and T. Podgorski.

The method they developed is a phase field method (they call it advected field method though) which is in some aspects very similar to the Level Set method. Therefore we set up a workgroup to exchange ideas about our experience of such methods. An article in about to be submitted, which makes a comparison of the two approaches [A14]. The basic differences between the two methods are the following. The Eulerian phase function Φ which captures the interface takes its values in $[0, 1]$. It is constant excepted in the neighborhood of the interface, where it varies quickly but smoothly from 0 to 1 (from the inner fluid to the outer fluid). The transition width is a parameter ε of the method, which compares to the one introduced in Level Set. The phase field function Φ corresponds to $H(\frac{\phi}{\varepsilon})$ in Level Set. A surface integral in this formulation does not involve a cut-off function ζ but the gradient of Φ, which is equivalent since $H' = \zeta$. The fundamental difference is thus not in this representation choice but rather in the equation used to move the phase function. While in Level Set the function is merely advected, recording some mechanical information on the interface (stretching), the phase field equation is a transport equation corrected with terms ensuring that the width of interface remains constant. This avoids the reinitialization or renormalization step which is mandatory in Level-Set, but another equation is needed to compute the stretching. Typically Φ verifies:

$$\Phi_t + u \cdot \nabla\Phi = \varepsilon_\Phi(\Phi(1 - \Phi^2) + \varepsilon^2(\Delta\Phi + c|\nabla\Phi|)) \tag{36}$$

the source terms maintaining values of Φ in $[0, 1]$, with a transition zone of width ε. In the original publication [31], the correction terms were found heuristically. The model has to be supplemented by some stretching equation, since this information is not included in the phase function. Recently, D. Jamet and C. Misbah [70] applied the second gradient theory, introducing a thermodynamic potential for this multi-physics problem. This potential has the phase function, its gradient and the stretching as variables. By differentiating this potential they obtained membrane and flexural forces and we prove in [A14] that the curvature forces (which are geometrical) coincide, while membrane forces could be identified up to a particular choice of the elastic constitutive law $E'(r) = \lambda \ln r$ in the Level Set method (which is nearly linear for small stretching).

On a numerical point of view, along with quantitative comparison between the methods [A14] , a stability study comparing the two methods in the case of a stiff membrane is still to be developed. While the Level Set method seems more natural since there is no extra term added in the advection equation, the spreading via a cut-off function of the elastic force seems to play a role in its stability. As indicated above, we investigated with Claire Bost numerical schemes which conserve some numerical energy, and for which it is still possible to control the width of interface. This work is still in development.

5.4.3 Application to phospholipidic vesicles

As a field of application we present in the static case the computation of 3D vesicles shapes. The problem is then to determine a surface of given area and enclosed volume, minimizing the

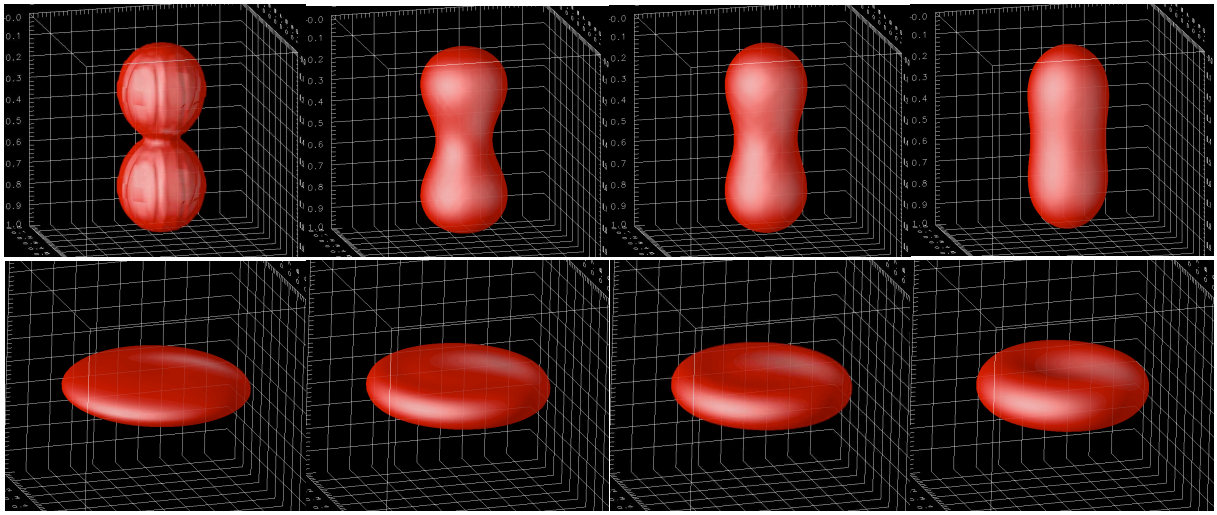

FIGURE 11: Computation of optimal shape for vesicles. Top: $\tau = 0.8$. Bottom: $\tau = 0.586$. From initialization to steady state from the left to the right. Computations by Thomas Milcent.

mean curvature energy. The swelling ratio is the parameter which determines the equilibrium shape. It is defined as the ratio of the vesicle area over the area of the sphere enclosing the same volume. Thanks to the isoperimetric inequality this number τ is between 0 and 1. For values close to 1, equilibrium shapes are ellipsoids, which when τ decreases turn to a peanut shape. A bifurcation appears for smaller values of τ where a donut (without a hole) shape appears. This is the classical shape that we know for red blood cell. For very small swelling ratios, vesicles can take very strange shapes [101] which are in effect observed in some pathologies of red blood cells. Figure 11 reproduces computations on the bove model which have been implemented by Thomas Milcent in his thesis [87] and were published in [A2].

The dynamical case is more interesting since the behavior of vesicles in a shear flow depends on the ratio of the inner fluid viscosity with respect to the outer fluid viscosity. Indeed for nearly equal viscosities, the vesicle reaches a steady state at a fixed angle, and its membrane rolls around in a tank-treading motion. As the vesicle is not spherical, dissipation occurs inside the vesicle. When the inner viscosity is too high, this dissipation is too costly from the energetic point of view. Then the vesicle tumbles around itself so that the inner fluid is nearly in a rigid motion. All these behaviors have been studied in detail in [31, 27, 88].

It is important in the dynamical case to perform a dimension analysis on our model to extract its relevant parameters. We recall the equation of conservation of linear momentum:

$$\rho(u_t + u\cdot\nabla u) - \operatorname{div}(\mu D(u)) + \nabla p = \left\{ \nabla[E'(|\nabla\phi|)] - \operatorname{div}\left[E'(|\nabla\phi|)\frac{\nabla\phi}{|\nabla\phi|}\right]\frac{\nabla\phi}{|\nabla\phi|} + \operatorname{div}\left[-G(\kappa(\phi))\frac{\nabla\phi}{|\nabla\phi|} + \frac{1}{|\nabla\phi|}\mathbb{P}_{\nabla\phi^\perp}\left(\nabla[|\nabla\phi|G'(\kappa(\phi))]\right)\right]\frac{\nabla\phi}{|\nabla\phi|}\right\}|\nabla\phi|\frac{1}{\varepsilon}\zeta\left(\frac{\phi}{\varepsilon}\right).$$

Let L, U, ρ_{ref} and μ_{ref} characteristic length, velocity, density and viscosity. Let $x = Lx'$, $u =$

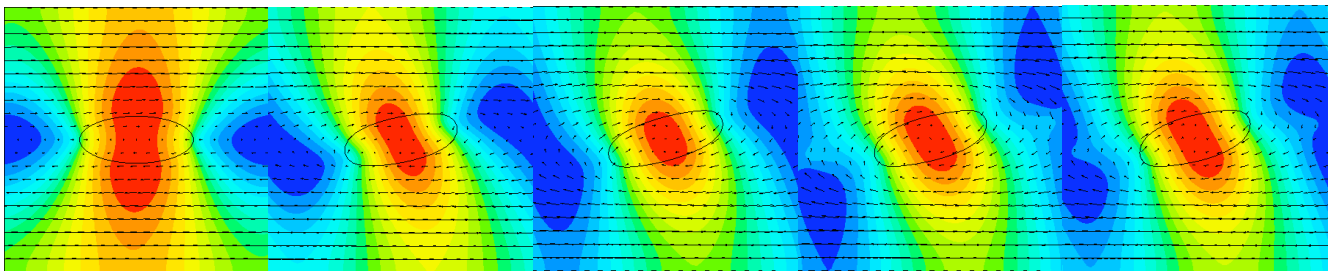

FIGURE 12: Tank-treading motion of a vesicle in a sear flow. Viscosity contrast: 1. Colors stand for iso-pressure lines.

Uu', $t = (L/U)t'$, $\rho = \rho_{\text{ref}}\rho'$, $\mu = \mu_{\text{ref}}r$, $p = \rho_{\text{ref}}U^2p'$, $\phi = L\phi'$, and $\varepsilon = L\varepsilon'$. Differentiating we find

$$u_t = \frac{U^2}{L}u'_{t'}, \quad \nabla u = \frac{U}{L}\nabla' u', \quad D(u) = \frac{U}{L}D'(u'), \quad \operatorname{div}(\mu D(u)) = \frac{U\mu_{\text{ref}}}{L^2}\operatorname{div}'(rD'(u')),$$
$$\nabla p = \frac{\rho_{\text{ref}}U^2}{L}\nabla' p', \quad \nabla\phi = \nabla\phi', \quad \kappa(\phi) = \frac{1}{L}\kappa'(\phi')$$

where $\kappa(\phi)$ is the curvature. In dimensionless variables (dropping the $'$), and for the particular case $E'(r) = \lambda(r-1)$ and $G(r) = \frac{1}{2}r^2$ we get:

$$\rho(u_t + u\cdot\nabla u) - \frac{1}{Re}\operatorname{div}(rD(u)) + \nabla p = \left\{\frac{1}{W_e}\left[\nabla[E'(|\nabla\phi|)] - \operatorname{div}\left[E'(|\nabla\phi|)\frac{\nabla\phi}{|\nabla\phi|}\right]\frac{\nabla\phi}{|\nabla\phi|}\right]\right.$$
$$\left. + \frac{1}{C_k}\operatorname{div}\left[-G(\kappa(\phi))\frac{\nabla\phi}{|\nabla\phi|} + \frac{1}{|\nabla\phi|}\mathbb{P}_{\nabla\phi^\perp}\left(\nabla[|\nabla\phi|G'(\kappa(\phi))]\right)\right]\frac{\nabla\phi}{|\nabla\phi|}\right\}|\nabla\phi|\frac{1}{\varepsilon}\zeta\left(\frac{\phi}{\varepsilon}\right)$$

where

$$R_e = \frac{LU\rho_{\text{ref}}}{\mu_{\text{ref}}}, \qquad W_e = \frac{\rho_{\text{ref}}U^2L}{\lambda}, \qquad C_k = \frac{\rho_{\text{ref}}U^2L^3}{\kappa}$$

In a shear flow one important quantity is the shear rate γ, from which we can express the characteristic velocity $U = \gamma L$. Substituting $LU\rho_{\text{ref}}$ by $R_e\mu_{\text{ref}}$ in W_e and C_k we finally get

$$R_e = \frac{LU\rho_{\text{ref}}}{\mu_{\text{ref}}}, \qquad W_e = R_e\frac{\mu_{\text{ref}}\gamma L}{\lambda}, \qquad C_k = R_e\frac{\mu_{\text{ref}}\gamma L^3}{\kappa}$$

which are the dimensionless parameters from [27] with $R_e = 1$ in W_e and C_k (in that article the Stokes equation is considered). The behavior of the vesicle is determined by the value of these parameters.

Below we plotted simulation results corresponding to generic situations (an intermediate regime has been discovered by C. Misbah [88]). On figure 12, which corresponds to $Re = 0.0001$, $W_e = 0.000025$, $C_k = 0.25$, visosity contrast 1, swelling ratio 0.7, we observe that the vesicle reaches a stationary angle.

By contrast on figure 13 which corresponds to the same parameters but with a viscosity ratio of 4 (the inner visosity 4 times greater than in the former test), we observe a tumbling motion. If rather than multipying the inner visosity by 4 we divide the outer by the same number ($Re = 0.0004$, $W_e = 0.000025$, $C_k = 0.25$, viscosity contrast 4) there is still tumbling but as the exterior fluid is less viscous the peanut shape of the vesicle is more evident (figure 14).

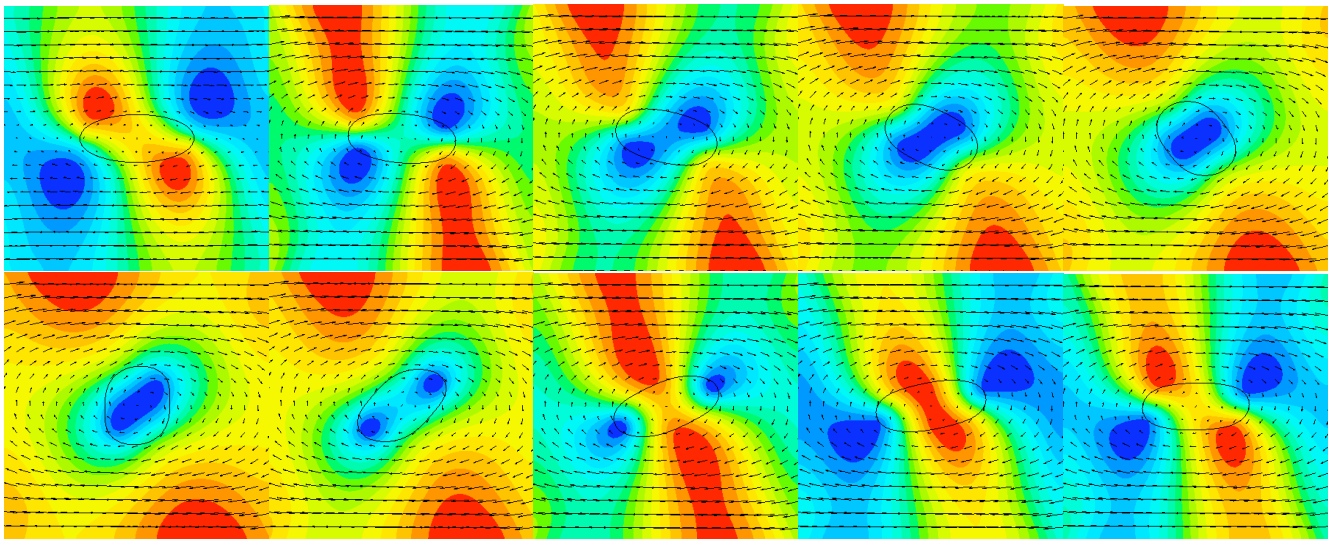

FIGURE 13: Tumbling motion of vesicle in a shear flow. Viscosity contrast: 4. Reynolds: 10^{-4}. Colors stand for iso-pressure lines.

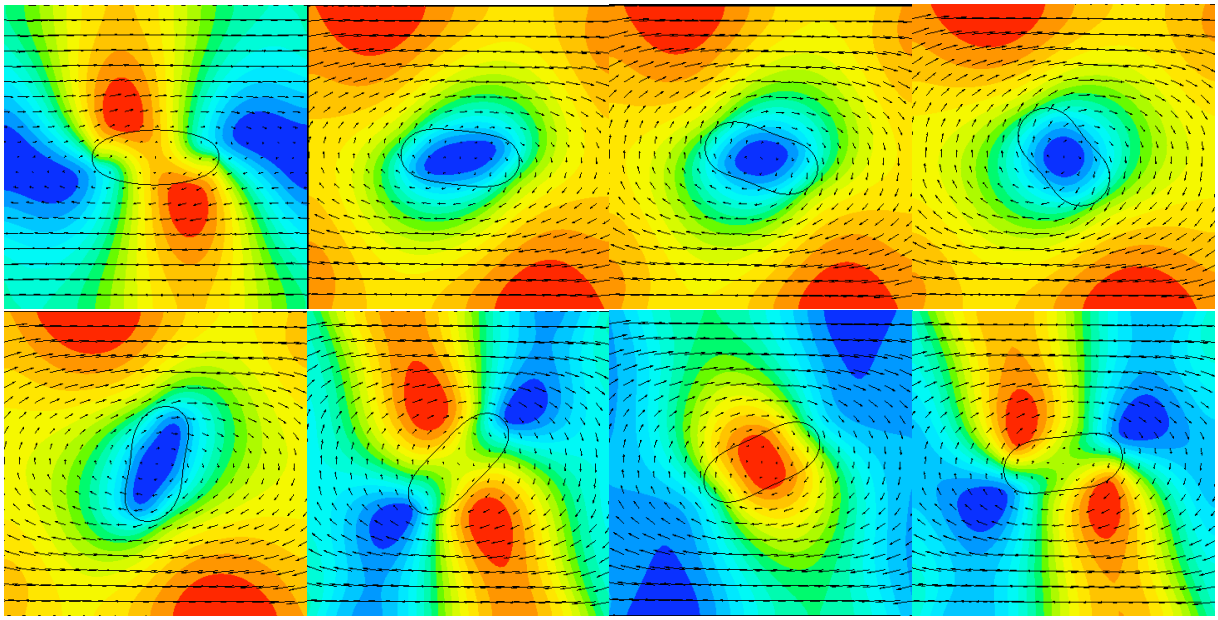

FIGURE 14: Tumbling motion of vesicle in a shear flow. Viscosity contrast: 4. Reynolds: 4.10^{-4}. Colors stand for iso-pressure lines.

5.5 Fluid-structure interaction: generic case

We now consider the case where the immersed elastic body is not thin but rather is a body of same dimension as the fluid.

5.5.1 Some comments on Eulerian elasticity

Remember that we consider the incompressible case (which is well relevant in the biological context) but that our methodology could be extended to compressible medium thanks to suitable insertion of jacobians, as pointed out in the membrane case (remark 5 page 30). For the time being, we consider the the elastic body occupies the whole domain Ω, the fluid-structure situation being restored later. As the velocity field is incompressible and vanishes on $\partial\Omega$, we are in the particular case where the reference configuration coincides with the deformed one from a geometrical point of view. This make the Eulerian formulation easier to settle. Let $\tau \to X(\tau; x, t)$ the characteristics of u. To simplify we set $X(\xi, t) := X(t; \xi, 0)$ for the forward characteristics. We also consider the backward characteristics $Y(x, t) := X(0; x, t)$. One important point of our approach is to remark that the backward characteristics verify a vectorial transport equation:

$$Y_t + u \cdot \nabla Y = 0, \quad Y(0) = x. \tag{37}$$

The first point in elasticity is to measure how distances change between the initial and deformed configurations. In Lagrangian elasticity, we usually make the following elementary computation: If ξ and $\xi + d\xi$ are two close (material) points in the initial configuration, the are after deformation in $X(\xi, t)$ and $X(\xi + d\xi, t)$ which are distant of $|X(\xi, t) - X(\xi + d\xi, t)|^2 \approx d\xi^T \nabla X^T \nabla X d\xi$ at order 1. The tensor $C = \nabla X^T \nabla X(\xi)$ therefore measure distance variations between initial and deformed configurations. Conversely in Eulerian elasticity we consider two close (geometrical) points x and $x + dx$ and we compute at which distance were two material points initially if the are on x and $x + dx$ at time t. Therefore we consider $|Y(x, t) - Y(x + dx, t)|^2 \approx dx^T (\nabla Y^T \nabla Y)(x) dx = dx^T (\nabla X \nabla X^T)^{-1}(\xi) dx$ at order 1, with $\xi = Y(x, t)$. Thus the tensor $B = \nabla X \nabla X^T(\xi) = \nabla Y^{-1} \nabla Y^{-T}(x)$ appears to measure this distance. This explain the central role played by B rather than C in Eulerian elasticity.

As a matter of fact, it is pleasant to remark that B et B^{-1} are solution to Eulerian PDE, that are

$$B_t + u \cdot \nabla B = \nabla u B + B \nabla u^T \qquad B_t^{-1} + u \cdot \nabla B^{-1} = -\nabla u^T B^{-1} - B^{-1} \nabla u. \tag{38}$$

while we would not obtain such relation for C.

5.5.2 Isotropic case

Due to the incompressibility assumption, the invariants of B are, in $\mathbb{R}^3$, $\operatorname{tr} B = |\nabla Y^{-1}|^2$ and $\operatorname{tr} B^{-1} = |\nabla Y|^2$, thus the stored energy may be written as [A3]

$$E = \frac{1}{2} \int_\Omega W(\operatorname{tr} B, \operatorname{tr} B^{-1})\, dx$$

where $(a, b) \to W(a, b)$ is a given function. Note that, from (38), we have

$$\begin{aligned} (\operatorname{tr} B)_t + u \cdot \nabla(\operatorname{tr} B) &= 2 \operatorname{tr}(\nabla u B) = 2B : \nabla u\,, \\ (\operatorname{tr} B^{-1})_t + u \cdot \nabla(\operatorname{tr} B^{-1}) &= -2 \operatorname{tr}(B^{-1} \nabla u) = -2B^{-1} : \nabla u\,. \end{aligned} \tag{39}$$

Taking the time derivative of E and using (39) gives

$$\begin{aligned}\frac{dE}{dt} &= \frac{1}{2}\int_\Omega \frac{\partial W}{\partial a}(\operatorname{tr} B)_t + \frac{\partial W}{\partial b}(\operatorname{tr}(B^{-1}))_t\,dx \\ &= \frac{1}{2}\int_\Omega \frac{\partial W}{\partial a}(-u\cdot\nabla(\operatorname{tr} B)) + \frac{\partial W}{\partial b}(-u\cdot\nabla(\operatorname{tr} B^{-1})) + \frac{\partial W}{\partial a}2B : \nabla u - \frac{\partial W}{\partial b}2B^{-1} : \nabla u\,dx \\ &= \int_\Omega -\frac{1}{2}u\cdot\nabla W + \left(\frac{\partial W}{\partial a}B - \frac{\partial W}{\partial b}B^{-1}\right) : \nabla u\,dx \\ &= \int_\Omega \left[-\frac{1}{2}\nabla W - \operatorname{div}\left(\frac{\partial W}{\partial a}B - \frac{\partial W}{\partial b}B^{-1}\right)\right]\cdot u\,dx.\end{aligned}$$

This expression should equal minus the power of stress forces, that is $-\int_\Omega \operatorname{div}\sigma\cdot u\,dx$. Therefore the incompressibility assumption leads to the following stress:

$$\sigma = -p\mathbb{I} + \frac{\partial W}{\partial a}(\operatorname{tr} B, \operatorname{tr} B^{-1})B - \frac{\partial W}{\partial b}(\operatorname{tr} B, \operatorname{tr} B^{-1})B^{-1}. \tag{40}$$

Note that thanks to Cayley-Hamilton theorem, $B^{-1} = \operatorname{tr} B^{-1}\mathbb{I} - (\operatorname{tr} B)B + B^2$. Therefore, up to a gradient term which is absorbed in the pressure, B^{-1} could be replaced by $(\operatorname{tr} B)B - B^2$, as in [91]. The Eulerian formulation of isotropic elasticity we just presented is summarized in the following proposition:

Proposition 8 *The deformation of an isotropic elastic material in Eulerian coordinates is governed by the following equations:*

$$\begin{cases} \rho(u_t + u\cdot\nabla u) - \operatorname{div}\left(\alpha_1 B - \alpha_2 B^{-1}\right) + \nabla p = f, & \text{on } \Omega\times]0,T[, \\ \operatorname{div} u = 0, & \text{on } \Omega\times]0,T[, \\ Y_t + u\cdot\nabla Y = 0, \qquad B = \nabla Y^{-1}\nabla Y^{-T}, & \text{on } \Omega\times]0,T[, \\ u = 0, & \text{on } \partial\Omega\times]0,T[, \\ u = u_0, \quad Y = id, & \text{on } \Omega\times\{0\}. \end{cases}$$

where the α_i are functions of $(\operatorname{tr} B, \operatorname{tr} B^{-1})$ defined as partial derivatives of an energy function W.

The following remark is important from the computational point of view. We recall that

$$B = \nabla Y^{-1}\nabla Y^{-T} = \nabla X \nabla X^T = \sum_{i=1}^{3} X_{,\xi_i}\otimes X_{,\xi_i}.$$

By definition, $\nabla Y_j \cdot X_{,\xi_i} = \delta_{ij}$. By the incompressibility of the elastic body we have $\det\nabla Y = 1$, and thus we have the followng simple expression of $X_{,\xi_i}$ in the Eulerian domain

$$X_{,\xi_1} = \nabla Y_2\times\nabla Y_3, \quad X_{,\xi_2} = \nabla Y_3\times\nabla Y_1, \quad X_{,\xi_3} = \nabla Y_1\times\nabla Y_2. \tag{41}$$

This has two consequences: first it means that the computation of B in the Eulerian model reduces to simple algebraic operations involving the derivatives of Y, which keeps the computational complexity of the model at reasonable level. Secondly, it allows to interpret B as

a sum of projections on lines where two different Level Set functions Y_i are constant (we will use that in 5.6.2 to link this equation to Born-Infeld model, see [38]).

As an example we write the expression of α_1 and α_2 in the case of the Saint-Venant Kirchhoff constitutive law (in $\mathbb{R}^3$). The energy density in this case is given by

$$\frac{\lambda_1}{2}(\operatorname{tr} E)^2 + \lambda_2 \operatorname{tr} E^2, \quad E = \frac{1}{2}(C - \mathbb{I}),$$

where λ_1 and λ_2 are the Lamé coefficients. It is easy to see that $\operatorname{tr} E = \frac{1}{2}\operatorname{tr}(B - \mathbb{I})$ and $\operatorname{tr} E^2 = \frac{1}{4}\operatorname{tr}(B - \mathbb{I})^2$. Expanding these terms and using the identity $\operatorname{tr}(B^2) = (\operatorname{tr} B)^2 - 2\operatorname{tr} B^{-1}$ (since $\det B = 1$) leads to:

$$W_{SK}(a, b) = \frac{1}{8}(\lambda_1 + 2\lambda_2)a^2 - (\frac{3\lambda_1}{4} + \frac{\lambda_2}{2})a - \frac{\lambda_2}{2}b + \frac{9\lambda_1 + 6\lambda_2}{8}$$

This corresponds to the following coefficients in proposition 8:

$$\alpha_1 = \frac{\lambda_1 + 2\lambda_2}{4}(\operatorname{tr} B - 3) + 2\lambda_2, \qquad \alpha_2 = -\frac{\lambda_2}{2}.$$

5.5.3 Transverse anisotropy

We now turn to the anisotropic case, that is when the elastic body exhibits preferred stretching directions. We have two particular reasons for considering this important case. First this is a case often encountered in biological tissues, an application which was one of the motivations for the present work. As a matter of fact, continuous elastic models in such tissues can generally be seen as an idealization of viscous fluids filled with one or two dimensional fibers. Secondly, thin anisotropic elastic bodies seem to be an appropriate setting if one wishes to recover membrane models in the limit of width tending to zero, a question we will investigate in 5.3.4. Let $\tau(y)$ be a preferred direction (at time $t = 0$) and assume that the material response is indifferent to arbitrary rotations about the direction τ and by replacement of τ by $-\tau$. Following [91], this leads to an energy function, which depends not only (in material coordinates) on $\operatorname{tr} C, \operatorname{tr} C^{-1}$, but also on $\tau^T C\tau$ and $\tau^T C^2\tau$. Note first that, due to the Cayley-Hamilton theorem, we can replace this last invariant by $\tau^T C^{-1}\tau$. As we will see below, this form has a more direct mechanical meaning. It is also more tractable in our Level Set approach. The energy may thus be written in Lagrangian coordinates under the following form

$$E = \int_\Omega W(\operatorname{tr} C, \operatorname{tr} C^{-1}, \tau(y)^T C\tau(y), \tau^T(y)C^{-1}\tau(y))\, dy.$$

The invariants of B and C are the same. We use the change of variables $y = Y(x, t)$ with unit Jacobian (due to incompressibility), to get (with the notation $\tau(Y)$ for $\tau(Y(x, t))$)

$$E = \int_\Omega W(\operatorname{tr} B, \operatorname{tr} B^{-1}, \left|\nabla Y^{-1}(x, t)\tau(Y)\right|^2, \left|\nabla Y^T(x, t)\tau(Y)\right|^2)dx.$$

Still applying our method of differentiation of energy we get the following stress:

$$\sigma = -p\mathbb{I} + \frac{\partial W}{\partial a}B - \frac{\partial W}{\partial b}B^{-1} - \frac{\partial W}{\partial c}\nabla Y^T\tau \otimes \nabla Y^T\tau + \frac{\partial W}{\partial d}\nabla Y^{-1}\tau \otimes \nabla Y^{-1}\tau.$$

In the case of a fiber material as the cardiomyocyte, τ will represent the direction of the fiber. The quantity $\left|\nabla Y^{-1}(x,t)\tau(Y)\right|$ represents the stretching in the direction of fiber. Let us now consider an elastic body of a given width, occupying initially a domain enclosed between two level sets of a function ϕ (that is, a thick membrane). Then we may consider as preferred direction $\tau(y) = \nabla\phi_0(y)$. Let $\phi(x,t) = \phi_0(Y(x,t))$ the transported function; we have

$$\nabla Y^T \tau(Y) = \nabla Y^T \nabla\phi_0(Y) = \nabla\phi(x,t)$$
$$\nabla Y^{-1}\tau(Y) = \nabla Y^{-1}\nabla\phi_0(Y) = \nabla Y^{-1}\nabla Y^{-T}\nabla Y^T\nabla\phi_0(Y) = B\nabla\phi(x,t).$$

Therefore, $|B\nabla\phi|$ records the stretching along the direction$\nabla\phi_0(Y)$ whereas $|\nabla\phi|$ carries the stretching in the direction $\nabla\phi$, or the area change of $\phi = 0$ in the incompressible case, as proved in proposition 5. These two directions do not coincide in general. This distinction was easier to state precisely in this Level Set representation, under which the stress tensor has a simpler expression than usual descriptions used (for instance in comprarison with (73) of [91], p. 79, or (6.209) in [62], p. 269):

$$\sigma = -p\mathbb{I} + \frac{\partial W}{\partial a}B - \frac{\partial W}{\partial b}B^{-1} - \frac{\partial W}{\partial c}\nabla\phi\otimes\nabla\phi + \frac{\partial W}{\partial d}B\nabla\phi\otimes B\nabla\phi. \tag{42}$$

We have established the following result:

Proposition 9 *The deformation of a transverse isotropic elastic material, with initial preferred direction $\nabla\phi_0(y)$, where ϕ_0 is a distance function, is governed by the following equations:*

$$\begin{cases} \rho(u_t + u\cdot\nabla u) - \operatorname{div}\sigma = f, & \text{on } \Omega\times]0,T[,\\ \operatorname{div} u = 0, & \text{on } \Omega\times]0,T[,\\ Y_t + u\cdot\nabla Y = 0, & \text{on } \Omega\times]0,T[,\\ \phi(x,t) = \phi_0(Y(x,t)), & \text{on } \Omega\times]0,T[,\\ u = 0, & \text{on } \partial\Omega\times]0,T[,\\ u = u_0, \quad Y = id, & \text{on } \Omega\times\{0\}. \end{cases}$$

where σ is given by (42) and the α_i are functions of $|\nabla Y|^2, |\nabla Y^{-1}|^2, |\nabla\phi|^2$, $|B\nabla\phi|^2$ defined as partial derivatives of an energy function W.

Remark 9 *(i) We could recover the form of Ogden and Holzapfel by taking their I_5 invariant based on C^2 instead of using C^{-1}. This would correspond in the above formulation to changing $|\nabla Y^{-1}\tau(Y)|$ into $|\nabla Y^{-T}\nabla Y^{-1}\tau(Y)|$ and make the Level Set formulation slightly less direct. (ii) If we consider an initial level-set function which is not a distance, and define $\tau(y) = \frac{\nabla\phi_0}{|\nabla\phi_0|}(y)$, then the corresponding part of the above stress has to be divided by $|\nabla\phi_0(Y(x,t))|$. (iii) We could have derived directly the stress from the fact that $\nabla\phi$ and $B\nabla\phi$ satisfy similar stretching equations, as seen from (38), namely*

$$\nabla\phi_t + u.\cdot\nabla(\nabla\phi) = -\nabla u^T\nabla\phi \qquad (B\nabla\phi)_t + u.\cdot\nabla(B\nabla\phi) = \nabla u B\nabla\phi$$

Annie Raoult recently clarifies in a deep way the field of anisotropic elastic energies, by studying the number of invariants that should be involved depending on the symmetry group that leaves the material invariant [98].

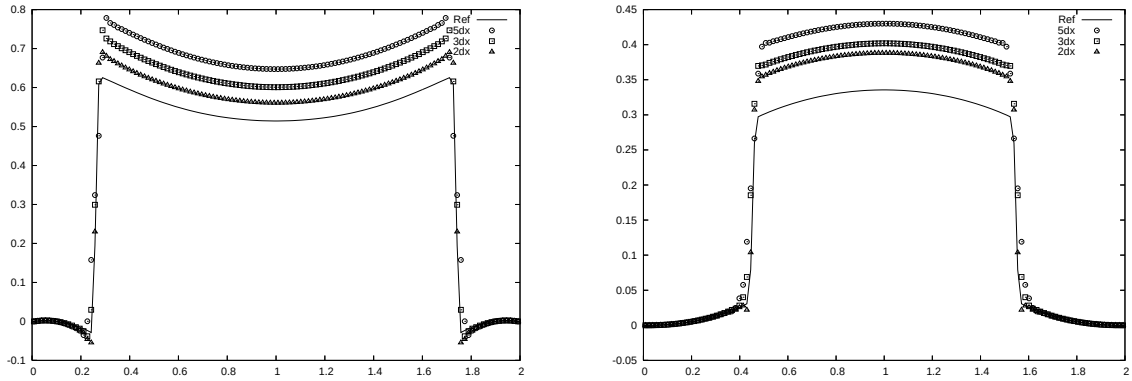

FIGURE 15: Convergence of pressure profiles at $t = 0.2$ (left) and $t = 2.2$ (right) to the reference profile (membrane) for different values of ε

Another remark concerns the existence theory for this model. The main difference with the immersed membrane case is that there is no dissipation in the solid. If we rather consider a visco-elastic solid it is straightforward to generalize our existence results under some regularity assumption on the coefficients α_i.

At last a small computation done in [A3] shows that in dimension 2, the stress tensor (42) can be expressed thanks to the last two terms, which gives

$$\sigma = -p\mathbb{I} - \beta_1(|\nabla\phi|, |B\nabla\phi|)\nabla\phi \otimes \nabla\phi + \beta_2(|\nabla\phi|, |B\nabla\phi|)B\nabla\phi \otimes B\nabla\phi. \tag{43}$$

An asymptotic analysis, as the thickness goes to zero, on this generic model recovers the immersed membrane model, a fact that we correlated numerically by considering a sequence of annular solids thiner and thiner and observing, on figure 15 the convergence of pressure profiles.

5.5.4 Multi-physics model of fluid-structure coupling

We are now in a position to derive generic fluid-structure interaction Eulerian models relying on Level Set functions. It essentially suffices to introduce an additional Level Set function to capture the fluid-solid interface and switch between the fluid and solid stress forms.

Let us denote by $\Omega_F(t)$ and $\Omega_S(t)$ respectively the moving fluid and solid domains and by $\Sigma(t)$ their interface. Assume that the interface $\Sigma(0)$ coincides with the zero level set of a smooth function Ψ_0 and that Ψ_0 is positive inside $\Omega_S(0)$. The densities of the fluid and solid are denoted by ρ_F and ρ_S. In the sequel, H denotes the Heaviside function. The following result gives a general Level Set formulation for fluid-structure interaction:

Proposition 10 *With the above notations, a generic fluid-structure interaction model is*

given by the following system of equations:

$$\begin{cases} \rho(\Psi)(u_t + u\cdot\nabla u) - \operatorname{div}\left(H(\Psi)\sigma_S + (1-H(\Psi))\sigma_F\right) = f, & \text{on } \Omega\times]0,T[\\ \operatorname{div} u = 0 & \text{in } \Omega\times]0,T[, \\ Y_t + u\cdot\nabla Y = 0 & \text{in } \Omega\times]0,T[, \\ \phi(x,t) = \phi_0(Y(x,t))\ ,\ \Psi(x,t) = \Psi_0(Y(x,t)) & \text{in } \Omega\times]0,T[, \\ u = 0 & \text{in } \partial\Omega\times]0,T[, \\ u = u_0, \quad \Psi = \Psi_0, \quad Y = Id & \text{in } \Omega\times\{0\}. \end{cases}$$

In the above system, $\rho(\Psi) = H(\Psi)\rho_S + (1-H(\Psi))\rho_F$, $\sigma_F = -pI + 2\mu D(u)$ is the fluid stress tensor, and σ_S is the elastic stress tensor. In the case of isotropic elasticity in Ω_S, σ_S is given by (40). For a transverse isotropic solid with preferred direction at time zero $\tau(y) = \nabla\phi_0(y)$, σ_S is given by (42) with $\phi(x,t) = \phi_0(Y(x,t))$.

This result merely states that the momentum conservation equation implicitly translates the fact that the deformations satisfy the flow equations in the fluid, the elasticity equations in the solid and fulfill continuity of velocity and stresses at the fluid-solid interface.

5.5.5 Application to cardiomyocyte contraction

In a recent article, Okada et al. [92] investigated the mechanism of calcium wave propagation in connection with cardiomyocyte contraction. They developed a $3D$ simulator using the model of Subramanian et al (2002) for the calcium dynamics and relying on the Negroni and Lascano's contraction model of Negroni et Lascano (1996) which couples calcium concentration with force generation. For the elastic part an isotropic Saint Venant-Kirchhoff hyperelastic model was assumed and myofibrills, Z-lines, sarcolemma, cytoskeleton and cytoplasm were represented by various finite element families. As presented above we use a Level Set approach of the fluid-structure coupling that occurs between the surrounding fluid and the cardiomyocyte, considering these two as a unique incompressible continuous medium. The microscopic internal structure of the cardiomyocyte is not described: the passive property of the myocyte is given by nonlinear elasticity, with a transverse isotropy assumption accounting for the topology of the sarcolemma.

Experiments developed in Montpellier on rat cardiomyocytes by physicians in collaboration with Y. Usson (biologist in Grenoble, TIMC) brought us the ability to work on real geometry. We consider an immersed cardiomyocyte and describe the fluid-structure interaction problem in Eulerian coordinates. For the calcium dynamics we used the model of Goldbeter which describes the CICR system (see [A2] for details and references). This dynamics is added in the stress tensor as an active part along the preferred direction τ, which is the actin/myosin fiber direction. More precisely, the stress tensor we consider is given by:

$$\sigma = -p\mathbb{I} + \alpha_1 B - \alpha_2 B^{-1} + (\alpha_4 + T_0\gamma(Z))\nabla Y^{-1}\tau\otimes\nabla Y^{-1}\tau,$$

where Z is the solution to the CICR reaction-diffusion system in the cardiomyocyte. Z is the calcium concentration and $\gamma(Z)$ is a threshold function which triggers the contraction when Z takes a sufficiently great value. Two cases are considered and happen in vivo: either Z is spatially uniform and the contraction is triggered in all the myocyte. This is the physiological case. Either Z propagates as a wave, which corresponds to the isolated cardiomyocyte case (the calcium wave is created by random calcium sparks).

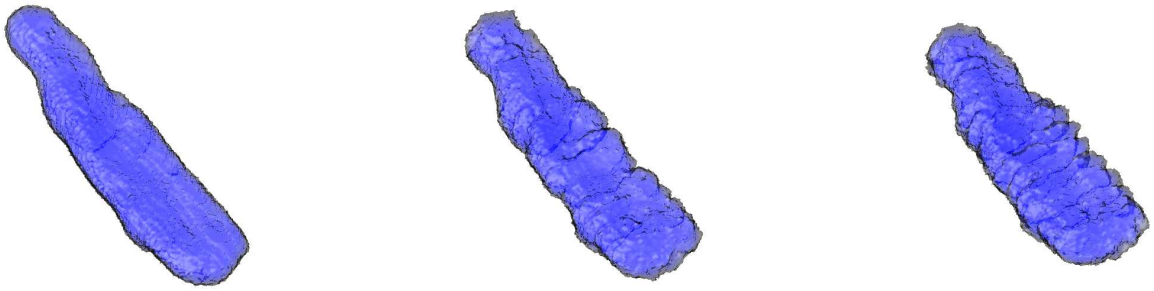

FIGURE 16: Uniform contraction of a cardiomyocyte under an homogeneous calcium release

Uniform contraction of an incompressible cylinder In order to test our computational code, we started by an incompressible cylinder in uniform contraction. The simulation is made on a MAC grid of size 100^3 and a contraction is computed in 3 hours on an AMD 64 processor 3GHz.

Uniform contraction in real geometry One strong aspect of our method is that the complicated interface of the cardiomyocyte is note resolved by the mesh but rather captured by a Level Set function, so that the computational code for a cylinder or for a real cardiomyocyte only differs in the function repsenting the object. Moreover this function is very simply extracted from the experimental data which consist of a binary $3D$ image, that is, an Heaviside function (figure 16). In the case of a calcium wave, the contraction, the contraction is of far less amplitude (figure 17). The biological data are given in [A2].

5.6 Links with other models

5.6.1 Optimal transportation

In [39], Y. Brenier establishes a link between optimal transportation and Boussinesq equations that he further generalizes. Let Ω be a bounded and connected domain of $\mathbb{R}^d$ and y^0 a map from Ω to $\mathbb{R}^d$. The optimal transportation problem is to find, among all rearrangements y of

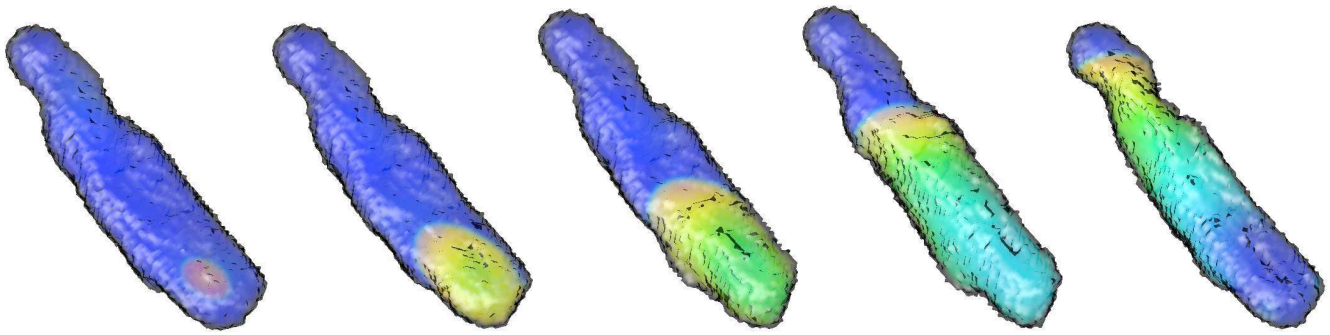

FIGURE 17: Calcium wave propagating in a cardiomocyte. The color represent the calcium concentration. Final time: 1s

y^0 the one minimizing the cost

$$\int_\Omega |y(x) - x|^2 dx.$$

To this aim the AHT model (for Angenent-Haker-Tannenbaum) consists in finding the steady state of the following system:

$$\partial_t y + (v \cdot \nabla) y = 0, \tag{44}$$

$$-\Delta v + \nabla p = y, \quad \operatorname{div} v = 0, \tag{45}$$

with the initial condition $y(x,0) = y^0$ and an homogeneous Dirichlet boundary condition for v. This system has a solution $(y, v, p) = (y(x,t), v(x,t), p(x,t)) \in \mathbb{R}^d \times \mathbb{R}^d \times \mathbb{R}$ whose expected behavior when $t \to +\infty$, is obtained from the identity proved in [39]:

$$\frac{d}{dt} \int_\Omega \frac{1}{2} |y(t,x) - x|^2 \, dx = - \int_\Omega |\nabla v|^2 \, dx. \tag{46}$$

Y. Brenier then introduces a generalization of (44-45) which contains the Boussinesq equations of fluid mechanics. This system reads

$$\epsilon(\partial_t v + (v \cdot \nabla) v) - \Delta v + \nabla p = F(x,y), \quad \operatorname{div} v = 0, \tag{47}$$

$$\partial_t y + (v \cdot \nabla) y = G(x,y), \tag{48}$$

where F and G are smooth functions. The Boussinesq case is recovered by setting $\varepsilon = \rho_0$, $G = 0$ et $F(x,y) = y$, y being a vectorial function with one non zero component. This component is equal to $g\delta\rho$, $\rho_0 + \delta\rho$ being the decomposition of density used in that model.

We observe that our immersed membrane model (or immersed solid) is similar to (47-48), with $G = 0$ and F depending on $(x, y, \nabla y, \nabla^2 y)$. We can rephrase our immersed membrane problem, for example, neglecting the inertia

$$\partial_t y + (v \cdot \nabla) y = 0, \qquad \phi = \phi^0(y),$$

$$-\Delta v + \nabla p = \operatorname{div} \left(E'(|\nabla\phi|) |\nabla\phi| \frac{\nabla\phi \otimes \nabla\phi}{|\nabla\phi|^2} \frac{1}{\varepsilon} \zeta(\frac{\phi}{\varepsilon}) \right), \quad \operatorname{div} v = 0,$$

with the initial condition $y(0,x) = y^0(x)$ and an homogeneous Dirichlet condition on v. The associated optimal transportation problem is to find among all rearrangements y of y^0 the one minimizing

$$\int_\Omega E(|\nabla\phi|(x))\frac{1}{\varepsilon}\zeta(\frac{\phi}{\varepsilon})dx \text{ with } \phi(x) = \phi^0(y(x)).$$

5.6.2 Born-Infeld model

In [38], the authors first consider a non conservative version of the equations of Born-Infeld (BI). These equations, in the weak field limit, gives Maxwell equations. Y. Brenier remarked that this system could be augmented by adding conservation laws of combination of BI unknowns (ABI system). This augmented system, written under the non conservative form is:

$$\begin{aligned}
\tau_t + u\cdot\nabla\tau - \tau\,\mathrm{div}\,u = 0,\\
u_t + u\cdot\nabla u - b\cdot\nabla b - d\cdot\nabla d - \tau\cdot\nabla\tau = 0,\\
b_t + u\cdot\nabla b - b\cdot\nabla u + \tau\nabla\times d = 0,\\
d_t + u\cdot\nabla d - d\cdot\nabla u - \tau\nabla\times b = 0.
\end{aligned}$$

In the limit for high fields, which corresponds to $\tau = 0$, we obtain the equations

$$\begin{aligned}
u_t + u\cdot\nabla u - b\cdot\nabla b - d\cdot\nabla d = 0,\\
b_t + u\cdot\nabla b - b\cdot\nabla u = 0,\\
d_t + u\cdot\nabla d - d\cdot\nabla u = 0.
\end{aligned}$$

Our model could be put under this form. Indeed, considering the vectorial transport equations satisfied by the backward characteristics (still in the incompressible case)

$$Y_t + u\cdot\nabla Y = 0,$$

with initial condition $Y(x,0) = x$, an elementary computation shows that

$$(\nabla Y^{-T})_t + u\cdot\nabla(\nabla Y^{-T}) = \nabla Y^{-T}\nabla u^T.$$

Applying the divergence operator (column vector made of divergences of row vectors) shows that $\mathrm{div}(\nabla Y^{-T})$ verifies a transport equation, which since it is initially zero, proves that $\mathrm{div}(\nabla Y^{-T}) = 0$ for all time (see also [80]). But in the incompressible case, $\nabla Y^{-T} = (\nabla Y_2\times\nabla Y_3, \nabla Y_3\times\nabla Y_1, \nabla Y_1\times\nabla Y_2)^T$ so that we have

$$\mathrm{div}(\nabla Y_i\times\nabla Y_j) = 0 \qquad \forall i,j. \tag{49}$$

Given that

$$(\nabla Y_i)_t + u\cdot\nabla(\nabla Y_i) + \nabla u^T\nabla Y_i = 0$$

we have also, arguing as in Lemma 3.1 of [A5],

$$(\nabla Y_i\times\nabla Y_j)_t + u\cdot(\nabla Y_i\times\nabla Y_j) = \nabla u(\nabla Y_i\times\nabla Y_j) = (\nabla Y_i\times\nabla Y_j)\cdot\nabla u. \tag{50}$$

Moreover using the decomposition of B as in (41) and considering the isotropic model of proposition 8 with $\alpha_1 = 1$ and $\alpha_2 = 0$ we have

$$u_t + u \cdot \nabla u - \operatorname{div}\left(\sum_{i<j} (\nabla Y_i \times \nabla Y_j) \otimes (\nabla Y_i \times \nabla Y_j)\right) + \nabla p = 0.$$

Since we have (49) there holds $\operatorname{div}(a \otimes b) = b \cdot \nabla a + (\operatorname{div} b)a$,

$$u_t + u \cdot \nabla u - \sum_{i<j} (\nabla Y_i \times \nabla Y_j) \cdot \nabla(\nabla Y_i \times \nabla Y_j) + \nabla p = 0. \tag{51}$$

We observe that we recover the ABI model under its non conservative form with a pressure term, if we choose two of the three fields. This is the Eulerian analog of membrane equation described by [38], and spatial or string equations are recovered taking respectively three or one field.

6 Level Set method and optimization of functional defined on surfaces [A1]

6.1 Introduction

This is a joint work with Fadil Santosa from University of Minnesota, who collaborates with a biomedical firm. The motivation is to identify polarization on the surface of myocardium from measures inside the ventricle. To determine an anomaly in this polarization, physicians insert a balloon probe through an artery up to inside the ventricle. This probe measures the potential at its surface. From this information we aim to reproduce the polarization wave on the myocardium surface. This is an ill posed problem, amounting to solve the Cauchy problem for a Poisson equation. Some regularization technics of Tikhonov type have been tried without fully satisfactory solving the problem. Fadil Santosa had the idea to regularize the problem by adding some extra information on the object to be identified. The polarization could be searched as a binary field: polarized/depolarized. This amounts to localize an interface between these two zones, which is moving onto the myocardium surface. As the separating curve could change topology, the natural way to represent it is by a Level Set method. We know from [46] that it is possible to represent a codimension 2 object in $\mathbb{R}^3$ thanks to two Level Set functions. But this turns the problem of moving a $1D$ curve on a $2D$ surface to a $3D$ problem, which is not so optimal.

Therefore we chose to introduce an hybrid method: indeed the myocardium surface which does not move a lot, and does not change topology (hopefully) could be safely represented in parametric form. The curve can then be represented by a Level Set function but in the parameter space, which is a $2D$ square in general. We then obtain an Eulerian method in a square of $\mathbb{R}^2$ to represent a curve on a surface in $\mathbb{R}^3$.

We first developed our method on some academic situation: the isoperimetric problem on a surface. The application to our identification problem is under progress.

Consider a smooth fixed surface S included in some bounded open set $\Omega \subset \mathbb{R}^3$. On this surface, we denote a closed curve by Γ. The arclength of the curve, denoted by $\ell(\Gamma)$, is to be minimized while the area enclosed by the curve is $A(\Gamma)$ is fixed. The optimization problem then is

$$\min_{\text{Area}(\Gamma)=C} \ell(\Gamma).$$

In the planar case, this is a classical problem whose solution is given by the isoperimetric theorem (the unique solution is a circle). On general surfaces the problem is harder and although there have been some recent advances, some open questions remain (see [65] and references therein). The goal of this work is to develop an effective numerical method for solving problems of this type.

Some notations:

- $\gamma(r,s) \ : \ J^2 \to \mathbb{R}^3$ is the parameterization of the fixed surface S. In component form $\gamma = (\gamma_1, \gamma_2, \gamma_3)^T$.
- $\nabla = (\partial_r, \partial_s)^T$. The 3-D cartesian gradient is denoted by ∇_x.
- $\phi(r,s) = 0$ is the Level Set function for the curve on S described in the parameter space.

- $$\nabla\gamma = \begin{pmatrix} \gamma_{1,r} & \gamma_{1,s} \\ \gamma_{2,r} & \gamma_{2,s} \\ \gamma_{3,r} & \gamma_{3,s} \end{pmatrix}, \qquad \nabla\gamma^T = \begin{pmatrix} \gamma_{1,r} & \gamma_{2,r} & \gamma_{3,r} \\ \gamma_{1,s} & \gamma_{2,s} & \gamma_{3,s} \end{pmatrix}.$$
- $$\nabla \times \gamma = \begin{pmatrix} -\gamma_{1,s} & \gamma_{1,r} \\ -\gamma_{2,s} & \gamma_{2,r} \\ -\gamma_{3,s} & \gamma_{3,r} \end{pmatrix}, \quad \nabla \times \gamma^T = \begin{pmatrix} -\gamma_{1,s} & -\gamma_{2,s} & -\gamma_{3,s} \\ \gamma_{1,r} & \gamma_{2,r} & \gamma_{3,r} \end{pmatrix}.$$
- $\nabla\phi = (\phi_r, \phi_s)^T$, and $\nabla \times \phi = (-\phi_s, \phi_r)^T$.
- For 2-vectors u and v,
$$u \otimes v = \begin{bmatrix} u_1 v_1 & u_1 v_2 \\ u_2 v_1 & u_2 v_2 \end{bmatrix}.$$
- Divergence of a 2-by-2 matrix is
$$\operatorname{div} A = \begin{bmatrix} A_{11,r} + A_{12,s} \\ A_{21,r} + A_{22,s} \end{bmatrix}.$$

Since the surface S is fixed, we can choose the following parametrization. Let J be an interval, and $\gamma : J^2 \to \mathbb{R}^3$ be such that

$$S = \{x \,|\, x = \gamma(r, s), \quad (r, s) \in J^2\}.$$

We will view the iterative optimization method as a discretization of a 'flow'. Therefore, it will be most convenient to consider the problem in the continuous setting. To this end, the curve on the surface is denoted by Γ_t, where the subscript t denotes its dependence on time t. The curve Γ_t is given a level-set representation in the parameter domain J^2. Let $\phi : J^2 \times (0, T) \to \mathbb{R}$ such that

$$\Gamma_t = \{x \,|\, x = \gamma(r, s), \quad \phi(r, s, t) = 0\}.$$

We will consider two cases:

(i) S has a boundary but the curve Γ_t does not touch this boundary. We assume $\phi > \alpha > 0$ on ∂J^2.

(ii) S has no boundary. In that case γ is taken periodic in r and s.

An obvious generalization is the case where S is a truncated cylinder, then γ will be periodic in one direction and ϕ will be constrainted to be positive on the boundary of the parameter space of the other direction. All that follows applies to that case as well.

To move the curve Γ_t, we will evolve the level-set function $\phi(r, s, t)$ according to a transport equation with a given velocity field. To constrain the area enclosed by the curve Γ_t on S, we will need to find a projection for the velocity field. These ideas are discussed in more detail below.

We note that in our formulation the surface is given explicitly whereas the curve on the surface is given implicitly as the zero-level set of function $\phi(r, s)$. This fact requires us to derive formulas for simple quantities such as arclength and area, which are substantially more complicated than those in [46]. We need to work with the parameter variables in order to obtain two-dimensional equations for the motion of the curve.

6.2 Arclength and surface area

The computation of arclength of Γ_t on the surface S takes a few steps. In [A1] we prove

$$\begin{aligned}\ell(\Gamma_t) &= \lim_{\varepsilon\to 0}\int_{J^2}\left|\nabla\gamma\frac{\nabla\times\phi}{|\nabla\phi|}\right||\nabla\phi|\frac{1}{\varepsilon}\zeta(\frac{\phi}{\varepsilon})\,drds\\ &= \lim_{\varepsilon\to 0}\int_{J^2}|\nabla\gamma\nabla\times\phi|\frac{1}{\varepsilon}\zeta(\frac{\phi}{\varepsilon})\,drds.\end{aligned}$$

We therefore consider for fixed $\varepsilon > 0$ the approximation of the length of Γ_t as cost function:

$$\ell_\varepsilon(\Gamma_t) = \int_{J^2}|\nabla\gamma\nabla\times\phi|\frac{1}{\varepsilon}\zeta(\frac{\phi}{\varepsilon})\,drds = \int_{J^2}|\nabla\times\gamma\nabla\phi|\frac{1}{\varepsilon}\zeta(\frac{\phi}{\varepsilon})\,drds. \tag{52}$$

In the case of a planar surface $|\nabla\times\gamma\nabla\phi| = |\nabla\phi|$ and we recover the usual formula.

The enclosed area Γ_t on S is likewise approximated by

$$\mathrm{A}_\varepsilon(\Gamma_t) := \int_{J^2}\left(1 - H\left(\frac{\phi}{\varepsilon}\right)\right)|\gamma_{,r}\times\gamma_{,s}|\,drds.$$

where$H(r) = \int_{-\infty}^{r}\zeta(s)ds$ is a regularized Heaviside function. Finally our problem could be stated in a regularized way as:

$$\min_{\Gamma_t}\ell_\varepsilon(\Gamma_t) \quad \text{under the constraint } \mathrm{A}_\varepsilon(\Gamma_t) = C. \tag{53}$$

We want to preserve this area while moving the curve with a velocity field w, which means as ϕ evolves as

$$\phi_t + w\cdot\nabla\phi = 0. \tag{54}$$

Writing that the time derivative of A_ε with respect to t is zero gives the following condition on w:

$$\mathrm{div}(|\gamma_{,r}\times\gamma_{,s}|w) = 0. \tag{55}$$

The next step is to find a velocity field that not only preserves the area, but also reduces the arclength.

6.3 Descent algorithm

Arguing by analogy with Eulerian mechanics we look for a fictitious force $F(\phi)$ such that

$$\frac{d\ell_\varepsilon(\Gamma_t)}{dt} = -\int_{J^2}F(\phi)\cdot w\,drds. \tag{56}$$

After some heavy computations we found in [A1] the following expression:

$$F(\phi) = -\,\mathrm{div}\left(\nabla\times\gamma^T\frac{\nabla\times\gamma\nabla\phi}{|\nabla\times\gamma\nabla\phi|}\right)\frac{1}{\varepsilon}\zeta(\frac{\phi}{\varepsilon})\nabla\phi. \tag{57}$$

The idea is now to choose w colinear to this force and to project it as in the resolution of Navier-Stokes equations in order to enforce the constraint (55). We therefore set

$$w = \frac{F}{|\gamma_{,r}\times\gamma_{,s}|^2} - \frac{\nabla p}{|\gamma_{,r}\times\gamma_{,s}|}. \tag{58}$$

with the "pressure" p such that

$$\Delta p = \operatorname{div}\left(\frac{F}{|\gamma_{,r} \times \gamma_{,s}|}\right). \tag{59}$$

The weights in the construction of w allows to get a simple Poisson equation for the pressure, and a decreasing energy. Obtaining such a simple equation allows to use fast FFT solvers (FISHPACK).

Substituting F for its expression in terms of w in (56) we obtain thanks to the boundary conditions i or (ii)

$$\frac{d\ell_\varepsilon(\Gamma_t)}{dt} = -\int_{J^2} |\gamma_{,r} \times \gamma_{,s}|^2 |w|^2 dr ds \leq 0.$$

Therefore we observe that moving the curve with the field w, makes the curve length decrease. This length will stop decreasing if, and only if, w vanishes.

6.4 Curve moving algorithm

To sum up, the minimization process is done by solving the following system of PDEs

$$\phi_t + w \cdot \nabla \phi = 0, \tag{60}$$

$$w + \frac{1}{|\gamma_{,r} \times \gamma_{,s}|} \nabla p = \frac{1}{|\gamma_{,r} \times \gamma_{,s}|^2} F(\phi), \tag{61}$$

$$\operatorname{div}(|\gamma_{,r} \times \gamma_{,s}| w) = 0. \tag{62}$$

The evolution terminates when the velocity field w becomes zero.

The divergence-free condition may be implemented by a slightly modified projection method. For example for the classical Chorin-type projection we perform these steps

$$\begin{aligned}
\frac{\phi^{n+1} - \phi^n}{\delta t} + w^n \cdot \nabla \phi^n &= 0, \\
\tilde{w}^{n+1} &= \frac{1}{|\gamma_{,r} \times \gamma_{,s}|^2} F(\phi^{n+1}), \\
\Delta p^{n+1} &= \operatorname{div}(|\gamma_{,r} \times \gamma_{,s}| \tilde{w}^{n+1}), \\
w^{n+1} &= \tilde{w}^{n+1} - \frac{1}{|\gamma_{,r} \times \gamma_{,s}|} \nabla p^{n+1}.
\end{aligned}$$

We may of course use some more advanced time-stepping scheme but this algorithm is presented here for the sake of simplicity. For example we can use $F(\frac{3}{2}\phi^{n+1} - \frac{1}{2}\phi^n)$ rather than $F(\phi^{n+1})$, so that w^{n+1} will approximate the velocity at time $n + \frac{3}{2}$ and the next step in the transport of ϕ will be more accurate.

6.5 Geodesic curvature

We will next provide a geometric interpretation of the force F in (57). When the miminization (53) is solved using the algorithm in (60)-(62), the process terminates when the velocity w is zero. Recall from differential geometry that curves which minimize their length under a fixed enclosed area constraint are linked to constant geodesic curvature curves [65]. We will

show that the geodesic curvature of the curves becomes constant when the velocity is zero. Further, the geodesic curvature provides a method for verifying numerical calculations. After lengthy computations we obtain the following equivalent form of (56):

$$F(\phi) = -|\gamma_{,r} \times \gamma_{,s}|\kappa_g \frac{1}{\varepsilon}\zeta\left(\frac{\phi}{\varepsilon}\right)\nabla\phi. \tag{63}$$

Then we can prove that our algorithm, if it converges, will produce a curve with constant geodesic curvature. Indeed we saw that its length stops decreasing if and only if w vanishes, which in (61) gives

$$\frac{1}{|\gamma_{,r} \times \gamma_{,s}|}\nabla p = \frac{1}{|\gamma_{,r} \times \gamma_{,s}|^2}F(\phi).$$

Observe that the force does not vanish since it still tend to reduce the length of the curve which is impossible due to the surface constraint. From (63) we have

$$\nabla p = -\kappa_g \frac{1}{\varepsilon}\zeta\left(\frac{\phi}{\varepsilon}\right)\nabla\phi = -\kappa_g \nabla\left[H(\frac{\phi}{\varepsilon})\right] \tag{64}$$

In order the right hand side of this equality to be a gradient, it is necessary and sufficient that κ_g is constant on level sets of ϕ, which in particular means that Γ_t has a constant geodesic curvature.

6.6 Numerical examples

In the context of moving a curve with given enclosed surface, our projection algorithm has a clear advantage over other algorithms that use a penalty term to enforce the fixed area constraint. Our implementation uses a MAC grid which ensures accurate divergence-free condition (Chorin type projection method), even in the case where γ is not identity (see [A1]). Thus the surface area constraint is not penalized but enforced. Surface area loss from initialization to stationary state in the case of an ellipse on a cylinder relaxing to a circle is about two percents for a 64×64 grid, under one percent (0.66 %) for a 128×128 grid and 0.06% for a 256×256 grid. Moreover, as the Poisson equation associated to the projection method lies on the rectangular parametric space, fast FFT solvers (e.g. FISHPACK) may be used, leading to very small computational costs.

The boundary conditions are of Dirichlet type in case of non-closed supporting surfaces, and periodic in one direction in the case of surfaces of revolution. Note however that our algorithm as presented above in its native form requires a regular parametrical representation of the supporting surface in the neighborhood of the moving curve. This fact rules out, for example, the case where the supporting surface is a closed sphere, unless if the curve remains away from the singular poles. In this last case the algorithm works since the force is localized around the curve. In order to deal with a sphere without any *a priori* extra information on the curve motion, we have to adapt the algorithm to handle parametrical patches. This work is under development.

We first demonstrate our minimization algorithm on a simple problem of finding the shortest closed curve on a paraboloid. The minimizer is known to be a circle. In figure 18, we show the evolution of the minimization starting with an ellipsoid on the paraboloid. As can be seen the flow ends with a horizontal circle.

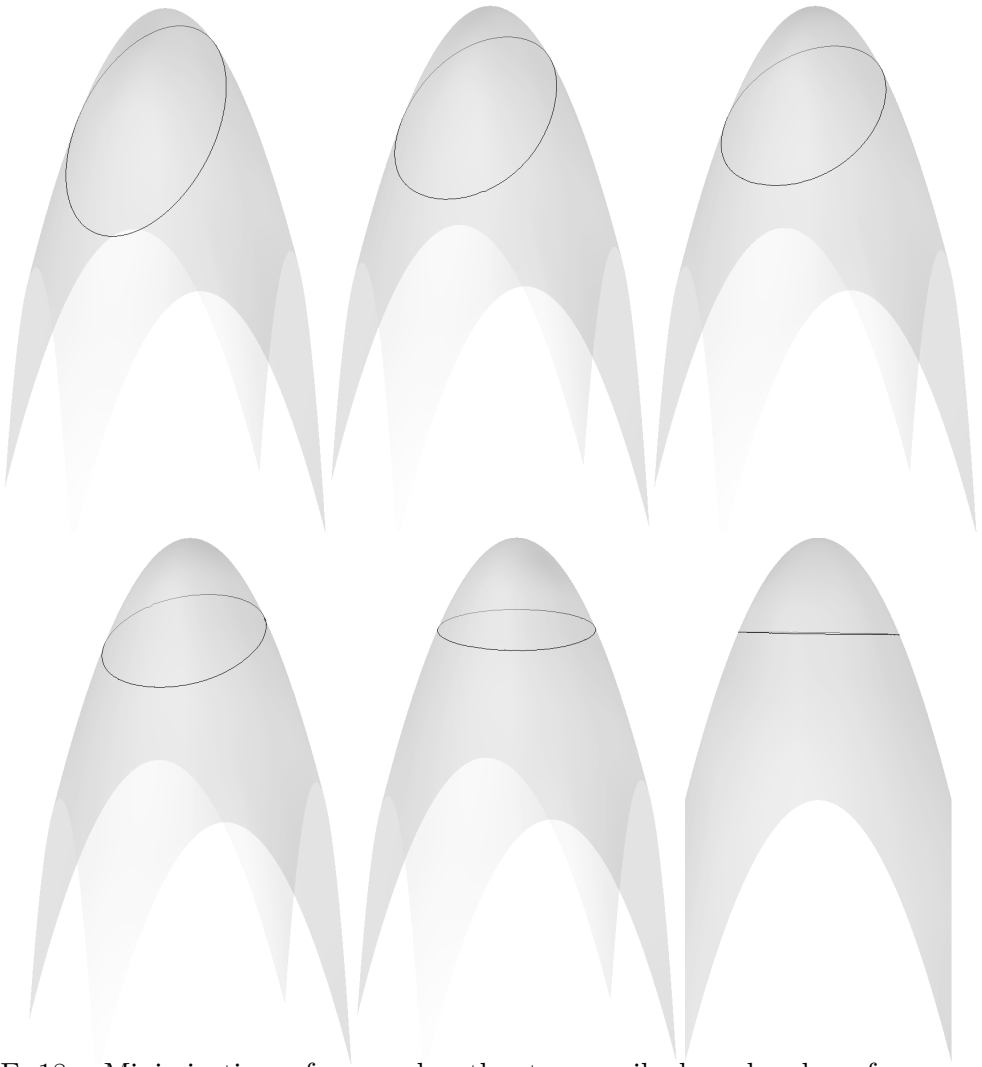

FIGURE 18: Minimization of curve length at prescribed enclosed surface area, on a paraboloid. Convergence toward the horizontal circle. Last picture shows a non-perspective plot of the final state.

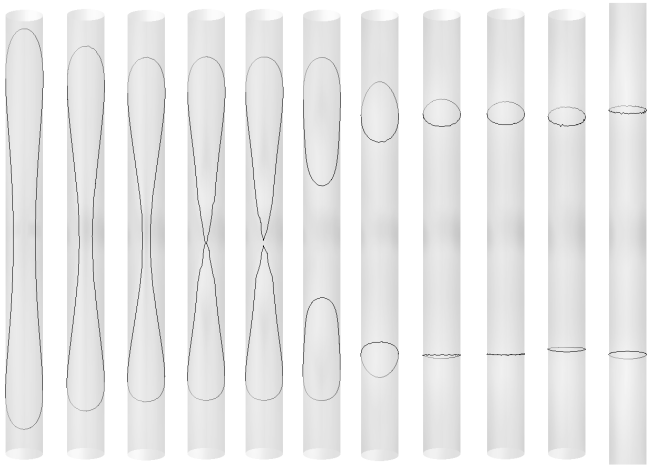

FIGURE 19: Minimization of curve length leading to a topological change. Last picture on the right is without perspective to demonstrate symmetry property.

In the next example, the supporting surface is a cylinder of radius $a = 1$. An ellipse in the parametric space is chosen as initialization, which gives the curve drawn on the leftmost picture in figure 19. This curve is wrapped around the cylinder: the top and bottom loops are running on the back part of the surface while the thinest part of domain enclosed by the curve is drawn on the front. Computations are made on a 128×128 grid. Due to the fact that the area enclosed by the curve is greater than $4\pi a^2$, the minimizing curve is known to be made of two circles [65], a fact that our computations recover. See `http//www-ljk.imag.fr/membres/Emmanuel.Maitre/Levelset/` for videos of the minimization process.

7 Conclusion and future work

My work has been mainly concerned by the modeling of physical or biological phenomenon with often a care about the efficiency of their implementation from the numerical point of view. In that respect it appeared that the Eulerian modeling in continuum mechanics did not attract all attention it deserves, speaking of its simplicity and efficiency. This is even more true in the modeling of biological systems where the concept of multiphysics medium is particularly relevant. Therefore I have several paths to further develop this topic.

The first one concerns the handling of a full elasticity in the elastic membrane model. Up to now, we were able to deal with an energy only function of the local area change. However, for the simulation of red blood cells, we have to add some membrane full elasticity, because these biological entities have an extra network of actin under the phospholipidic bilayer membrane. While this should not play a role in the equilibrium shapes, we expect a modified behavior in shear flow. The same model could also be relevant for the case of an isotropic fabric. We therefore work in that direction with our Physicists colleagues of LSP.

The stability question is central in fluid-structure coupling problems, and number of publications are devoted to that issue, independently of the method used. In her thesis Claire Bost proposed an elementary $1D$ model which allows to recover the stability conditions usually used in the literature. The study of efficient numerical schemes, stable for stiff elastic objects remains a challenging question. In that respect it seems that the discretization of singular source terms in multiphysics methods plays a role which remains to be studied. This bringsus back to the question of Eulerian representation of the interface and discussion between Level Set and phase field methods that we addressed in [A14]. On a close topic a joint work with John Stockie about parametric instability of an immersed $3D$ membrane is under development.

Identifying the polarization on the myocardium surface that we aim to implement from our academic work with Fadil Santosa is already started in dimension 2. More generally I am thinking about the use of this Level Set method in the parameter space in the case where the surface is the manifold of parameters to some dynamical system. Could we write some descent like optimization algorithms to look for optimal trajectories of this system ?

At last and more generally we developed with Georges-Henri Cottet these last years several techniques of multiphysics type to deal with fluid-structure interaction problems (elastic and rigid). All these tools will be integrated into a coherent computational library which could be used by other researchers. For the time being Iker Bellicot is integrating some part of our code inside the software SOFA of the INRIA team EVASION of our laboratory. We aim at providing a software where non specialists could deal with the interaction of rigid, elastic bodies and fluids with as few software development as possible.

The numerical implementation of all these models was very exciting for me, as well as exchanges I developed with my physicists colleagues, among who I want to single out Chaouqi Misbah and Philippe Peyla. I am convinced that model analogies, from which multiphysics takes its origin, are very useful to reformulate problems and bring new insight to solve issues, at the mathematical and numerical level.

Publications list[3] and references

— International journals —

[A1] Emmanuel Maitre and Fadil Santosa. Level set methods for optimization problems involving geometry and constraints II. Optimization over a fixed surface. *J. Comp. Phys.*, 2008. in press, available online.

[A2] Emmanuel Maitre, Thomas Milcent, Georges-Henri Cottet, Annie Raoult, and Yves Usson. Applications of level set methods in computational biophysics. *Math. Comput. Model.*, 2008. in press, avaible online.

[A3] Georges-Henri Cottet, Emmanuel Maitre, and Thomas Milcent. Eulerian formulation and level set models for incompressible fluid-structure interaction. *ESAIM-Math. Model. Numer. Anal.*, 42:471–492, 2008.

[A4] Georges-Henri Cottet and Emmanuel Maitre. A level set method for fluid-structure interactions with immersed surfaces. *Math. Models Meth. Appl. Sci.*, 16(3):415–438, 2006.

[A5] Georges-Henri Cottet and Emmanuel Maitre. A level-set formulation of immersed boundary methods for fluid-structure interaction problems. *C. R. Math.*, 338(7):581–586, 2004.

[A6] Emmanuel Maitre. On a nonlinear compactness lemma in $L^p(0,T;B)$. *Int. J. Math. Math. Sci.*, 2003(27):1725–1730, 2003.

[A7] Samir Akesbi and Emmanuel Maitre. Theoretical and numerical analysis of a minimal residual solver for 2D Boltzmann transport equation. *J. Comput. Appl. Math.*, 150(2):357–374, 2003.

[A8] Emmanuel Maitre and Patrick Witomski. A pseudo-monotonicity adapted to doubly nonlinear elliptic-parabolic equations. *Nonlinear Anal.-Theory Methods Appl.*, 50(2):223–250, 2002.

[A9] Emmanuel Maitre. Numerical analysis of nonlinear elliptic-parabolic equations. *ESAIM-Math. Model. Numer. Anal.*, 36(1):143–153, 2002.

[A10] Nadjombé Faré and Emmanuel Maitre. Existence de solutions pour un modèle de drapé d'un tissu. *C. R. Acad. Sci., Paris, Sér. I, Math.*, 333(10):967–972, 2001.

[A11] Samir Akesbi and Emmanuel Maitre. Minimal residual method applied to the transport equation. *Numer. Algorithms*, 26(3):235–249, 2001.

[A12] Samir Akesbi and Emmanuel Maitre. Méthode du résidu minimal en dimension infinie pour l'équation de transport neutronique. *C. R. Acad. Sci., Paris, Sér. I, Math.*, 330(5):385–390, 2000.

[A13] Emmanuel Maitre and Patrick Witomski. Transport equation with boundary conditions for free surface localization. *Numer. Math.*, 84(2):275–303, 1999.

[3] pdf are downloadable on `http//ljk.imag.fr/membres/Emmanuel.Maitre/pdf/`

[A14] E. Maitre, E. Bonnetier, C. Misbah, P. Peyla, and A. Raoult. Comparison between advected-field and level-set methods in the study of vesicle dynamics. *en préparation*, 2009.

— Invited conferences —

[B15] Georges-Henri Cottet, Emmanuel Maitre, and Thomas Milcent. *An Eulerian method for fluid-structure interaction with biophysical applications.* European Conference on Computational Fluid Dynamics, ECCOMAS CFD 2006, Delft, Pays-Bas, September 2006. Invited mini-symposium conference.

[B16] Georges-Henri Cottet and Emmanuel Maitre. *A combined level-set / immersed boundary approach to describe the motion of an elastic curve in a fluid.* EUCOR Worshop on fluid-structure coupling, Mulhouse, France, October 2003. Invited conference.

[B17] Georges-Henri Cottet, Emmanuel Maitre, and Philippe Tracqui. *Cell Dynamics: From a 1D model to a Combined Level Set-Immersed Boundary Approach.* International Symposium on Modeling of Physiological Flows, Lausanne, Suisse, September 2003. Invited conference.

— References —

[18] S. Akesbi. Splitting d'opérateur pour l'équation de transport neutronique en géométrie bidimensionnelle plane. *ESAIM : M2AN*, 34(6):1109–1122, 2000.

[19] S. Akesbi, M.R. Laydi, and M. Mokhtar-Kharroubi. Décomposition d'opérateurs et accélération de la convergence en neutronique. *C.R. Acad. Sci. Paris*, 319:765–770, 1994.

[20] S. Akesbi, M.R. Laydi, and M. Mokhtar-Kharroubi. Schemes and acceleration in transport theory. *To appear in Journ. of Transport Theory and Statistical Physics*, 1999.

[21] S. Akesbi and M. Nicolet. Nouveaux algorithmes performants en théorie du transport. *M2AN*, 32(3):341–358, 1998.

[22] R. E. Alcouffe, B. A. Clark, and E. W. Larsen. The diffusion-synthetic acceleration of transport iterations, with application to a radiation hydrodynamics problem. In *Multiple time scales (A86-47618 23-64). Orlando, FL, Academic Press, Inc.*, pages 73–111, 1985.

[23] K. Ammar and P. Wittbold. Existence of renormalized solutions of degenerate elliptic-parabolic problems. *Proceedings of the Royal Society of Edinburgh: Section A Mathematics*, 133:477–496, 2003.

[24] S. F. Ashby, P. N. Brown, M. R. Dorr, and A. C. Hindmarsh. A linear algebraic analysis of diffusion synthetic acceleration for the boltzmann tranport equation. *SIAM Journal on Numerical Analysis*, 32(1):128–178, 1995.

[25] H. Bauschke. The approximation of fixed points of composition of nonexpansive mappings in Hilbert space. *Journal of Mathematical Analysis and Applications*, 202:150–159, 1996.

[26] J. T. Beale and J. Strain. Locally corrected semi-lagrangian methods for stokes flow with moving elastic interfaces. *J. Comp. Phys.*, 227(8):3896–3920, 2008.

[27] J. Beaucourt, F. Rioual, T. Séon, T. Biben, and C. Misbah. Steady to unsteady dynamics of a vesicle in a flow. *Physical Review E*, 69(1):011906, 2004.

[28] Ph. Bnilan, M.G. Crandall, and A. Pazy. Nonlinear evolution equations in Banach spaces. *preprint book to appear*, 1991.

[29] Ph. Bnilan and P. Wittbold. On mild and weak solutions of elliptic-parabolic problems. *Adv. Diff. Equ.*, 1:1053–1073, 1996.

[30] Ph. Bnilan and P. Wittbold. Sur un problme parabolique-elliptique. *Mathematical Modelling and Numerical Analysis (M2AN)*, 33(1):121–127, 1999.

[31] T. Biben and C. Misbah. Tumbling of vesicles under shear flow within an advected field approach. *Physical Review E*, 67:031908, 2003.

[32] T. Biben, K. Kassner, and C. Misbah. Phase-field approach to three-dimensional vesicle dynamics. *Physical Review E*, 72(4):041921, 2005.

[33] D. Boffi, L. Gastaldi, and L. Heltai. Numerical stability of the finite element immersed boundary method. *M3AS*, 17:1479–1505, 2007.

[34] D. Boffia, L. Gastaldi, and L. Heltai. Stability results and algorithmic strategies for the finite element approach to the immersed boundary method, preprint available on http//www.ing.unibs.it/˜gastaldi/paper.html. *Proceeding of the Sixth European Conference on Numerical Mathematics and Advanced Applications*, pages 557–566, 2005.

[35] S. Bohnet, R. Ananthakrishnan, A. Mogilner, J.-J. Meister, and A. Verkhovsky. Weak force stalls protrusion at the leading edge of the lamellipodium. *Biophys. J.*, 90:1810–1820, 2006.

[36] C. Bost. *Méthodes Level-Set et pénalisation pour le calcul d'interactions fluide-structure.* Thèse de l'Université de Grenoble, oct 2008.

[37] J. Brackbill, D. Kothe, and C. Zemach. A continuum method for modelling surface tension. *J. Comput. Phys.*, 100:335–354, 1992.

[38] Y. Brenier and W.-A. Yong. Derivation of particle, string, and membrane motions from the born–infeld electromagnetism. *Journal of Mathematical Physics*, 46(6):062305, 2005.

[39] Y. Brenier. Optimal transport, convection, magnetic relaxation and generalized boussinesq equations. *preprint HAL, http//hal.archives-ouvertes.fr/hal-00202710/fr/*, 2008.

[40] D. Bresch, Th. Colin, E. Grenier, B. Ribba, O. Saut, O. Singh, and C. Verdier. Quelques méthodes de paramètre d'ordre avec applications à la modélisation de processus cancéreux. *ESAIM: Proceedings*, 18:163–180, 2007.

[41] D. Bresch, T. Colin, E. Grenier, B. Ribba, and O. Saut. Computational modeling of solid tumor growth: the avascular stage. *soumis*, 2009.

[42] A. Berger, H. Brézis, and J. Rogers. A numerical method for solving the problem $u_t - \Delta f(u) = 0$. *RAIRO Modél. Math. Anal. Numér.*, 13:297–312, 1979.

[43] L. Caffarelli, R. Kohn, and L. Nirenberg. Partial regularity of suitable weak solutions of the Navier-Stokes equations. *Comm. Pure and Applied Math.*, 35:771–831, 1982.

[44] P. Causin, J.-F. Gerbeau, and F. Nobile. Added-mass effect in the design of partitioned algorithms for fluid-structure problems. *Computer Methods in Applied Mechanics and Engineering*, 194:4506–4527, 2005.

[45] Y.C. Chang, T.Y. Hou, B. Merriman, and S. Osher. A level set formulation of eulerian interface capturing methods for incompressible fluid flows. *J. Comp. Phys.*, 124:449–464, 1996.

[46] L.-T. Cheng, P. Burchard, B. Merriman, and S. J. Osher. Motion of curves constrained on surfaces using a level set approach. *J. Comp. Phys.*, 175:604–644, 2002.

[47] P.G. Ciarlet. *Elasticité tridimentionnelle*. Masson, 1985.

[48] P.G. Ciarlet. *Mathematical Elasticity II, Theory of plates*. North Holland, 1997.

[49] P.G. Ciarlet and D.Coutand. An existence theorem for nonlinearly elastic flexural shells. *J. Elasticity*, 50:261–277, 1998.

[50] R. Cortez, C.S. Peskin, J.M. Stockie, and D. Varela. Parametric resonance in immersed elastic boundaries. *SIAM Journal on Applied Mathematics*, 65(2):494–520, 2004.

[51] D. Coutand. Existence d'un minimiseur pour le modle proprement invariant de plaque en flexion non linairement lastique. *C.R.Acad.Sci, Paris, srie I*, 324:245–248, 1997.

[52] G. Duvaut. *Mécanique des milieux continus*. Dunod, 1998.

[53] B. Engquist, A.-K. Tornberg, and R. Tsai. Discretization of dirac delta functions in level set methods. *Journal of Computational Physics*, 207(1):28–51, 2005.

[54] L.C. Evans and R. Gariepy. *Measure theory and fine properties of functions*. CRC Press, 1992.

[55] M. Fernandez, J.-F. Gerbeau, and C. Grandmont. A projection semi-implicit scheme for the coupling of an elastic structure with an incompressible fluid. *International journal for numerical methods in engineering*, 69(4):794–821, 2007.

[56] C. Galusinski and P. Vigneaux. Level-Set method and stability condition for curvature-driven flows. *C. R. Acad. Sci. Paris, Series I - Mathematics*, 344(11):703–708, 2007.

[57] C. Galusinski and P. Vigneaux. On stability condition for bifluid flows with surface tension : application to microfluidics. *J. Comp. Phys.*, 227(12):6140–6164, 2008.

[58] B.E. Griffith and C.S. Peskin. On the order of accuracy of the immersed boundary method: Higher order convergence rates for sufficiently smooth problems. *J. Comp. Phys.*, 208:75–105, 2005.

[59] E. Girardi. *Couplage de méthodes et décomposition de domaine pour la résolution de l'équation du transport des neutrons.* CEA Cadarache / Thèse de doctorat d'état de l'Université Evry Val d'Essone, 2004.

[60] O. Grange and F. Mignot. Sur la Résolution d'une Équation et d'une Inéquation Paraboliques non Linéaires. *J. Funct. Anal.*, 11:77–92, 1972.

[61] B. Halpern. Fixed points of nonexpansive mappings. *Bull. Amer. Math. Soc.*, 73:957–961, 1967.

[62] G. A. Holzapfel. *Nonlinear solid mechanics : a continuum approach for engineering.* Wiley, 2000.

[63] T. Y. Hou and Z. Shi. Removing the stiffness of elastic force from the immersed boundary method for the 2D Stokes equations. *in press for J. of Comp. Phys.*, 2008.

[64] T. Y. Hou and Z. Shi. An efficient semi-implicit immersed boundary method for the NavierStokes equations. *in press for J. of Comp. Phys.*, 2008.

[65] H. Howards, M. Hutchings, and F. Morgan. The isoperimetric problem on surfaces. *The American Mathematical Monthly*, 106(5):430–439, 1999.

[66] W. Jäger and J. Kačur. Solution of Porous Medium Type Systems by Linear Approximation Schemes. *Numer. Math.*, 60:407–427, 1991.

[67] W. Jäger and J. Kačur. Solution of Doubly Nonlinear and Degenerate Parabolic Problems by Relaxation Schemes. M^2AN, 29(5):605–627, 1995.

[68] D. Jamet, O. Lebaigue, N. Coutris, and J.M. Delhaye. The Second Gradient Method for the Direct Numerical Simulation of Liquid–Vapor Flows with Phase Change. *J. of Comp. Phys.*, 169:624–651, 2001.

[69] D. Jamet, D. Torres, and J.U. Brackbill. On the theory and computation of surface tension: the elimination of parasitic currents through energy conservation in the second-gradient method. *J. of Comp. Phys.*, 182:262–276, 2002.

[70] D. Jamet and C. Misbah. Towards a thermodynamically consistent picture of the phase-field model of vesicles: Local membrane incompressibility. *Physical Review E*, 76(5):051907, 2007.

[71] J. Kačur, A. Handlovičová, and M. Kačurová. Solution of Nonlinear Diffusion Problems by Linear Approximation Schemes. *SIAM J. Numer. Anal.*, 30(6):1703–1722, 1993.

[72] J. Kačur. Solution of Some Free Boundary Problems by Relaxation Schemes. *SIAM J. Numer. Anal.*, 36(1):290–316, 1999.

[73] T.J. Kang and W.R. Yu. Drape simulation of woven fabric by using finite-element method. *J. Text. Inst.*, 86(4), 1995.

[74] K. M. Khattab and E. W. Larsen. Synthetic acceleration methods for linear transport problems with highly anisotropic scattering. *Nuclear Science and Engineering*, 107(3):217–227, 1991.

[75] E.W. Larsen. Unconditionally stable diffusion-synthetic acceleration methods for the slab geometry dicrete-ordinates equations. *Nucl. Sci. and Eng.*, parts I-II, 1988.

[76] P. Lascaux and R. Théodor. *Analyse numérique matricelle appliquée à l'art de l'ingénieur*, volume 2. Masson, 1987.

[77] L. Lee and R.J. Leveque. An immersed interface method for incompresible navier-stokes equations. *SIAM J. Sci. Comp.*, 25(3):832–856, 2003.

[78] R. J. LeVeque and Z. Li. Immersed interface methods for Stokes flow with elastic boundaries or surface tension. *SIAM J. Sci. Comput.*, 18(3):709–735, 1997.

[79] H. Le Dret and A. Raoult. The membrane shell model in nonlinear elasticity: A variational asymptotic derivation. *J. Nonlinear Sci.*, 6(1):59–84, 1996.

[80] F.-H. Lin, C. Liu, and P. Zhang. On hydrodynamics of viscoelastic fluids. *Communications on Pure and Applied Mathematics*, 58(11):1427–1471, 2005.

[81] P.-L. Lions. Approximation de points fixes de contractions. *C. R. Acad. Sci. Paris Sér. A.*, 284:1357–1359, 1977.

[82] J.-L. Lions. *Quelques Méthodes de Résolution des Problèmes aux Limites Non Linéaires*. Dunod, 1969.

[83] E. Magenes, R.H. Nochetto, and C. Verdi. Energy Error Estimates for a Linear Scheme to Approximate Nonlinear Parabolic Problems. *RAIRO Modél. Math. Anal. Numér.*, 21(4):655–678, 1987.

[84] E. Maitre. *Sur une classe d'équations à double non linéarité : application à la simulation numérique d'un écoulement visqueux compressible*. Thèse, Université Grenoble I, 1997.

[85] T.A. Manteuffel and K.J. Ressel. Least-squares finite-element solution for the neutronic transport equation in diffusive regimes. *SIAM Journal on Numerical Analysis*, 35(2):806–835, 1998.

[86] T. Manteuffel, S. McCormick, J. Morel, and G. Yang. A fast multigrid algorithm for isotropic transport problems ii. with absorption. *SIAM Journal on Scientific Computing*, 17(6):1449–1474, 1996.

[87] T. Milcent. *Formulation eulerienne du couplage fluide structure, analyse mathématique et applications en biomécanique*. Thèse de l'Université de Grenoble, nov 2008.

[88] C. Misbah. Vacillating breathing and tumbling of vesicles under shear flow. *Physical Review Letters*, 96(2):028104, 2006.

[89] J. E. Morel and T. A. Manteuffel. An angular multigrid acceleration technique for s_n equations with highly forward-peaked scattering. *Nuclear Science and Engineering*, 107:330–342, 1991.

[90] D. Ölz, C. Schmeiser, and V. Small. Modelling of the Actin-cytoskeleton in symmetric lamellipodial fragments. *to appear in Cell Adhesion & Migration*, 2008.

[91] R.W. Ogden. *Nonlinear elasticity, anisoptropy, material staility and residual stresses in soft tissue (edited by G.A. Holzapfel and R.W. Ogden).* CISM Course and Lectures Series 441, Springer, 2003.

[92] J. Okada, S. Sugiura, S. Nishimura, and T. Hisada. Three-dimensional simulation of calcium waves and contraction in cardiomyocytes using the finite element method. *Am. J. Physiol. Cell. Physiol.*, 288:C510–C522, 2005.

[93] S. Osher and R. P. Fedkiw. *Level set methods and Dynamic Implicit Surfaces.* Springer, 2003.

[94] F. Otto. L^1-Contraction and Uniqueness for Quasilinear Elliptic-Parabolic Equations. *J. Differential Equations*, 131:20–38, 1996.

[95] C.S. Peskin. Numerical analysis of blood flow in the heart. *J. Comp. Phys.*, 25:220–252, 1977.

[96] C.S. Peskin. The immersed boundary method. *Acta Numerica*, 11:479–517, 2002.

[97] S. Peskin and B.F. Printz. Improved volume conservation in the computation of flows with immersed boundaries. *J. Comput. Phys.*, 105:33–46, 1993.

[98] A. Raoult. Symmetry groups in nonlinear elasticity: An exercise in vintage mathematics. *preprint HAL - CCSD, http//hal.archives-ouvertes.fr/hal-00275450/en/*, 2008.

[99] P.A. Raviart. Sur la Résolution de Certaines Équations Paraboliques non Linéaires. *J. Funct. Anal.*, 5:299–328, 1970.

[100] K. Sbihi and P. Wittbold. Existence of renormalized solutions for a nonlinear Stefan problem. *Comptes Rendus Mathematique*, 345(11):629–632, Déc. 2007.

[101] U. Seifert K. Berndl and R. Lipowsky. Shape transformations of vesicles: Phase diagram for spontaneous- curvature and bilayer-coupling models. *Phys. Rev. A*, 44(2):1182–1202, 1991.

[102] F. Simondon. Sur l'équation $b(u)_t - \operatorname{div} a(u, \nabla u) = 0$ par la méthode des semi-groupes dans L^1. Séminaire d'analyse non linéaire, Laboratoire de Mathématiques de Besançon, 1984.

[103] M. Slodička. Approximation of a nonlinear degenerate parabolic equation via a linear relaxation scheme. *Comptes Rendus Mathematique*, 21(2):191–212, 2005.

[104] P. Smereka. The numerical approximation of a delta function with application to level-set methods. *J. Comp. Phys.*, 211:77–90, 2003.

[105] A. Smolianski. Finite-element/level-set/operator-splitting (FELSOS) approach for computing two-fluid unsteady flows with free moving interfaces. *International Journal for Numerical Methods in Fluids*, 48(3):231–269, 2005.

[106] V.A. Solonnikov. Estimates for solutions of nonstationary Navier-Stokes equations. *J. Soviet Math.*, 8(4):467–529, 1977.

[107] J. Stockie. Analysis of stiffness in the immersed boundary method and implications for time-stepping schemes. *J. Comp. Phys.*, 154:41–64, 1999.

[108] M. Sussman, E. Fatemi, P. Smereka, , and S. Osher. An improved level set method for incompressible two-phase flows. *Comp. Fluids*, 27:663–680, 1998.

[109] M. Sussman and E. Fatemi. An efficient, interface-preserving level set redistancing algorithm and its application to interfacial incompressible fluid flow. *SIAM J. Sci. Comp.*, 20(4):1165–1191, 1999.

[110] M. Sy, D. Bresch, F. Guillén-González, J. Lemoine, and M.A. Rodríguez-Bellido. Local strong solution for the incompressible korteweg model. *C. R. Acad. Sci. Paris, Ser. I*, 342:169–174, 2006.

[111] A. Tizaoui. *Principe de préconditionnement et de décomposition d'opérateurs pour l'équation de transport neutronique.* Thèse de l'Université de Haute-Alsace - Mulhouse, 2005.

[112] A. Tizaoui and S. Akesbi. Gmres algorithm and symmetric gauss-seidel preconditioning solver for 2-d boltzmann transport equation. *J. Fusion Energ.*, 27:225–232, 2008.

[113] C. Tu and C.S. Peskin. Stability and instability in the computation of flows with moving immersed boundaries: A comparison of three methods. *SIAM J. Sci. Statist. Comput.*, 13:1361–1376, 1992.